ASTROPHYSICS

THE KINEMATICS PARAMETERS OF THE GALAXY USING DATA OF MODERN ASTROMETRIC CATALOGUES

V.S. Akhmetov[1], P.N. Fedorov[1,2], A.B. Velichko[1], V.M. Shulga[2,1]

[1] Institute of Astronomy of Kharkiv National University, Sums'ka 35, 61022 Kharkiv, Ukraine, *akhmetov@astron.kharkov.ua*

[2] Institute of Radio Astronomy, National Academy of Sciences of Ukraine, Chervonopraporna 4, 61002, Kharkiv, Ukraine, *shulga@rian.kharkov.ua*

ABSTRACT. Based on the Ogorodnikov-Milne model, we analyze the proper motions of XPM2, UCAC4 and PPMXL stars. To estimate distances to the stars we used the method of statistical parallaxes herewith the random errors of the distance estimations do not exceed 10%. The method of statistial parallaxes was used to estimate the distanes to stars with random errors no larger than 14%. The linear solar veloity relative to the local standard of rest, which is well determined for the loal entroid (d 150 p), was used as a referene.

We have established that the model component that describes the rotation of all stars under consideration about the Galactic Y axis differs from zero. For the distant (d < 1000 pc) PPMXL and UCAC4 stars, the mean rotation about the Galactic Y axis has been found to be M_{13}^{-} = -0.75±0.04 mas yr^{-1}. As for distances greater than 1 kpc M_{13}^{-} derived from the data of only XPM2 catalogue becomes positive and exceeds 0.5 mas yr^{-1}. We interpret this rotation found using the distant stars as a residual rotation of the ICRS/Tycho-2 system relative to the inertial reference frame.

Keywords proper motions, reference systems, Galaxy: kinematics and dynamics: late-type.

1. Introduction

The method used in this work allows not only to determine kinematic parameters of the Galaxy but also to estimate the inertiality of the proper catalogues from the study of components of the solid-body rotation tensor, which describe the rotation about the X, Y axes in the galactic coordinate system.

Since the Sun is located inside the giant stellar-gaseous complex known as the Gould belt (≈ 500 pc in radius), the involvement of sufficiently distant stars, which would be free of the effects of both the near-solar flows and the local stellar system on the whole, is vital for the reliable application of the method.

The aim of this work is to study kinematic parameters of the large number of stars depending on their distances. To estimate the latter we applied the method of comparison of statistical parallaxes with the velocity of the Sun (Olling R. at all.: 2003), which is currently known quite reliably (Schönrich R. et al., 2010). $(U,V,W) = (\mathbf{11.1}^{+0.69}_{-0.75}, \mathbf{12.24}^{+0.47}_{-0.47}, \mathbf{7.25}^{+0.37}_{-0.36})$ km s^{-1}

2. The model

In the present work, we use a rectangular galactic coordinate system with the axes directed in the following way: from the observer towards the galactic center ($l = 0°$, $b = 0°$, axis X or axis 1), along the galactic rotation ($l = 90°$, $b = 0°$, axis Y or axis 2), and towards the Northern pole of the Galaxy ($b = 90°$, axis Z or axis 3). Within the Ogorodnikov-Milne model, we use the designations introduced by Clube S. (1972, 1973) and applied in the works by du Mont D. (1977, 1978). As is known, (Ogorodnikov, 1965), when using only the proper motions of stars, one of the diagonal elements of the local deformation tensor remains to be undefined. That is why we determine the differences of the form: $(M_{11}^{+} - M_{22}^{+})$ and $(M_{33}^{+} - M_{22}^{+})$.

The conditional equations are written in the following form:

$$\begin{aligned}\mu_l \cos b \;=\;& (1/r)(X_0 \sin l - Y_0 \cos l) \\ & - M_{32}^{-} \cos l \sin b - M_{13}^{-} \sin l \sin b \\ & + M_{21}^{-} \cos b + M_{12}^{+} \cos 2l \cos b \\ & - M_{13}^{+} \sin l \sin b + M_{23}^{+} \cos l \sin b \\ & - 0.5(M_{11}^{+} - M_{22}^{+}) \sin 2l \cos b, \qquad (1)\end{aligned}$$

$$\begin{aligned}\mu_b \;=\;& (1/r)(X_0 \cos l \sin b + Y_0 \sin l \sin b - Z_0 \cos b) \\ & + M_{32}^{-} \sin l - M_{13}^{-} \cos l \\ & - 0.5\, M_{12}^{+} \sin 2l \sin 2b + M_{13}^{+} \cos l \cos 2b \\ & + M_{23}^{+} \sin l \cos 2b \\ & - 0.5(M_{11}^{+} - M_{22}^{+}) \cos^2 l \sin 2b \\ & + 0.5(M_{33}^{+} - M_{22}^{+}) \sin 2b, \qquad (2)\end{aligned}$$

where X_0, Y_0, Z_0 are components of the peculiar velocity of the Sun, $M_{12}^-, M_{13}^-, M_{23}^-$ - components of the vector of the solid-body rotation of the small circumsolar vincinity about the corresponding axes. According to the rectangular coordinate system we selected, the following rotations are positive: from axis 1 to axis 2, from axis 2 to axis 3, and from axis 3 to axis 1.

M_{21}^- and M_{12}^+ values (mas yr^{-1}) are connected with the Oort constants A and B (km s^{-1} kpc^{-1}) respectively through the proportionality factor of 4.74. Each of the $M_{12}^+, M_{13}^+, M_{23}^+$ values describes deformation of the velocity field in the corresponding plane.

The diagonal terms of the local deformation tensor $M_{11}^+, M_{22}^+, M_{23}^+$ describe the general contraction or extension of the whole stellar system. The set of conditional equations (1), (2) involves eleven unknown variables which are found using the least squares method. As can be seen from the equation (1), two pairs of unknown variables M_{13}^- and M_{13}^+ as well as M_{32}^- and M_{23}^+ have the same coefficients *sin l sin b* and *cos l sin b*, respectively. This has the result that the unknowns are resolved poorly. A quantity $1/r$ is a parallactic factor, which is put to equal unity in solving the system of equations (1), (2). In this case stars are projected to the unit sphere. With this approach all parameters under determination are proportional to the heliocentric distance of the considered centroid and expressed in the same units as components of proper motions of stars namely in mas yr^{-1}. Applying a such approach allow us to eliminate completely the effect of the distance errors in data analyzed. Indeed, when the method with known distances to the stars is applied left-hand side of (1) and (2) equations have to be multiplied by 4.74 r, while right-hand side - by r, and then the desired unknowns will be distorted by the errors in determining the stellar distances. At present, the reliable distances to individual stars (with errors of <10%) allow the circumsolar vicinity of 100 pc in radius to be analyzed, but this is insufficient for the purposes of the present work.

3. Used catalogues

XPM2. The XPM2 astrometric catalogue recently created in the Research Institute of Astronomy of the V. N. Karazin Kharkiv National University but until now unpublished is presently the only bulk one that contains highly accurate proper motions of about one billion stars. There is a full coverage of the sky in the declination range $90^\circ \leq \delta \leq 90^\circ$. The accuracy of proper motions of faint stars in the XPM2 catalogue is within 3 to 10 mas yr^{-1}. As concerns its own proper motions, the XPM2 catalogue is a realization of the optical reference system independent on HCRF.

UCAC4. The UCAC4 astrometric catalogue (Zacharias, 2013), at present, is a catalogue, which contains highly accurate proper motions of stars up to 16 mag. The sky coverage is full in the declination interval $90^\circ \leq \delta \leq 90^\circ$. The accuracy of proper motions for faint stars ranges from 3 to 10 mas yr^{-1}. The catalogue expands the system of ICRS/Tycho-2 towards the faint stars.

PPMXL. The PPMXL catalogue contains 910,468,710 entries, including stars, galaxies, and bogus entries. Of these, 412,410,368 are in 2MASS, i.e., 2MASS is used to determine proper motions and the J,H,Ks magnitudes are given in the catalogue. The resulting typical individual mean errors of the proper motions range from 4 mas yr^{-1} to more than 10 mas yr^{-1} depending on observational history. We used only those stars from the catalogue, for which at least one of the stellar magnitudes $b1$ or $b2$ is given. If both of them are presented, the magnitude was accepted to equal $(b1 + b2)/2$. Ultimately, a number of stars we used from the PPMXL catalogue, made 750 millions.

4. Estimation of the group distances

To obtain the estimates of distances to the stars, we used a statistical method (Olling R. et al., 2003). For the value of the known velocity of the Sun's peculiar motion relative to the LSR values from the work (R. Schonrich R. et al., 2009) wewr adopted. $(U, V, W) = (\mathbf{11.1}^{+0.69}_{-0.75}, \mathbf{12.24}^{+0.47}_{-0.47}, \mathbf{7.25}^{+0.37}_{-0.36})$ km s^{-1}. The parallax has been calculated from the formulas:

$$\pi U = 4.74\ X/U;\ \pi W = 4.74\ Z/W, \qquad (3)$$

where X and Y are the are the components of the group velocity of stars (in mas yr^{-1}) received from the solution of equations (1), (2). Since component Y can be distorted by the asymmetric drift velocity (Dennen et. al, 1998), it was not used to determine the group parallaxes. The distance d is found from the relationship: $d = 1/\pi$. In this case the error of distance can be estimated from the relationship

$$e_d = \left(\frac{e_\pi}{\pi}\right) d, \qquad (4)$$

while the e_π value for the motion along Z coordinate was estimated in the following way:

$$e_\pi^2 = 4.74(e_W/W)^2 Z^2 + 4.74(e_Z/W)^2 \qquad (5)$$

A similar relationship can be derived for the motion along the X coordinate.

At first we apply this method to the HIPPARCOS catalogue. Grouping was based on trigonometric parallaxes of the catalogue, herewith $e_\pi/\pi < 1$. Derived statistical distances to the stars depending on trigonometric ones are presented in Fig. 1. It is seen from the figure that no significant systematic distortions in statistical distances are observed, as well as the fact that

for the distances larger that 200 pc, the errors in determining statistical distances are less that the errors of trigonometric distances. Further, we apply the method to the analysis of stars from the UCAC4, XPM2 and PPMXL catalogues.

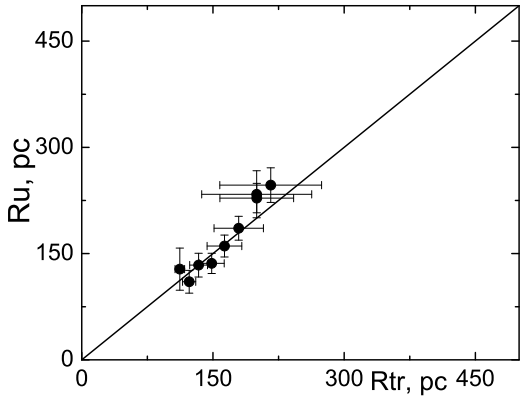

Figure 1: Statistical distances of stars depending on trigonometric ones calculated by data of the HIPPARCOS catalogue.

5. Results of calculations

The several results of solving (1), (2) equation system derived on the basis of stars of mixed spectral composition from XPM2, UCAC4 and PPMXL catalogues depending on the distance are presented in Fig. 2. We have used virtually all stars from the XPM2 catalogue (about 1 billion), with a constraint imposed on the modulus of a star tangential velocity $|\mu_t| = \sqrt{(\mu_\alpha \, cos \, \delta)^2 + (\mu_\delta)^2} < 150$ mas yr^{-1}. All the stars have been grouped according to their magnitudes, with the magnitude interval width of 1 mag in each group. Each of these intervals, in turn, was divided into 1633 Sharlie areas. The resulting data (the mean proper motions) were used to solve the system of equation (1), (2). Thus, the average distance derived using the procedure described above was assigned to the each interval of magnitudes. Random errors of all parameters under determination are 0.05 - 0.10 mas yr^{-1}, while those of $(M_{11}^{+} - M_{22}^{+})$ and $(M_{33}^{+} - M_{22}^{+})$ are twice as much in the each interval of magnitudes. The procedures for obtaining the data needed to solve the system of equations (1), (2) for XPM2, UCAC4 and PPMXL catalogues are the same.

The distances found and utilized in the work show that the considered stars are located on average outside the boundaries of the local spiral arm (Orion arm), or the Local stellar system. This serves as a reason to consider the rotation about the galactic axis Y found

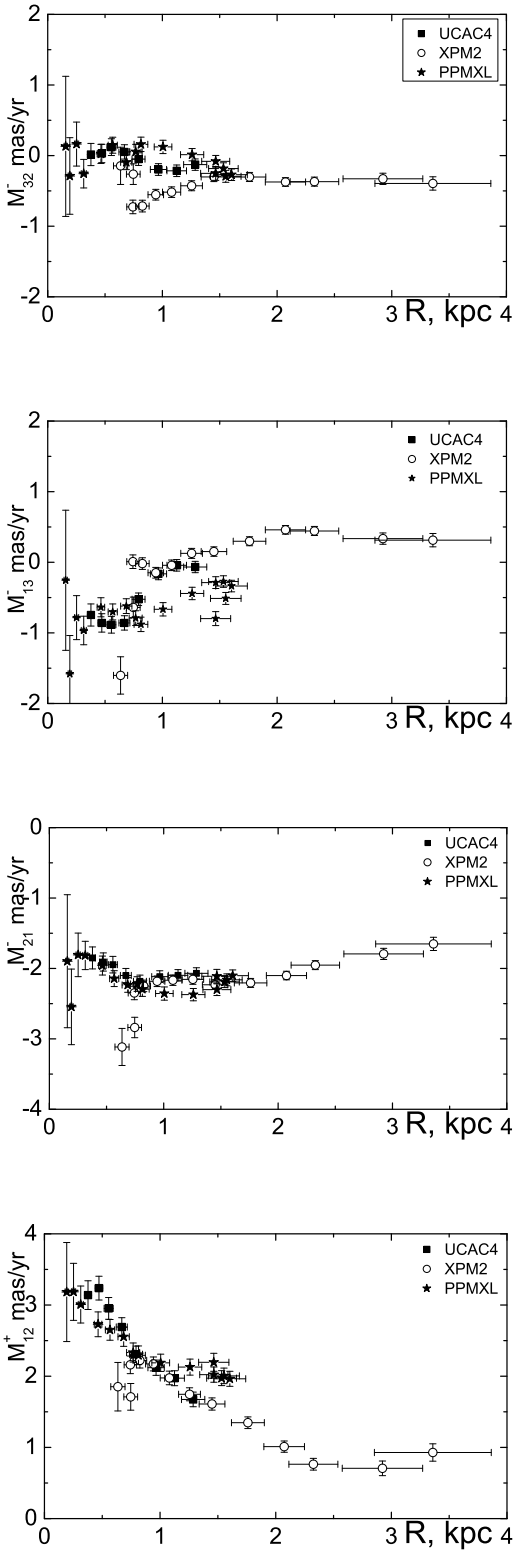

Figure 2: Kinematic parameters inferred from the proper motions of XPM2, UCAC4 and PPMXL stars vs. distances.

with the use of relatively faint stars, as a residual rotation of the ICRS/Tycho-2 (Hög, 2000) system relative to the extragalactic system of coordinates.

As can be seen from the figures, the dependences of kinematic parameters derived from the data of XPM2 catalogue are provided from the distance of about 600-700 pc. It is well seen that the components of rotation tensor for the stars of UCAC4 and PPMXL catalogues are almost coincided with each other within the interval of distances from 0 to 1 kpc and slightly different from those for XPM2 catalogue.

We also show a component of the deformation tensor in the XY plane for all the three catalogues. As can be seen from Fig. 2, the dependences of parameters M_{12}^{+} are very similar in the range from 0 to 1.5 kpc. The dependence is extended by the data from only the XPM2 catalogue at distances greater than 1.5 kpc and these data do not contradict the previous ones. We present in the Fig. 3 the dependence of the angular velocity of the Galaxy rotation obtained from the formula $\omega = (M_{21}^{-} - M_{12}^{+})$ on the heliocentric distance.

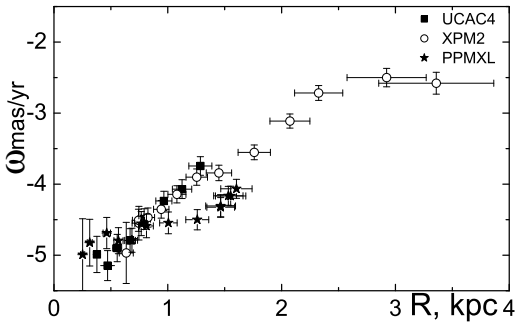

Figure 3: The dependence of the angular velocity of the Galaxy rotation on the heliocentric distance: $\omega = (M_{21}^{-} - M_{12}^{+})$

As can be seen from this figure, there are no differences in the behavior of the dependence of ω on the heliocentric distance to the stars from XPM2 and UCAC4 catalogues up to 1.25 kpc. As for larger distances (only XPM2 catalogue) the behavior of this dependence does not change. The angular rotation velocity derived from the data of the PPMXL catalogue differs from values derived from the data of XPM2 and UCAC4 catalogues by more than 0.5 mas yr^{-1} at the distance interval from 1 to 1.6 kpc. It was surprising for us that although the PPMXL catalogue contains virtually the same amount of stars as the XPM2 one, the distances derived from statistical parallaxes of PPMXL stars do not exceed 1.6 kpc.

6. Conclusions

As a result of the work performed, it was established that for relatively close stars ($d < 1000$ pc) one component of the Ogorodikov-Milne model which describes the rotation about the galactic axis Y and two components which describe deformations in the YZ and XY planes, depend on the heliocentric distance. We associate it with the kinematic specialities of the Local group of stars. As for farther stars, in average, the existence of the deformations in YZ and XY planes is seen.

Besides, for the distant stars of the Tycho2/UCAC4 and Tycho2/PPMXL catalogue systems, located in the distance > 1000 pc from the Sun, the mean value of the rotation about the galactic axes Y is about $+0.30$ mas yr^{-1} that we interpret as the residual rotation of the ICRS/Tycho-2 system relative to the inertial coordinate system.

The angular rotation velocity of the Galaxy can be represented by the linear dependence on the heliocentric distance and change from -5 mas yr^{-1} to -3 mas yr^{-1} in the distance range from 0.5 kpc to 2 kpc.

References

Olling R. et al.: 2003, *ApJ*, **599**, 275.
Schönrich R. et al.: 2010, *MNRAS*, **403**, 1829.
Clube S.: 1972, *MNRAS*, **159**, 289.
Clube S.: 1973, *MNRAS*, **161**, 445.
du Mont D.: 1977, *A&A*, 61, 127.
du Mont D.: 1978, *A&A*, 66, 441.
Ogorodnikov K.F.: 1965, *Dynamics of stellar systems.* Fizmatgiz [in russian].
Zacharias N. et al.: 2013, *ApJ*, **145**, 44.
Dennen W. et al.: 1998,*MNRAS*, **298**, 387.
Roeser S. et al.:2010, *ApJ*, **139**, 2440.
Hög E. et al.: 2000, *A&A*, **355**, L27.

"ASYMPTOTIC PARABOLA" FITS FOR SMOOTHING GENERALLY ASYMMETRIC LIGHT CURVES

K.D.Andrych [1], I.L.Andronov [2], L.L.Chinarova [1], V.I.Marsakova [1]

[1] Department of Astronomy and Astronomical Observatory, Odessa National University, Marazlievskaya 1V, 65014, Odessa, Ukraine, katyaandrych@gmail.com, *lidia_chinarova@mail.ru*, *v.marsakova@onu.edu.ua*

[2] Department "High and Applied Mathematics, Odessa National Maritime University, Mechnikova Str., 34, 65029, Odessa, Ukraine, *tt_ari@ukr.net*

ABSTRACT. A computer program is introduced, which allows to determine statistically optimal approximation using the "Asymptotic Parabola" fit, or, in other words, the spline consisting of polynomials of order 1,2,1, or two lines ("asymptotes") connected with a parabola. The function itself and its derivative is continuous. There are 5 parameters: two points, where a line switches to a parabola and vice versa, the slopes of the line and the curvature of the parabola. Extreme cases are either the parabola without lines (i.e.the parabola of width of the whole interval), or lines without a parabola (zero width of the parabola), or "line+parabola" without a second line. Such an approximation is especially effective for pulsating variables, for which the slopes of the ascending and descending branches are generally different, so the maxima and minima have asymmetric shapes. The method was initially introduced by Marsakova and Andronov (1996OAP.....9...127M) and realized as a computer program written in QBasic under DOS. It was used for dozens of variable stars, particularly, for the catalogs of the individual characteristics of pulsations of the Mira (1998OAP....11...79M) and semi-regular (200OAP....13..116C) pulsating variables. For the eclipsing variables with nearly symmetric shapes of the minima, we use a "symmetric" version of the "Asymptotic parabola". Here we introduce a Windows-based program, which does not have DOS limitation for the memory (number of observations) and screen resolution. The program has an user-friendly interface and is illustrated by an application to the test signal and to the pulsating variable AC Her.

Keywords: Stars: variable – stars: binary – stars: cataclysmic – stars: pulsating

1. Introduction

Variable stars are important sources of information on structure and evolution of stars, They are observed by many professional and amateur astronomers, which have generally different photometrical systems. In this case, it is not easy to reduce all the data to some effective system, thus such observations are used for high-amplitude variables, e.g. Mira – type stars, cataclysmic binaries or semi – regular variables. A huge part of observations of such objects was obtained by amateurs and stored in national (but really international) databases like AAVSO (http://aavso.org), AFOEF (http://cdsarc.u-strasbg.fr/afoev/), VSOLJ (http://vsolj.cetus-net.org/). Photographical surveys ("Sky Patrol") produced "one or few per night" observations, which are not suitable for short – period (or aperiodic stars with a short time – scale of variability). The most abundant collections of photo negatives are stored in the AAVSO (Harvard Observatory), Sonneberg observatory, and Astronomical Observatory of the Odessa National University. Nowadays, there are numerous "photometric surveys" based on the CCD observations from ground-based and space telescopes. They are very important in studying variable stars (including the newly discovered ones) "in the past".

However, for eclipsing and pulsating variables, there is another very popular mode of observations: time series, which are obtained during a time interval, which is shorter than a photometric period – close to the minimum of eclipsing binaries, or to the maximum of pulsating variables. Then from the light curve is determined a single parameter – the moment of the extremum and its accuracy (needed, but often ignored). These individual extrema are published in the journals "Variable Stars. Supplement" ("Peremennye Zvezy. Prilozhenie"), "Information Bulletion on Variable Stars", "Open European Journal on Variable Stars" et al. and are used for studies of the period changes using the method of the "O-C" diagrams (see Tsessevich, 1971 for more details).

The methods for determination of the extrema were based on the Pogson's method of chords, Hertzsprung's method of fitting the data to some "standard curve", method of "tracing paper" (see e.g. Tsessevich (1971) for a review). Kwee and van der Woerden (1956) proposed a very popular method, which was implemented in some computer programs. However, it generally produces unreal small error estimates and thus is to be replaced by fitting the data with some approximating function (e.g. Andronov, 1994, 2005; Andronov & Marsakova, 2006; Mikulašek, 2007).

These methods are based on the assumptions of "symmetry" (suitable for eclipses of binary stars) and "asymmetry" (suitable for maxima of pulsating and cataclysmic variables). For latter, Marsakova and Andronov (1996) proposed the method of "asymptotic parabolae"), which was successfully used for determination of characteristics of thousands of maxima and minima of individual cycles of variability of

single and binary stars of different types (Marsakova & Andronov, 1998).

As in the electronic tables (Microsoft Excel, Open/Libre Office, GNUmeric), the smoothing functions are algebraic polynomials. The polynomials were applied for the determination of more than 6500 extrema (and the error estimates) of semi-regular variables by Chinarova and Andronov (2000).

The method was also realized later in the programs VSCalc (Breus, 2007) and PERANSO (http://peranso.com).

2. Basic Equations

In this work, we present application of algebraic polynomials and asymptotic parabolae for determination of extrema. Following Andronov (1994, 2005), we make a mathematical model (smoothing function) for the signal:

$$x_C(t) = \sum_{\alpha=1}^{m} C_\alpha f_\alpha(t) \qquad (1)$$

Here C_α are called "the coefficients" and $f_\alpha(t)$ – "the basic functions". The coefficients C_α are usually determined by minimizing the test function

$$\Phi_m = \sum_{jk=1}^{n} h_{jk}(x_j - x_{Cj})(x_k - x_{Ck}), \qquad (2)$$

which uses the observed x_j and computed $x_{Cj} = x_C(t_j)$ values. Obviously, results are dependent on the matrix h_{jk}, which is similar to the "metric tensor" in the differential geometry. In the electronic tables, the matrix h_{jk} is oversimplified to the unitary matrix (Kronecker symbol) δ_{jk} (equal to 1, if $j = k$, and else 0). More general case is $h_{jk} = w_k \delta_{jk}$, $w_k = \sigma_0^2 / \sigma_k^2$, σ_0 – the "unit weight error" and σ_k – the accuracy of the observation x_k.

For the derivative of degree s, the Eq. (1) may be extended to

$$x_C^{(s)}(t) = \sum_{\alpha=1}^{m} C_\alpha f_\alpha^{(s)}(t) \qquad (3)$$

Obviously, the case $s = 0$ corresponds to the initial function, $s = -1$, to the integral etc. The error estimate of this value is

$$\sigma[x_C^{(s)}(t)] = \sum_{\alpha\beta=1}^{m} R_{\alpha\beta} f_\alpha^{(s)}(t) f_\beta^{(s)}(t), \qquad (4)$$

Where $R_{\alpha\beta}$ is the covariation matrix of the statistical errors of the coefficients. Usually it is replaced by a simplified expression

$$R_{\alpha\beta} = \sigma_{0m}^2 A_{\alpha\beta}^{-1}, \qquad (5)$$

$$A_{\alpha\beta} = \sum_{jk=1}^{m} h_{jk} f_\alpha(t_j) f_\beta(t_k) \qquad (6)$$

This approximation (5) is valid, only if the matrix $h_{jk} = \sigma_0^2 \mu_{jk}^{-1}$, where μ_{jk} is the covariation matrix of errors of the observations and σ_0^2 is an arbitrary positive constant. Andronov (1997) studied even more complicated case, when h_{jk} are dependent on the time shift (like in the wavelet analysis). The classical case $w_k = \sigma_0^2 / \sigma_k^2$ was described e.g. by Anderson (??), Andronov (1994, 2003), Mikulášek (2007, 2015).

Marsakova and Andronov (1996) proposed a method of asymptotic parabola. The idea is that the part of the light curve near an extremum is approximated by two straight lines, which are connected by a piece of the parabola in a way that the function and its first derivative are continuous.

Free parameters for this approximation are the transition points between the parabola and straight lines corresponding to the ascending and descending branches. Extreme cases are the ordinary parabola and a broken line. The remaining three parameters – the slope of the lines and the vertical offset defined by the method of least squares.

The extremum of the smoothing function is determined in an usual way, by solving equation for the first derivative: $x'_C(t) = 0$ analytically or numerically by determining a maximum or minimum at a discrete grid of arguments, and then using iterations

$$t_e := t_e - \frac{x'_C(t)}{x''_C(t)} \qquad (7)$$

with a corresponding statistical error estimate:

$$\sigma[t_e] = \frac{\sigma[x'_C(t_e)]}{|x''_C(t_e)|} \qquad (8)$$

(cf. Andronov 1994, Mikulášek 2007). Obviously, this estimate is valid for a parabolic shape of the extremum and is not valid for flat extrema (e.g. total eclipses in binary stars). To determine of the statistically optimal number of parameters, we have computed approximations for few values of m=2…$m_{\max}$, where $m_{\max}$= 10 or smaller, and used m, which corresponds to the minimum of $\sigma[t_e]$. The computations stopped, when the degree of degeneracy

$$\gamma = \det(\mathbf{A}) / \prod_{\alpha=1}^{m} A_{\alpha\alpha}$$

of the matrix of normal equation becomes smaller than the limiting value $\gamma_{\min} = 10^{-9}$.

3. Applications

For an illustration, we have used a part of the light curve of the RV – type pulsating star AC Her. We have used the international AAVSO database (http://aavso.org). After filtering of the photometrical data for outliers and other filters, the total number of the observations N=23540. The detailed analysis is in preparation. We have chosen a smaller part well covered by the observations.

In Fig. 1, the approximation using the "asymptotic parabola" is shown for few dozens cycles.

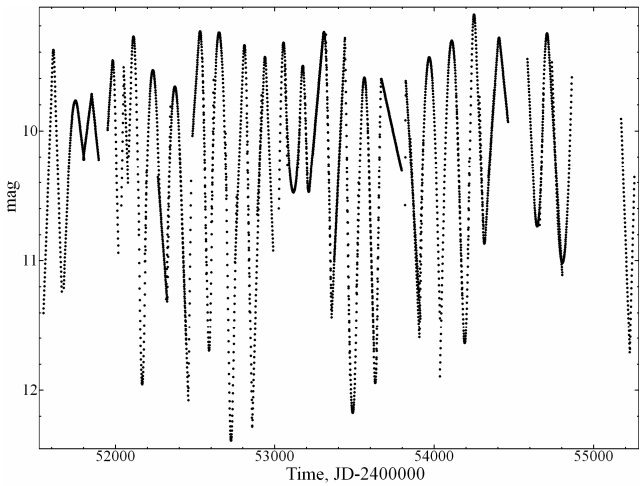

Figure 1: The "asymptotic parabola" approximation to the light curve of AC Her. The curve is compiled from the individual approximations of observations in the intervals surrounding maxima and minima.

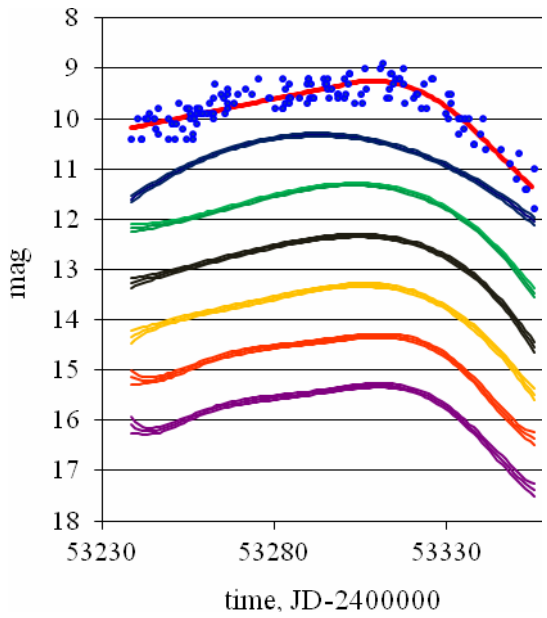

Figure 2: Original data (circles), approximations and "$\pm 1\sigma$ error corridor" (lines) for the asymptotic parabola (upper curve) and algebraic polynomials with number of parameters m=3..8.

An excellent approximation is seen at those parts where approximations near minimum and maximum overlap. Totally we determined characteristics of 749 extrema.

Fig. 2 shows approximations using the "asymptotic parabola" and low-order algebraic polynomials of one of the extrema.

One may note that a maximum of the parabola is significantly shifted as compared to other approximations. However, the parabola corresponds to the best accuracy estimate of the time of extremum.

The dependences of the error estimates of the smoothing function are shown in Fig. 3. For this data set, the most accurate approximation corresponds to m=3 (parabola), the statistical errors increase with m.

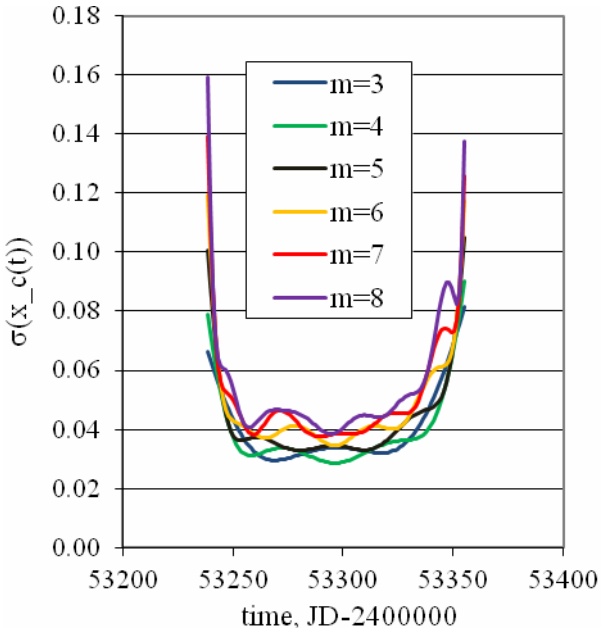

Figure 3: Scheme of internal and external contacts in eclipse.

4. Conclusions

The program was developed in the computer language VBA for Excel. It allows to determine the characteristics of extrema (maxima or minima) using the polynomial approximation with choosing a statistically optimal degree.

Results are applied to the pulsating variable S Aql.

The program will be used for further determination of extrema of variable stars of different types using our observations as well as observations from the virtual observatories and photometric databases like AAVSO, AFOEV, VSOLJ etc.

References

Andronov I.L.: 1994, *Odessa Astron. Publ.*, **7**, 49 (1994OAP.....7...49A).
Andronov I.L.: 2003,*ASPC*,**292**,391 (2003ASPC..292..391A)
Andronov I.L.: 2005, *ASPC*, **335**, 37 (2005ASPC..335...37A)
Andronov I.L., Marsakova V.I.: 2006, *Ap*, **49**, 370 (2006Ap.....49..370ª).
Breus V.V. //Odessa Astron. Publ., 2007, v.20. P. 32 (2007OAP....20...32B).
Chinarova L.L., Andronov I.L.: 2000, *OAP.*, **13**, 116 (200OAP....13..116C).
Kwee K.K., van Woerden H.: 1956, BAN, 12, 327, (1956BAN....12..327K).
Marsakova V.I., Andronov I.L.: 1996, Odessa Astron. Publ., **9**, 127 (1996OAP.....9...127M).
Marsakova V.I., Andronov I.L.: 1998, Odessa Astron. Publ., **11**, 79 (1998OAP....11...79M).
Mikulášek Z.: 2007, *OAP* **20**, 138,(2007OAP....20..138M)
Mikulášek Z.: 2015, *A&A*, **584A**, 8, (2015A&A...584A...8M).
Tsessevich V.P.: 1980, *Variable Stars and their Observations* (in Russ.), Moscow, Nauka, 176pp.

A MODIFICATION OF GAUSS' METHOD FOR PRELIMINARY DETERMINATION OF A CELESTIAL BODY'S ORBIT

A.A.Bazyey

Dpt of Astronomy, Odessa National University
Shevchenko Park, Odessa 65014, Ukraine

ABSTRACT. A modification of classical Gauss' method for determination of Keplerian elements from the observed positions is considered in this paper. The modification involves the exhaustive enumeration of all possible orbital plane positions in order to improve the method's reliability. It has been shown that such an approach requires a priori information on the pattern of the celestial body's motion, particularly, whether its motion is direct or retrograde.

Key words: orbit determination methods, celestial mechanics

Introduction

The method for determination of orbital elements of celestial bodies was developed by C.F.Gauss as early as at the beginning of the 19th century when the first asteroids were discovered. Up to the present time, this method has been successfully employed for preliminary orbit determination for both circumsolar and near-Earth orbital motion.

However, the method presents some limitations in its usage (Samotokhin et al., 2014). In particular, the orbital arc whose length is used for calculations should not be too long as in this case difficulties with solution of some equations may emerge. On the other hand, the orbital arc should not be too short as in this case uncertainties associated with observational errors may occur.

Numeral experiment

These and other limitations of Gauss' method can be overcome by exploiting capabilities of modern computers. Keplerian elements define the size and shape of the conic (the semi-major axis and eccentricity); a celestial body's position at a given instant of time (the time of perigee passage); the conic section orientation within the orbital plane (the argument of perigee); and, finally, the orbital plane position with regard to the reference coordinate system (the inclination and longitude of the ascending node).

At a two-body approximation the orbital plane always intersects the centre of gravity. With this fact the orbital plane position can be independently determined using the method of exhaustive enumeration of all possible values of inclination and longitude of the ascending node (Bondarenko et al., 2014a). All orbital elements can be derived for each pair of elements i and Ω using Gauss' method for determination of orbital elements from two position vectors and instants of time (Escobal, 1970). Based on these orbital elements, it is possible to define a celestial body's position for the current *i* and Ω. Using the differences between the observed and calculated in such a manner positions (O-C), it is possible to select the inclination and longitude of the ascending node which define the actual position of the orbital plane. It is evident that it is the minimum difference (O-C) that corresponds to the actual position of the orbital plane.

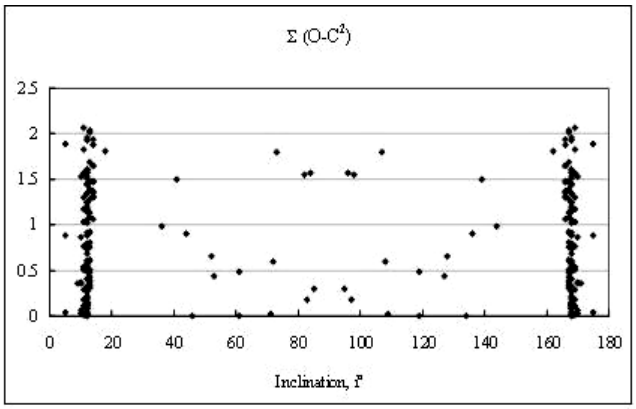

Figure 1. The distribution of the sum of squared differences between the observed and calculated positions of the test celestial body for different orbital inclinations.

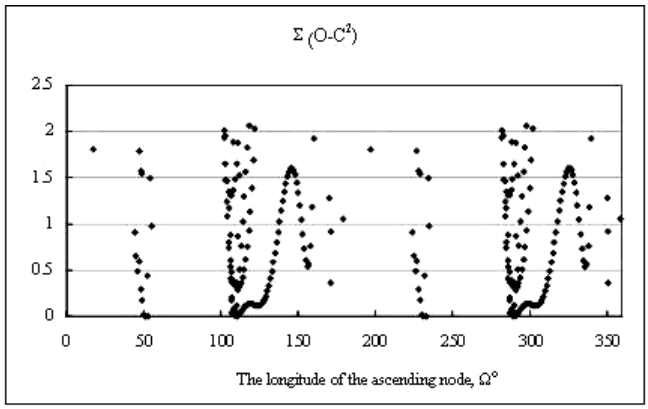

Figure 2. The distribution of the sum of squared differences between the observed and calculated positions of the test celestial body for different longitudes of the ascending node.

To study the behaviour of the dependence of the sum of squared differences (O-C) on the adopted values of inclination and longitude of the ascending node, we set up a numerical experiment. In this experiment we simulated the search of the position of a test celestial body's orbital plane. Keplerian elements for the heliocentric orbit were selected as follows:

the semi-major axis a=2.48255 AU;
the eccentricity e=0.15326;
the time of perigee passage 19.06.2011;
the argument of perigee ω=79.325°;
the longitude of the ascending node Ω=108.395°;
the inclination i=10.252°.

Using the methods described in (Bondarenko et al., 2014b), we determined the sums of squared differences $(O-C)$ for all possible pairs of orbital elements, namely the inclination $0 \le i \le 180^o$ and longitude of the ascending node $0 \le \Omega < 360^o$. From this data set we selected only those values which meet the following requirement:

$$\Sigma\sqrt{(O-C)^2} \le 1.4'.$$

The obtained dependencies are shown in Figs. 1 and 2.

The dependence of $\Sigma(O-C)^2$ on the inclination is reflection symmetric with regard to the value i=90°, and it exhibits the largest number of the selected values $\Sigma(O-C)^2$ near i=10.5° and i=169.5°.

The dependence of $\Sigma(O-C)^2$ on the longitude of the ascending node is the same for the ranges $0 \le \Omega < 180^o$ and $180^o \le \Omega < 360^o$, and it exhibits the largest number of the selected values $\Sigma(O-C)^2$ near Ω=108.5° and Ω=288.5°.

Conclusion

Thus, to ultimately determine the orbital plane using a modified Gauss" method suggested in (Bondarenko et al., 2014a), a priori information on the pattern of the celestial body's motion is required, particularly, whether its motion is direct or retrograde. This requirement is similar to that one for the application of Gauss' method for determination of orbital elements from two position vectors and instants of time (Escobal, 1970).

References

Bondarenko Yu.S., Vavilov D.E., Medvedev Yu.D.: 2014, *Solar System Research*, **48**, No 3, 212-216.

Bondarenko Yu.S., Vavilov D.E., Medvedev Yu.D.: 2014, *Astronomical News Letter*, **48**, No 3, 1-5.

Escobal P. *Methods of Orbit Determination*. Moscow: Mir, 1970.

Samotokhin A.S., Khutorovskiy Z.N.: 2014, *The Working Papers of M.V.Keldysh Institute of the Applied Mathematics*, No **44**, 31.

RESULTS OF DOUBLE STARS OBSERVATIONS AT NIKOLAEV OBSERVATORY

D.V.Bodryagin, N.V.Maigurova
Research Institution "Mykolaiv Astronomical Observatory",
Observatorna St.1, 54030, Mykolaiv, Ukraine

ABSTRACT. The results of double stars observations at Nikolayev Observatory during 2013-2014 are presented. The Washington Double Stars Catalogue (WDS) was used for observation program composing. The observation volume was obtained with usage two telescopes equipped CCD-cameras. Precise modern epoch CCD-observations allowed to make new proper motion values. The position angles and separations for 214 double stars were measured. Results are going to be submitted to WDS.

Keywords: Stars: double stars, binary stars, proper motions

1. Introduction

The main reason to be interested in double stars is a possibility to obtain total mass of a double-star system from studying their relative motions. Mass estimates are of huge importance to theorists on stellar evolution. According to modern double stars researches, the percentage of stars included into double or multiple systems is in range from 30 to 70%. The main source of information about these objects is the Washington Double Star Catalog (WDS) [1]. WDS contains more than 132,000 objects on July, 2015 each of which gives measures for the positional angle and separation of two components. Visual double stars are two that appear close together in the sky visually, but are not necessarily anywhere near one another in space. If visual doubles are gravitationally attached they are called visual binaries. Similar proper motions for both components is one of criteria for distinguish them. If the difference of their proper motions is small comparing to their common proper motion, the pair is probably physical. The proper motions for 1.5% of main component and for 20% second component are absent in WDS catalog. The most of the doubles are available for observations with small telescopes. That's why we have performed double stars observations in Nikolaev.

2. Observations: Instrumentation, Program

The observations were made at two telescopes which were created in the RI NAO: mobile multi-channel automatic telescope (Mobitel) with D=500 mm, F=3000 mm and Axial meridian circle (AMC) with D=180 mm, F=2500 mm.

Both telescopes are equipped with the CCD cameras and getting images in drift scan mode. We have obtained frames with scale 1.32″ and 0.83″per pixel and field of view 24′×28′ and 42.6′×42.6′ for AMC and Mobitel, respectively. These parameters allow us to have enough reference stars for astrometric reductions and obtaining positions of the stars with high accuracy.

For observational program we selected WDS objects which are most apropriate to be observed by our telescope and in the expected time frame (the full time of exposure is 102^s and 85^s at equator). For the main selection criteria we used a magnitude limit of 17^m and 14.5^m and a separation bigger than two FWHM.

The regular observations of double stars were carried out during 2013-2014. The statistical information about volume of observations is given in table 1. There are not only program objects in column 4; we also selected other WDS doubles from the other observations, which appeared in the imaged field.

Table1. Statistics of observations

Period	Telescope	Σ stars	Mean N*
2013	AMC	2420	4
2014	AMC	1848	3.5
2013	Mobitel	124859	8
2014	Mobitel	87767	9

*The average number of star observations

3. Processing and Results

Processing of obtained observations included two steps: getting astrometrical parameters (coordinates, proper motions, magnitudes) and measures of double stars parameters (position angle and separation).

Astrometric reductions for equatorial coordinates of objects were performed with Astrometrica software [2]. Connection model between the tangential and the measured coordinates was polynomial 2nd order for AMC and polynomial 4th order for Mobitel. The catalogs UCAC2 [3] and UCAC4 [4] were used as reference catalogs. After processing whole volume of observations the coordinates in right ascension and declination at mean observational epoch were averaged. The mean standard errors of catalog position were about 30 mas in both coordinates and that allows us to obtain new proper motions with accuracy about 4-5 mas/year when the catalog USNO A2.0 was used as source of second epoch positions. Then we cross-matched our positional data with WDS catalog and other astronomical catalogs for calculations new proper motions of the primary and secondary double components and for selection all WDS doubles which were appeared in the imaged field. The results of search WDS double stars and following cross-matching are summarized in table 2. Cross-matching was made with usage

service CDS-Upload X-Match realized by TOPCAT software [5].

Table 2. Results of cross-matching

	WDS	USNO A2.0	PPMXL	2mass	UCAC4	TYCHO2
AMC	127	118	123	127	127	74
Mobitel	234	216	222	234	230	55

The comparison of obtained proper motions has shown a good agreement with other sources. The mean external accuracy of the obtained proper motions is about 8 mas/year in both coordinates based on the comparison with other catalogs (Tycho2, PPMXL, UCAC4, WDS).

The comparison results of obtained proper motions with WDS proper motions are shown in figure 1.

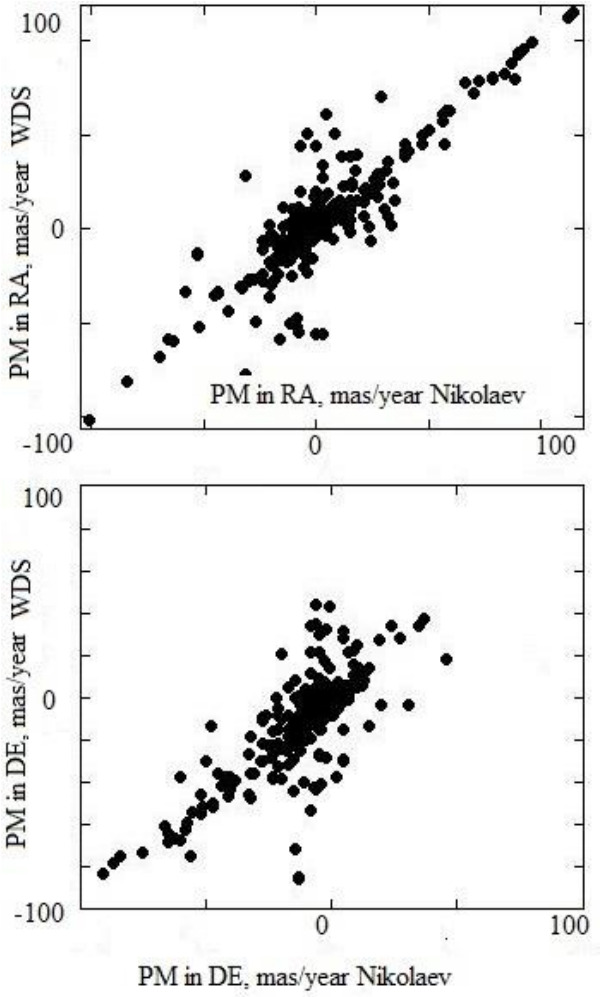

Figure 1: Obtained proper motion vs WDS proper motions (top – right ascension, bottom – declination).

The figure 1 have shown that criteria of common proper motions for distinguishing visual binary stars work better for stars with high proper motions, when values of their error much less than values of proper motions.

Measures of double stars were made with usage REDUC software [6]. We used previously determined exact values of orientation angle and image inclination regarding the celestial equator from astrometric reductions for calibration. Unfortunately, the AMC limiting magnitude fallen down significantly by the technical reasons and we can't see the secondary component in most frame there. We have measured only observations obtained at Mobitel.

There were obtained 1802 positions for 199 WDS stars. The mean number of measurements of a star is about 8. The distributions of observations in stellar magnitudes and magnitude differences between main and secondary component measured by REDUC are given in figure 2.

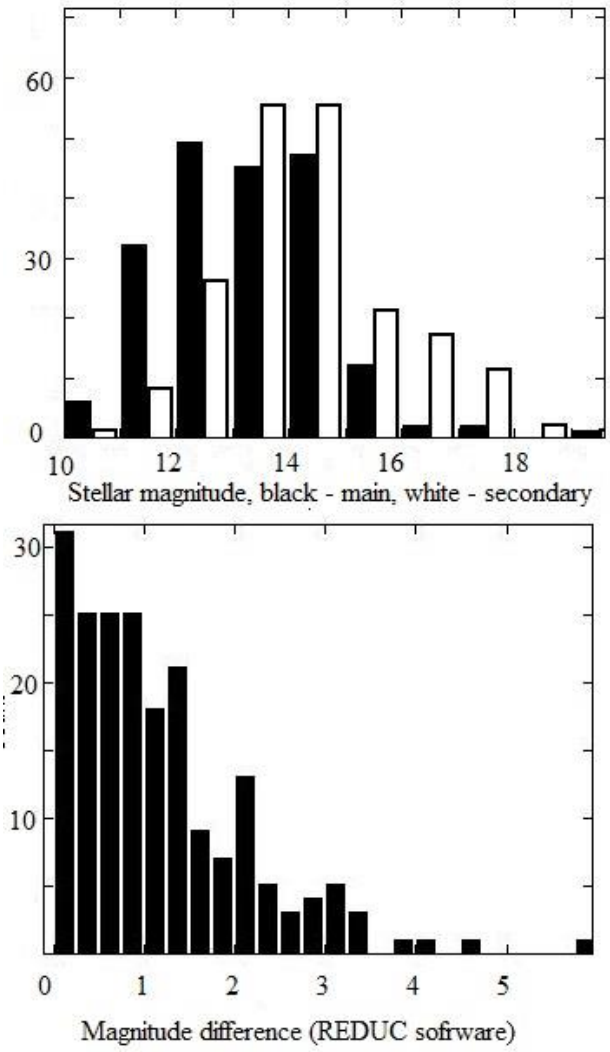

Figure 2: Distribution of double stars in stellar magnitude (top – stellar magnitude of main (black column) and secondary (white column), bottom – magnitude difference between the components, obtained REDUC software)

The position angle (PA) of the secondary with respect to the primary and angular distance between the two stars (separation) between components were measured. The mean standard error of PA is 0.5°, separation – 0.15″. The distribution of standard errors in PA and separation are shown in figure 3.

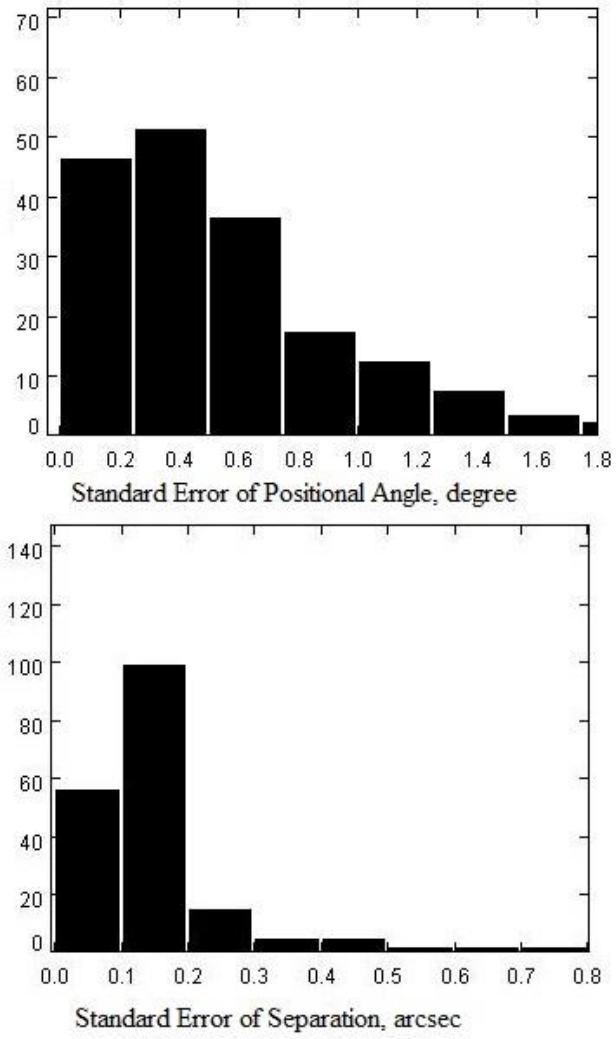

Figure 3: Distribution of standard errors of measurements

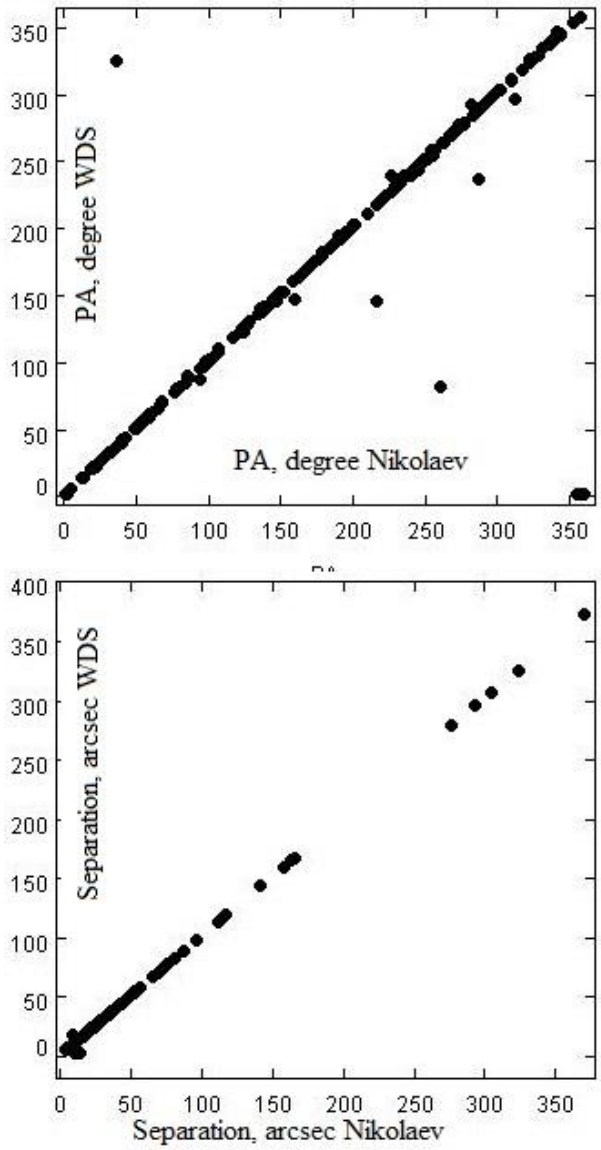

Figure 4: Measured values of separation and PA over separation and PA from WDS catalog (only double stars with separations between components more than about double FWHM were measured)

We have compared our results with WDS data. It can be seen from figure 4 that they are in good accordance with each other.

4. Conclusions

The equatorial coordinates and proper motions of 361 WDS stars were obtained basing on CCD observations during 2013-2014 yr. Average accuracy of the catalog star position is about 30 mas in both coordinates. The new proper motions for WDS star were calculated with usage USNO A2.0 as the first epoch. Parameters for 199 WDS doubles (PA and separations) were obtained. The standard deviation is 0.5° for PA and 0.15″ for separation.

The results of measurements are going to be sent to WDS database.

References

1. Mason B.D. et al: 2001, Astron. J., 122, 3466
2. http://www.astrometrica.at/
3. Zacharias N. et al: 2004, Astron. J., 127, 3043
4. Zacharias N. et al: 2013, Astron. J., 145, 44Z
5. http://www.star.bris.ac.uk/~mbt/topcat/
6. http://www.astrosurf.com/hfosaf/uk /tdownload.htm

INVESTIGATION OF DIFFUSE INTERSTELLAR BANDS OF ORGANIC MOLECULES IN THE SPECTRA OF CEPHEID STARS

Kashuba S.V.[1], Andrievsky S.M.[1], Chehonadskih F.A.[1],
Korotin, S.A.[1], Kovtyukh V.V.[1], Luck R.E.[2]

[1] Astronomical Observatory, Odessa National University,
Shevchenko Park, 65014, Odessa, Ukraine

[2] Department of Astronomy, Case Western Reserve University, 10900 Euclid Avenue, Cleveland, OH 44106-7215, USA

ABSTRACT. We describe an effective method of investigation of the Diffuse Interstellar Bands (DIBs) in the spectra of Cepheid stars. DIBs are believed to originate from the absorption of such carriers as polycyclic aromatic hydrocarbons in the interstellar gaseous clouds located between an observer and the stars whose spectra were recorded. We performed a detailed consideration of the DIB at 6613 A in our sample of spectra for more than 250 stars. The quantitative characteristics of the DIB absorption features will be studied in connection with the interstellar absorption data, and after that, they will be used in the mapping of the Galactic disc.

Keywords: ISM: bands – variables: cepheids

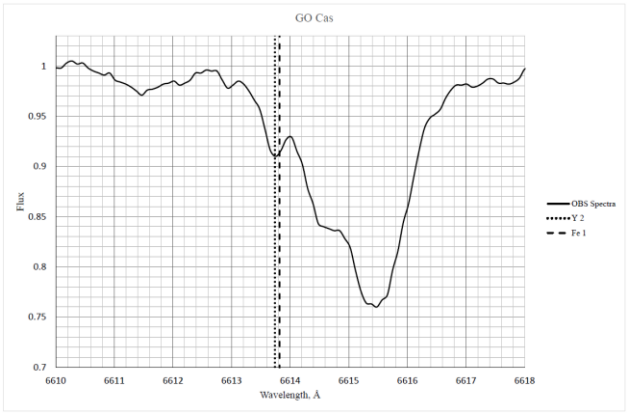

Figure 1: The DIB at 6613 Å in spectrum of GO Cas

1. Introduction

The Diffuse Interstellar Bands (DIBs) are observed in spectra of astronomical objects in ultraviolet, visible and infrared wavelengths. The central wavelengths of DIBs don't correspond to any known spectral lines of a chemical elements. This phenomena is one of the most difficult conundrums for astrophysics. However, presence the unknown bands in the spectra of stars confirms existence the inhomogeneous distribution of the interstellar medium. Therefore, we investigated in detail the one of the DIBs of organic molecules in the spectra of Cepheid stars for determining of some characteristics ISM.

2. Data

We used the spectra of Cepheid stars with resolution of 30000, which had been obtained by R. E. Luck with the Hobby–Eberly Telescope Spectrograph (McDonald Observatory, Texas, United States). Using spectra of the variable stars for investigation DIBs is unique. In our research, we analyzed 253 spectra.

3. The method

The object of the research was DIB at 6613 Å. As a rule it blend with two stellar spectral lines: Y II at 6613.73 Å and Fe I at 6613.82Å. But sometimes our band don't blend with any stellar spectral lines.

We had to neutralize the influence of these two lines on our DIB. For this purpose, we developed an effective method, which consists of the following stages:

1. Verifying oscillator strength for Y II at 6613.73 Å and Fe I at 6613.82Å. We used spectra of Sun with high resolution (Kurucz et al. 2004) and VALD (Vienna Atomic Line Database).
2. Creating synthetic spectra of Cepheid stars. For that, we used the basic atmospheric parameters stars, which are presented in the paper Luck & Lambert (1). The models of stellar atmospheres were generated with program ATLAS9 (Kurucz, 2004). The synthetic spectra were calculated with the SynthV program (Tsymbal, 1996). We also used the chemical structure database from the paper Luck et al. (2).
3. The observed spectra processing. All procedures of spectra processing were conducted in DECH20t (Galazutdinov).
4. The observed spectrum was divided by the synthetic and we received a «clean» profile of the DIB.

Our aims were to analyze the «clean» profiles of the DIB at 6613 Å and to make map of the distribution density of interstellar matter in the Galactic disc.

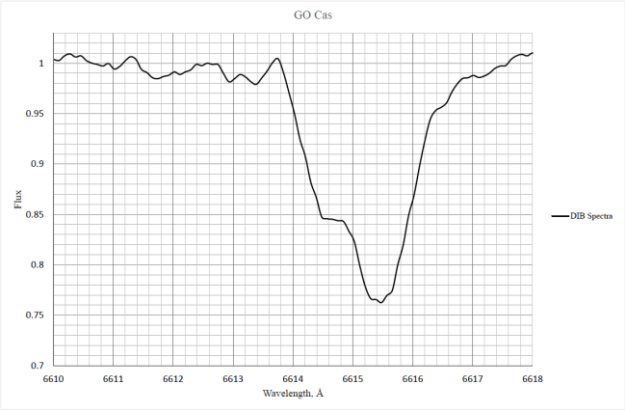

Figure 2: The «clean» profiles of the DIB at 6613 Å in spectrum of GO Cas

In our paper, we investigated the DIB of organic molecules at 6613 Å in the 253 spectra of Cepheid stars.

We «cleared» the chosen DIB's profiles of the stellar spectral lines Y II at 6613.73 Å and Fe I at 6613.82Å.

We defined the equivalent width of DIB at 6613 Å in 253 spectra.

Finally, we made map of the distribution density of interstellar matter in the Galactic disc. Our results were presented in tables and graphs.

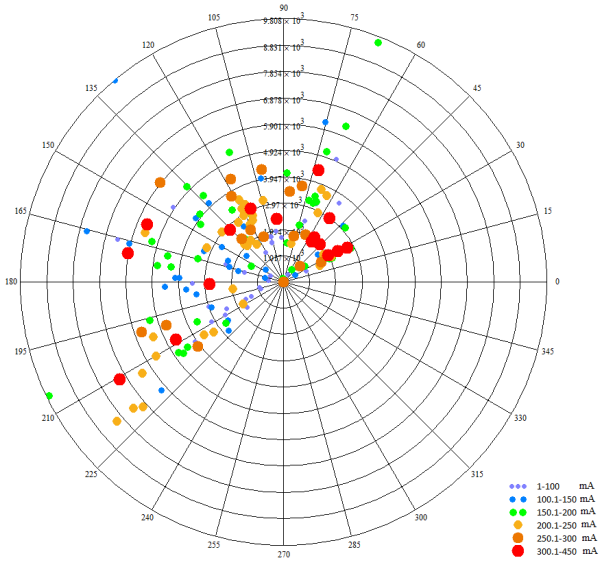

Figure 1: The Map of the Distribution Density of Interstellar Matter in the Galactic Disc

References

Luck, R.E., & Lambert, D. L. 1981, *ApJ*, 245, 1018.
Luck R.E. et al.: 2007, *ApJ*, **133**, 2464.

NUCLEAR MAGICS AT MAGNETOROTATIONAL SUPERNOVA EXPLOSION

V.N.Kondratyev [1,2], Yu.V.Korovina [3], T.V.Mishenina [4]

[1] Physics Department, Taras Shevchenko National University of Kyiv, 03022-UA Kyiv, Ukraine, *vkondrat@univ.kiev.ua*
[2] BLTP, JINR, 141980-RU Dubna, Russia
[3] Moscow Institute of Open Education, 125167-RU Moscow, Russia
[4] Astronomical Observatory, Odessa National University, 65014-UA Odessa, Ukraine

ABSTRACT. Nucleosynthesis at magnetorotational supernova explosion is considered by employing arguments of nuclear statistical equilibrium. Effects of ultra-strong nuclear magnetization are demonstrated to enhance the portion of titanium product. The relation to an excess of ^{44}Ti revealed from the Integral mission data and galactic chemical evolution is discussed.

Keywords: Stars: supernovae, magnetic field. – Nucleosynthesis: abundances, galactic chemical evolution.

1. Introduction

Supernovae (SNe) represent promising sites for synthesis of heavy atomic nuclei (Woosley, Heger & Weaver, 2002) and give major stellar nucleosynthetic contributions to nuclide inventories during the Galaxy chemical evolution. Magnetization of hot dense plasma due to magnetorotational instability (MRI) is considered as an inherent feature and makes plausible explosion mechanism. In present study we argue that such a feature affects nucleosynthesis (cf., e.g., (Kondratyev, 2004; 2014 and refs. therein) and, in particular, magnetic effects lead to an increase of titanium portion in the synthesis of nuclides close to the iron "peak". Consequently, the characteristic lines of respective nuclei in spectra of astrophysical objects are considerably enhanced and allow for an analysis of synthesized elements. The radioactive decay chain ^{44}Ti→ ^{44}Sc→ ^{44}Ca gives rise to an emission of lines with energies of 67.9 keV and 78.4 keV (from ^{44}Sc *) and 1157 keV (from ^{44}Ca *) of approximately equal intensity. The respective image-mosaics from Integral data (Kondratyev, 2004; 2014) for the Cassiopeia region in various energy ranges of registered photons are presented in Fig. 1. The color (brightness) is proportional to the gamma-quanta flux: as larger the flux as lighter (brighter) the color of a pixel. As is seen the SNR CAS A gives the brightest spot for energies matching ^{44}Sc lines.

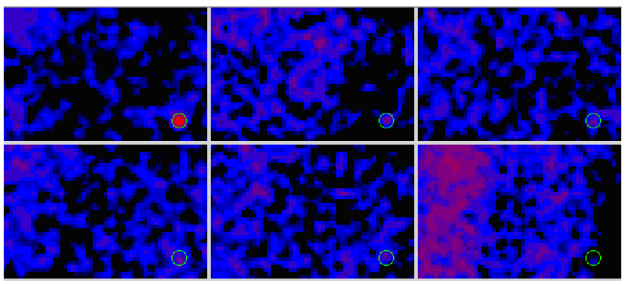

Figure 1: Direction (pixel number) dependence of the registered gamma-ray flux at different energy ranges. top: left – 20–50 keV, middle – 50–67 keV, right – 67–70 keV, bottom: left – 70–77 keV; middle – 77–82 keV, right – 82-100 keV; for the Cassiopeia region. SNR CAS A, (J2000) R.A. 350.86°, decl. 58.81°, indicated by circle.

Table 1: Volume $M_{\rm Ti}$ of nuclides ^{44}Ti (in solar masses $M_{\rm Sun}$) initially synthesized in young SNe, Tycho, CAS A and SN1987A (see Kondratyev & Korovina, 2015).

SN	$M_{\rm Ti}[10^{-4}\,M_{\rm Sun}]$
CAS A	$3.3^{+0.9}_{-0.7}$
SN1987A	3.1 ± 0.8
Tycho	< 0.84

Then ^{44}Ti half-life, about 60 years, allows to determine this isotope initial mass in SN remnants. Table. 1 shows the observational results for the total mass of ^{44}Ti nuclide synthesized in SN explosions from (Kondratyev & Korovina, 2015). These values are significantly larger as compared to model predictions, see. (Woosley, Heger & Weaver, 2002), giving the mass of initially synthesized ^{44}Ti, $M_{\rm Ti} \sim 10^{-5}\,M_{\rm Sun}$ (in solar masses $M_{\rm Sun}$) in an absence of magnetic effects.

2. MRI explosive nucleosynthesis

Abundances of iron group and nearby nuclides are described very successfully within nuclear statistical equilibrium (NSE) approach for over half a century (Woosley, Heger & Weaver, 2002). At such conditions nuclide abundance is determined mainly by the binding

energy of corresponding atomic nuclei. The magnetic effects in the NSE were considered by Kondratyev (2014) and refs. therein. Recall that at temperatures ($T \le 10^{9.5}$ K) and field strengths ($H \ge 0.1$ TT), the magnetic field dependence of relative output value $y = Y(H)/Y(0)$ is determined by a change in the binding energy of nuclei in a field and can be written in the following form

$$y = \exp\{\Delta B / kT\} . \qquad (1)$$

We consider examples of ^{56}Ni and ^{44}Ti. Such a choice of symmetric nuclei, double magic and anti-magic for vanishing magnetization, gives a clear picture of magnetic effects in the formation of chemical elements and fundamental conclusions about transmutation and synthesis of nuclei in ultramagnetized plasma.

The binding energy B can be written as $B = B_{\rm LDM} + C_{\rm n} + C_{\rm p}$, where shell corrections $C_{\rm i}$ for protons and neutrons, and the component $B_{\rm LDM}$ is calculated in semiclassical liquid drop model and varies only slightly in the magnetic field, according to the Bohr-van Leuven theorem, see (Kondratyev, 2014).

Spin magnetization of Pauli type dominates for the neutron magnetic reactivity. Interaction of a field and the spin-magnetic moment corresponding to a spin projection $m_{\rm n}$ on a field vector gives rise to a linear shift of energy levels $\Delta = m_{\rm n} g_{\rm n} \omega_{\rm L}$, where $\omega_{\rm L} = \mu_{\rm N} H$ with nucleon magneton $\mu_{\rm N}$, and $g_{\rm n}$ – neutron g –factor. Accordingly, the shell energy in a field H is modified as follows

$$C_{\rm n}(H) = C_{\rm n}^{+}(E_{\rm F} + \Delta) + C_{\rm n}^{-}(E_{\rm F} - \Delta) , \qquad (2)$$

where the indices + and – indicate a sign of the projection of spin magnetic moment on field direction. The proton magnetic response is represented by a superposition of the field interaction with spin and orbital magnetic moments and exceeds the neutron component for an open shell.

As is demonstrated by Kondratyev & Korovina (2015) at field strengths $H < 10$ TT, the binding energy shows nearly linear H dependence for considered nuclei $B = B_0 + \kappa_i H$ [MeV] with magnetic susceptibility parameters κ_i depending on a nucleus $nucleus = {}^{A}_{N}Z$. For ^{44}Ti the value of this parameter is positive $\kappa_{\rm Ti} \sim 0.3$ MeV/TT, and in case of ^{56}Ni it becomes negative $\kappa_{\rm Ni} \sim -0.3$ MeV/TT. Evidently, for anti-magic at zero field strength nuclei the shell energy always increases with field H, and for magic one - decreases, indicating positive and negative values of magnetic susceptibility κ_i, respectively. Then for an average relative yield over MRI region V, see sect. 1, $\langle y \rangle = V^{-1} \int_V d^3 r y(H(\mathbf{r}))$ one gets (Kondratyev & Korovina, 2015)

$$\langle y \rangle = b^{-1}\left(\exp\{a\} + \int_1^b \exp\{a/x\}\, dx\right)$$

$$= \left(\exp\{a/b\} + \frac{a}{b}\left[\mathrm{Ei}(a) - \mathrm{Ei}(a/b)\right]\right) , \qquad (3)$$

where $a = \kappa_i H_0 / kT$, $b=(r_{\rm a}/r_0)^2$. The radius r_0 relative to the MRI center corresponds to a maximum in field strength H_0, and radius $r_{\rm a}$ is determined from conditions of comparable values for magnetic pressure gradients and gravitational force at R corresponding to material irruption, i.e., $dH^2(r)/dr = 4H_0^2/b^2 r_{\rm a} \sim 8\pi$ GM n(R)/R^2. Here the gravitational constant G, and the star mass M inside the bifurcation radius R is related to the matter density n(R) as $4\pi R^2$ n(R) = -dM/dR, and the integral exponential function $\mathrm{Ei}(x) = \int_{-\infty}^{x} \frac{\exp\{t\}}{t} dt$.

In Fig. 2 one sees significant difference for magnetic field dependence of nuclide output, magic and anti-magic at vanishing field. For anti-magic nuclei and, therefore, increasing binding energy with increasing field strength or positive magnetic susceptibility relative volume of nucleosynthesis increases significantly with increasing a. At the same time, the relative production of magic nuclides, i.e., negative value a, is not substantially changed with increasing field. This behavior significantly differs from the case of a spatially uniform magnetization, see Fig. 2, which corresponds to the exponential dependence of $\langle y \rangle$ or $b = 1$ in Eq. (3). In this case the coefficients of suppression and enhancement are the same with the same absolute value of a. The presence of the diffusion layer, corresponding to a fade-out field strength with increasing r (or $b > 1$) in a real MRI region leads to substantial differences of relevant factors. Significant increase in a synthesis of anti-magic nuclei is accompanied by a slight change in mass volume magic nuclides. Model predictions in the absence of magnetic effects, see. (Woosley, Heger & Weaver, 2002), give the mass of initially synthesized ^{44}Ti, $M_{\rm Ti} \sim 10^{-5} M_{\rm Sun}$ (in solar masses $M_{\rm Sun}$). For realistic characteristics of Type II SN explosion (sect. 1) enhancement factor $\langle y \rangle_{\rm Ti} \sim 30 - 300$ corresponds to a mass $M_{\rm Ti} \sim 10^{-3.5} - 10^{-2.5} M_{\rm Sun}$. It is worthy to notice that not all the material ejected from the central part of a star is formed in MRI areas, see (Kondratyev, 2014). Such an enhancement of ^{44}Ti is in an agreement with direct observations in yang SN II remnants, see Table I. At the same time for SN I the ^{44}Ti volume is significantly smaller. One might expect, therefore, noticeable correlations in enrichment of anti-magic nuclides with other metals, e.g., ^{56}Fe, ^{26}Al.

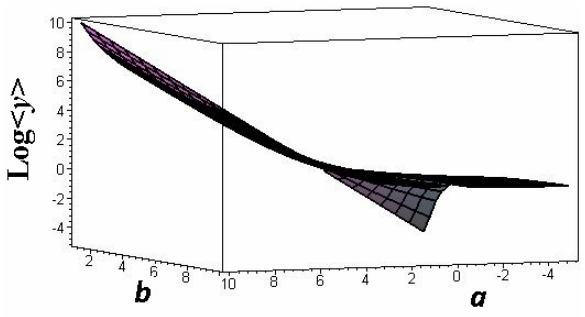

Figure 2: Relative field of nucleosynthesis products depending on parameters a and b.

3. Galactic chemical evolution

An important application of the nucleosynthesis computations is represented by a description of the enrichment of our Galaxy and the Universe as a whole with various chemical elements. Despite considerable progress in the chemical evolution modeling, as well as in the nucleosynthesis computations, a number of issues remain unresolved. In this paper, we dwell on potential sources of calcium and titanium production.

For this purpose we use the abundances of these elements, which we had obtained earlier for the Galactic disc dwarfs (Mishenina et al., 2008), and compared them with the chemical evolution computations (Timmes, Woosley & Weaver, 1995) (Figs. 3, 4). In the recent study (Timmes, Woosley & Weaver, 1995) the yields of isotopes ^{48}Ti and ^{44}Ca, produced by massive supernovae, from Woosley & Weaver (1995) were used to develop a Galactic chemical evolution model. As can be seen from Figs. 3 and 4, the employed data describe the trend of [Ca /Fe] vs. [Fe/H] quite well; however, the adopted yield of isotope ^{48}Ti is insufficient to describe the behavior of [Ti/Fe] vs. [Fe/H]. A similar pattern for calcium and titanium is presented in the study by Timmes, Woosley & Weaver (1995; see their Figs. 25 and 27). It proves that the investigated sources of calcium production, such as massive stars, are dominant suppliers of calcium in the interstellar medium while further improved computations for the titanium sources are required. In respect with titanium the authors point out that "both the ^{48}Ti yield and the ration [Ti/Fe] are sensitive to the parameters of the explosion and the amount of material that falls back onto the neutron star". The nucleosynthesis computations (Woosley & Weaver, 1995) were carried out not accounting for the magnetic field.

We suggest another possible mechanism of additional titanium enrichment when taking into account the increased yield of anti-magic nuclides in ultramagnetized astrophysical plasma. As is seen on an example of the radioactive isotope ^{44}Ti the direct observational data, see sect. 1, confirm such an enrichment which can be understood in terms of magnetic effects. The resulting enrichments of M44 isobars are collaborated with observational data

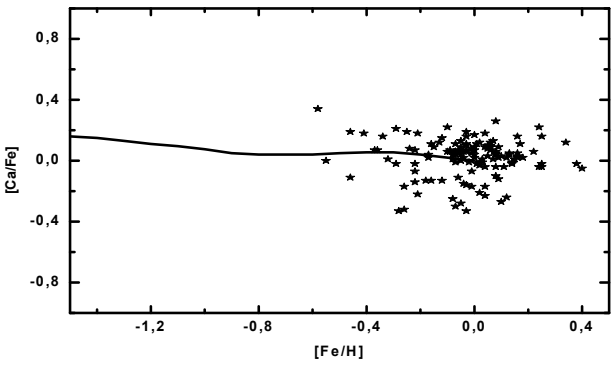

Figure 3: Comparison of observed abundance of Ca (Mishenina et al., 2008, marked as asterisks) with the trend of galactic chemical evolution (Timmes, Woosley & Weaver, 1995, marked as solid line).

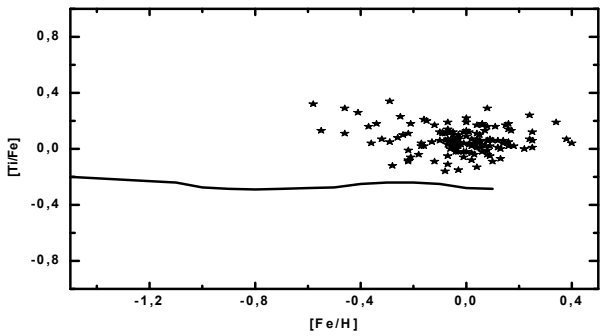

Figure 4: The same as Figure 3, but for Ti abundance.

(Kondratyev, 2014; Magkotsios, 2010). The proton magnetic reactivity dominates in a change of binding energy, see Eq. (2). Therefore, one can expect to meet a noticeable increase in production of other titanium isotopes, as well. At the same time a yield calcium isotopes can be expected unchanged because of the proton shell closure, see Eq. (3).

4. Conclusion

Effects of ultra-magnetized astrophysical plasma in supernovae on synthesis of chemical elements were investigated at conditions of nuclear statistical equilibrium. Magic-antimagic switches in the nuclear shell structure in varying magnetic field lead to an increase of titanium binding energy and, consequently, to a noticeable increase of the portion of ^{44}Ti in explosive nucleosynthesis products. Magnetic effects in nuclide creation are favorably compared to observational Integral data and galactic chemical composition.

Acknowledgements. This work is supported in part by Integral scientific data center and by the Swiss National Science Foundation (SCOPES project No.~ IZ73Z0152485).

References

Kondratyev V.N. et al.: 2004, *Proc. 54th Intern.Symp. on Nuclear Spectroscopy and Structure of Atomic Nuclei* (Belgorod, Russia), p. 83.

Kondratyev V.N.:2014, *EPJ A*, **50**, 7.

Kondratyev V.N., Korovina Yu.V.: 2015, *JETP L,* **102**, 131.

Mishenina T.V., Soubiran C., Bienayme O. et al.: 2008, *Astron. Astrophys*., **489**, 923.

Magkotsios G. et al.: 2010, *ApJS*, **191**, 66.

Woosley S.E., Weaver T.A.: 1995, *Astrophys. J. Suppl. Ser*., **101**, 181.

Woosley S.E., Heger A., Weaver T.A.: 2002, *Rev. Mod. Phys.,* **74**, 1015.

Timmes F.X., Woosley S.E., Weaver T.A.: 1995, *Astrophys. J. Suppl. Ser*., **98**, 617.

THREE-DIMENSIONAL NUMERICAL HYDRODYNAMICAL SIMULATION OF LOW/HARD AND HIGH/SOFT STATES IN ACCRETION DISCS OF MICROQUASARS AND QUASARS ON BASE OF UNDEFINED PRECESSION

V.V. Nazarenko, S.V. Nazarenko

Astronomical Observatory of I.I.Mechnikov Odessa National University,
Odessa, Ukraine, *astro@paco.odessa.ua*

ABSTRACT. In this study, the models of slaved precession of accretion disc and donors radiation-driven wind were performed using three-dimensional numerical astrophysical methods by the example of microquasar Cyg X-1. As is shown, in the course of precession of the accretion disc blown by the donor's wind the states with high and low temperature (low and high mass accretion rate, respectively) start being generated in the centre of disc. Our computations of disc precession performed on base of undefined precession that means each point of rotation axis of accretion disc makes unclosed difficult curve instead of a circle as it is in case of definite precession. In this case, the transition between states of high and low temperature takes place irregularly and not depend on precession period. The duration of transition between these both states is less than intervals of states on several orders of magnitudes.

Key words: Stars: close binary system; microquasars; quasars.

1. Introduction

In present work we continue to simulate high/soft and low/hard (ON- OFF-: active and passive) states in accretion discs of microquasars and quasars. Our idea consists in that in precession accretion disc having been blown by the donor's wind begins to generate the states of low and high temperature in the disc centre. Since these states are unti correlated with mass accretion rate we interpreted them as ON- and OFF-states in accretion discs of microquasars. In the previous our work (Nazarenko, 2014) we had simulated ON- and OFF-states on the base of defined precession. The result of it was the transition between ON- and OFF-states was every precession period. But it occurs irregularly in real microquasars and not depends from precession period. By such the way to improve the results of previous work in the present one we simulate ON- and OFF-states on the base of undefined precession. It means that each point of rotation axis of accretion disc makes unclosed curve. Thus our goal in the present research is to make the change between both ON- and OFF-states to be irregular and don't depended from precession period.

2. The numerical approach

To obtain the goal stated above we use special numerical technique. This one is as follows: to simulate 3D mass flow in the calculation area from initial time to stationary state we use non-stationary Euler's hydrodynamical equations. We resolve these equations by astrophysical variant of 'Big-particles' code by Belotserkovsky and Davydov (Nazarenko, 2014). This astrophysical variant is distinct to the standard 'Big-particles' code (Belotserkovskii et al., 1982) that in this one the internal energy on first time substep is used (in standard code the total energy on first time substep is used). To decrease the effects of numerical viscosity attributing the cold in use we use the special technique to decrease radial velocity in accretion disc and do the temperature in calculation area to the real one. We use rectangular numerical grid and also the rectangular Cartesian coordinate system that is connected hardly with the donor. To simulate the precession of accretion disc we use the slaved precession. In the chosen coordinate system the accretor makes the unclosed curve.

To decrease large computer expenses and order to run our calculation over long time we use the accretion disc precession period equal to orbital one. In the present calculation we use the following dimensionless units: the velocities are given in units of the orbital speed; the temperatures are given in units 10^4K; the numerical time units are such that 2π is corresponding to the orbital period; mass accretion rate is given in units of solar mass per year in logarithmic scale. We cut the space around the accretor with the radius of

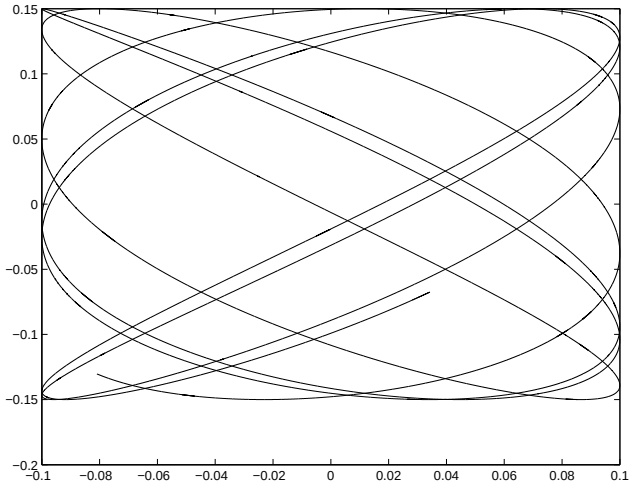

Figure 1: The time change of the accretor's coordinates in z-y plane.

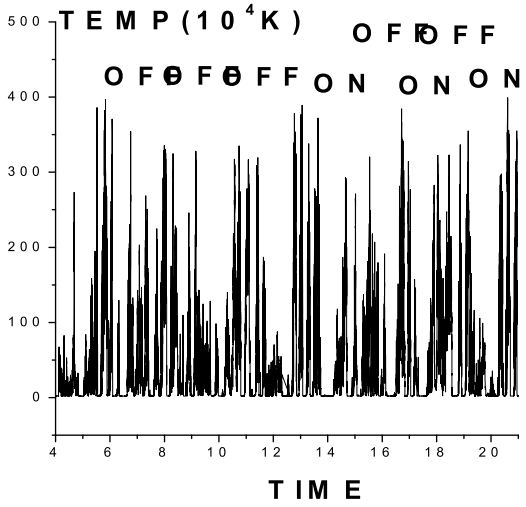

Figure 2: The dependance of the temperature in the disk's centre versus time.

0.025 (10% of the outer disc radius) to avoid singularity. This space has the size of 5000 Schwarzschild radii and it means that our simulations are running far away from accretor.

The time changes of the accretor's coordinates are given below.

$$x_{ac1} = 1.0, \qquad \text{if } t < 0$$
$$y_{ac1} = 0.0, \qquad \text{if } t < -0.25$$
$$z_{ac1} = 0.0, \qquad \text{if } t < 0$$

$$x_{ac1} = 1.0 + A\sin(2\pi\tfrac{t}{P_x}), \qquad \text{if } t > 0$$
$$y_{ac1} = 0.0 + B\cos(2\pi\tfrac{t}{P_y}) \cdot N_{prec}, \quad \text{if } t > -0.25$$
$$z_{ac1} = 0.0 + C\sin(2\pi\tfrac{t}{P_z}), \qquad \text{if } t > 0$$

where $A = B = C = 0.15$, $N_{prec} = -1$ for retrograde precession, $N_{prec} = 1$ for prograde precession and P_x, P_y, P_z are precession periods for appropriate accretor's coordinates. The time is given in units of precession period.

3. The numerical results

The unclosed curve made by the accretor over on the time of calculation is shown in Fig. 1. The evolution of the accretion disc central temperature in time is shown in Fig. 2. The dependance of mass accretion rate of our accretion disc model versus time is shown in Fig. 3. The mass accretion rate is negative since it is accretion process. As it is led from Fig. 2 we run our calculation over long time as large as 17th precession period. It shows that the essential physical values are strong conserved in our present simulation in code in use. First we see in Fig. 2 it is the high temperature interval is from 4 to 13.5 precession period. The interval of low temperature in Fig. 2 is on 13.75-14.50 precession period. This interval is over 0.75 precession period. We have interpreted these intervals of low and high temperature as generation low/hard and high/soft states in our accretion disc model. We have make such the interpretation since the both time intervals of temperature stated above are unti correlated with mass accretion rate in our accretion disc model (see Fig. 2 and Fig. 3). Accordingly mentioned above we may say that the change between both low/hard and high/soft states is not making every precession period in our present calculation and is strong irregular. As we think such the fine result occurs due to the using undefined precession in the present work. To show the time structure of low/hard and high/soft states in more details we have plotted partially low/hard state (Fig. 4) and high/soft one (Fig. 5). As it is good seen from these figures, the time characteristics of low/hard state in first turn are strong discrete i.e. it is in the view of partial peaks. The amplitudes of these peaks are in the interval from 2 to 400 (maximal values). By the other words, the central disc temperature is changing in time in 200 times. As it is led from Fig. 4 and Fig. 5, the relation between both low/hard and high/soft states time intervals is order of 10. This magnitude is in good accordance with the corresponding value in real Cyg X-1 in which the low/hard states are over several years and the high/soft states are over several months (Lachowicz et al., 2006). In order to see in more details the transition between both low/hard and high/soft states on time of 13.75 (see Fig. 2) we are plotted the vicinity of this time on high resolution scale (see Fig. 6). As it is led from these figures, the time interval of the transition stated above is order of 0.005 of precession period or 40 minutes of orbital time.

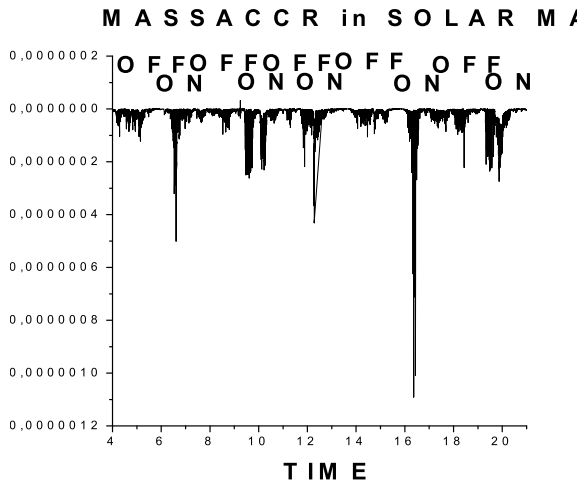

Figure 3: The dependance of the mass accretion rate in the disk's centre versus time.

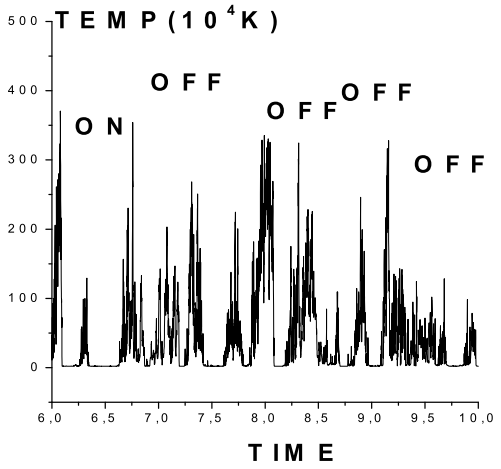

Figure 4: The dependance of the temperature in the disk's centre versus time over the interval of 6-10 precession periods.

The work of the mechanism to produce low/hard and high/soft states is very simple in the present paper. In the precession accretion disk having been blown by the donor's wind to states of low and high densities in the centre of disk is formed. When the densities in the disk centre are low, the radiation cooling is not efficient and instantly due to the action of the disk viscosity the kinetic energy of the disk rotation are transformed in thermal one. In this case the temperature in the disk centre is high. When the densities in the disk centre are high, the radiation cooling is strong effective and temperature in the disk centre is low.

4. Summary and discuss

Analyzing the numerical results described above we may say that the goal stated introduction is obtained and we have simulated low/hard and high/soft states and the change between both states is irregularly and is not depending from precession period. We may to mark also that the essential microquasar properties were have simulated in our present work. First of all, we show that the relation between both states is the factor of 10; the changes of central disc temperature and mass accretion rate in both states are order of 200 and 100 respectively; the transition between both states is order of 40 minutes of orbital time; the time structure of low/hard state has discrete character in the present simulation. All four properties of low/hard and high/soft states are qualitatively and quantitatively in a good accordance with observations (Lachowicz et al., 2006; Fender et al., 2003; 2004). The evolution of our calculation in the future works we see to run jet produc-

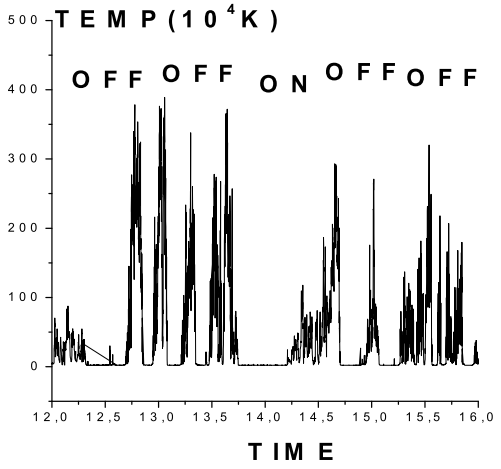

Figure 5: The dependance of the temperature in the disk's centre versus time over the interval of 12-16 precession periods.

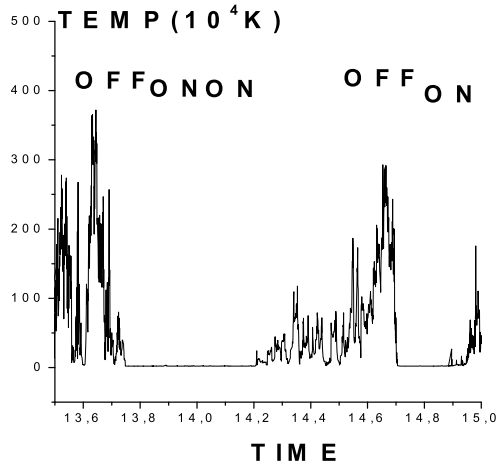

Figure 6: The dependance of the temperature in the disk's centre versus time on the high time scale over the interval of 13.6-15.0 precession periods.

tion and also its appearance and disappearance in simulated low/hard and high/soft states by us. We have planned to simulate radiation-driven jets since with our point of view such the jets may easy explained the microquasar phenomenon. Such the conclusion is based on three points on our opinion:

1) In low/hard state the temperature near the accretor in disc hot corona is increased by factor of 10 (from 10-20 KeV to 100 KeV, Fender et al., 2003; 2004). The last means that in these terms the radiation pressure will be rather able to produce jets.

2) The luminosities of microquasars are close to super critical one by factor of 0.3 - 0.7 (Fender et al., 2003; 2004).

3) The formation of radiation-driven jets in the view of narrow stream may be easy explained by radiation flux configuration on the bottom of the funnel of disc hot corona: this flux is distance from zero only in the direction in parallel to the disc rotation axis, since namely in this direction the disc central source radiation may freely leave a funnel.

In the last conclusion we implicitly imply that funnels are exist in all the microquasars.

References

Belotserkovskii O.M., Davydov Yu.M.: 1982, "The big particles code in gas dynamics", Moskaw, Scientist, 391.

Fender R.P., Gallo E., Jonker P.: 2003, *MNRAS,* **343**, 99.

Fender R.P., Belloni T., Gallo E.: 2004, *MNRAS,* **355**, 1105.

Lachowicz P., Zdziarski A.A., Schwarzenberg-Czerny A., et al.: 2006, *MNRAS,* **368**, 1025.

Nazarenko V.V., Nazarenko S.V.: 2014, *OAP,* **27**, 137.

THE RELATIVE WAVELENGTH INDEPENDENCE OF IR LAGS IN ACTIVE GALACTIC NUCLEI: IMPLICATIONS FOR THE DISTRIBUTION OF THE HOT DUST

V.L. Oknyansky[1], C.M. Gaskell[2], E.V. Shimanovskaya[1]

[1] Moscow M.V. Lomonosov State University, Sternberg Astronomical Institute, Moscow, 119991, Russian Federation, *oknyan@mail.ru*

[2] Department of Astronomy and Astrophysics, University of California, Santa Cruz, USA, *mgaskell@ucsc.edu*

ABSTRACT. We show that, contrary to simple predictions, most AGNs show at best only a small increase of lags in the J, H, K, and L bands with increasing wavelength. We suggest that a possible cause of this near simultaneity of the variability from the near-IR to the mid-IR is that the hot dust is in a hollow bi-conical outflow of which we only see the near side. Although most AGNs show near simultaneity of IR variability, there was at least one epoch when NGC 4151 showed the sharply increasing IR lag with the increase of the wavelength. This behaviour might also be present in GQ Comae. We discuss these results briefly. The relative wavelength independence of IR lags simplifies the use of IR lags for estimating cosmological parameters.

Keywords: galaxies: active – galaxies: nuclei – galaxies: Seyfert – infrared: galaxies – galaxies: individual: NGC 4151, NGC 6418, NGC 7469, NGC 5548, NGC 3783, Fairall 9, GQ Comae, WPVS48, PGC 50427, Ark 120, Mrk 509, MCG-6-30-15; optical and IR variability, time delay, data analysis, dust torus, cosmology.

1. Introduction

The variable near-IR radiation of active galactic nuclei (AGNs) is usually associated with the part of the optically-thick dusty torus closest to the central source (Hönig & Kishimoto 2011). The presence of such a torus is the key to explaining the observed differences in the spectra of type-1 and type-2 Seyfert nuclei by the torus blocking our direct view of the broad emission lines and the thermal continuum emitted by the accretion disc (AD). It is also believed that the dusty torus radiates in the infrared, as a result of heating by shorter wavelength radiation from the accretion disc and X-ray emitting corona. Closer to the centre the dust is completely (or largely) sublimated and delayed infrared variability gives us the estimate of radius of the "dust holes" around the central source (Oknyanskij & Horne 2001), i.e., the radius of the region where the dust is absent. The work we present here is a continuation of our series of papers in which we measure the radius of the "dust holes" in the NGC 4151 and other AGNs from the delay of the variability in the near infrared relative to the optical variability (see details and references at Oknyanskij et al. 1999, Oknyanskij & Horne 2001, Oknyansky et al. 2014a,b). Despite the significant growth in theoretical and observational studies of AGNs in the IR, our knowledge of the dust, its origin, kinematics, and detailed morphology remains very incomplete.

The number of IR lags determined at different wavelengths for AGNs is not large. At the time of publications by Oknyansky et al. (1999), Oknyanskij & Horne (2001), there were just a few estimates of IR lags at different wavelengths. The first results were somewhat controversial. Some objects (NGC 4151, GQ Comae) showed a sharp increase of lag with wavelength in the IR. These differences in the lags (the lags in the L band were 3 times longer than in the K band) were in a good agreement with simple model predictions that cooler dust is farther from the centre than hotter dust (Barvainis 1987). Therefore Oknyansky & Horne (2001) considered those results to be normal and used the observed increase to correct observed IR lags for red shift. However, at that time at least one object, Fairall 9, was known to have about the same lags for the H, K and L bands. Oknyanskij et al. (1999) interpreted this in the following way: if the minimum distance from the central source to the dust clouds corresponds to a brighter state of the nucleus well before the interval under study, then the differences in the lags for K and L will be insignificant, as was observed in the Fairall 9. If, alternatively, this minimum radius roughly corresponds to the maximum nuclear luminosity in the interval under consideration,

then a marked difference in the lags for K and L must be observed, as it was the case for NGC 4151. This interpretation gives us observational prediction for NGC 4151 - at another time when it goes into a low state we will see similar IR lags for different IR wavelengths. This was indeed found for NGC 4151 in subsequent papers by Oknyansky et al (2006, 2014a,b). In order to investigate the reliability of these results, we have been collecting all available time lag data in different IR bands for AGNs to see how often this phenomenon is observed.

2. Observed IR time lags

Table 1 gives published and new measurements of time lags between variations in different near- and mid-IR bands relative to variability of the optical or UV continuum for as many AGNs as possible. Some new results in Table 1 were obtained applying our MCCF (Modified Cross-Correlation Function) method (Oknyanskij 1993)) to published photometric data. Examples of MCCFs are given just for NGC 7469 in Fig. 1. In most cases our results are in a good agreement with results obtained before using other methods. In a few cases, our new results (for Ark 120, Mrk 509) disagree with the values obtained before by Glass (2004). These differences arise in part because of possible misprints in Glass (2004), some differences in the optical data sets used, reduction to a common photometric system, and the cross-correlation methods used. Glass took into consideration some unpublished optical data whereas we have used some additional published optical data, which were not used by Glass. Support for our values for the IR lags for Ark 120 and Mrk 509 comes from them being in good agreement with the luminosity–IR delay relation (Oknyanskij 1999; Okyanskij & Horne 2001). As can be seen from Table 1, for most of the objects, time lags at different IR bands are similar. Only for one object, GQ Comae, do we see difference at about a factor of three between lags in the L and K bands. A similar difference was seen for NGC 4151 but only during the long, very high state which was the only one during last 110 years (Oknyanskij et al. 2013). The probability of observing an object exactly in its highest state is not large. Perhaps this is the reason why we see similar IR lags at different wavelengths for most of objects. The similar IR lags at the near and mid-IR were recently predicted in the model of a compact IR region as a part of dust torus by Hönig & Kishimoto (2011). They considered the case in which the dust is located much farther then the sublimation distance. For the more realistic case of an IR region that is not too compact, the predicted values of the peak of the cross-correlation functions are too low in comparison to observed ones. Some new observations show that hot dust clouds radiating in the mid-IR are located more in the polar regions (Hönig et al. 2013) than in the torus. Those results were explained by optically-thin, dusty wind which is launched from the hottest and inner region of an optically-thick dusty disk. The beginning of this outflow with the hottest dust can be connected also with near-IR radiation. So we considered an alternative model where the variable near- and mid-IR radiation arises from the near side of a hollow, bi-conical outflow of dust clouds.

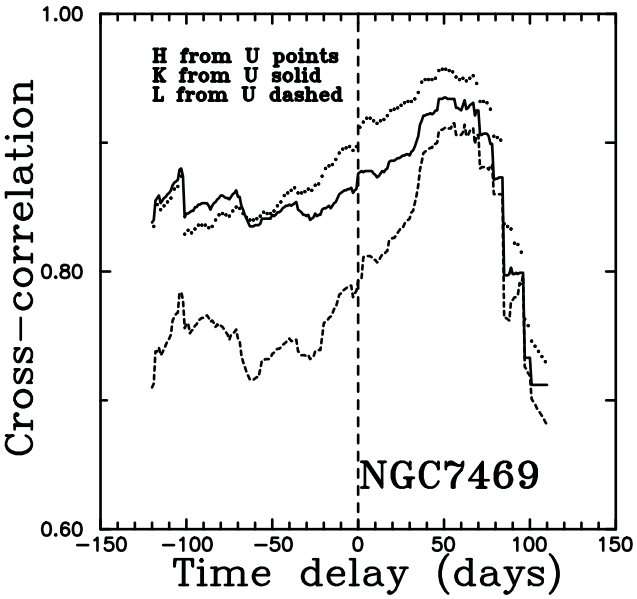

Figure 1: Cross-correlation functions calculated with the MCCF method for NGC 7469 using IR (Glass 1998) and optical (Lyuty 1995) observations during 2008-2013. See also Oknyansky (1999) and Oknyanskij & Horne (2001) where the IR lags for the object were found first time.

3. A hollow, bi-conical, outflow model

If, as it is often depicted, the dust is in a flattened distribution in a plane approximately perpendicular to the line of sight, the lag, τ, gives the distance, $c\tau$, of the emitting region from the central source. Therefore, if the IR lags are similar, as seems here usually to be the case, dust of different temperatures would be at approximately the same radii. An alternative possibility, that does not require dust of different temperatures to be at similar radii, is that the hot dust is the inner surface of a hollow conical outflow. As it is shown in Fig. 2, the part of the cone on the nearside of the AGN has its surface approximately tangential to the iso-delay surfaces for response to variations of the continuum when viewed from near face-on (as is usually the case for type-1 AGNs). The cone on the far side gives a much more spread out response and, since the

Table 1: Infrared lags in different bands, previously published and measured in this work.

Object	Time delay, days (1 from 2)	Bands 1(2)	Time Interval	References to results	References to data (for new results)
NGC4151	18 ± 6	K(U)	1969-1980	Oknyanskij (1993)	
	24 ± 6	L(U)		Oknyanskij & Horne(2001)	
	35 ± 8	K(U)	1985-1998	Oknyanskij et al. (1999)	
	8 ± 4	H(U)			
	97 ± 10	L(U)			
	104 ± 10	K(U)	1998-2003	Oknyanskij et al (2006)	
	94 ± 10	H(U)			
	105 ± 10	L(U)			
	41 ± 5	KH(U)	2003-2006	Oknyanskij et al. (2008)	
	105 ± 5	L(U)			
	94 ± 10	L(J)			
	37 ± 5	K(U)	2003-2007		
	40 ± 6	JHKL(B)	2008-2013	Oknyansky et al. (2014a,b)	
NGC 6418	37 ± 2	3.6μm(B)	2011-2013	Vazquez et al.(2015)	
	47 ± 3	4.5μm(B)			
	40 ± 5	3.6μm(B)		This work	Vazquez et al.(2015)
	50 ± 5	4.5μm(B)			
NGC 7469	52 ± 15	K(U)	1984-1996	Oknyanskij & Horne(2001)	Glass(1998), Luyty(1995)
	60 ± 10	L(U)			
	50 ± 10	H(U)		This work	
	88	K(V)	2001	Suganuma et al.(2006)	
	54	K(V)	2002		
	87	K(V)	2001-2002		
	70 ± 5	H(V)	2001	This work	Suganuma et al.(2006)
	88 ± 5	H(V)	2002		
	53 ± 5	K(V)			
	48 ± 5	H(V)			
NGC 5548	47	K(V)	2001-2003	Suganuma et al.(2006)	
	48	K(V)	2001		Suganuma et al.(2006)
	48 ± 4	K(V)	2001-2003	This work	
	37 ± 6	H(V)			
	55 ± 4	K(V)	2001		
	52 ± 4	H(V)			
NGC 3783	41 ± 8	J(B)	2006-2009	Lira et al. (2011)	
	66 ± 6	H(B)			
	76 ± 14	K(B)			
	74 ± 5	J(B)		This work	Lira et al. (2011)
	75 ± 8	H(B)			
	86 ± 8	K(B)			
F9	-20 ± 100	J(UV)	1982-1998	Clavel et al.(1989)	
	385 ± 100	K(UV)			
	250 ± 100	H(UV)			
	410 ± 110	L(UV)			
GQ Comae	250	K(UV)	1980-1989	Sitko et al. (1993)	
	700	L(UV)			
	260 ± 20	K(UV),K(V)		Oknyanskij (1999)	Sitko et al. (1993)
	70 ± 20	L(V)			
WPVS48	66 ± 4	J(B)	2013	Pozo Nuñez et al. (2014)	
	74 ± 5	K(B)			
	68 ± 4	K(B)		This work	Pozo Nuñez et al. (2014)
PGC 50427	48 ± 2	J(B)	2013	Pozo Nuñez et al. (2015)	
	47 ± 2	K(B)			
M 509	100	K(U)	1985-2001	Glass (2004)	
	60	L(U)			
	104 ± 20	J(B)		This work	Glass (2004)
	139 ± 20	HK(B)			Chuvaev et al.(1997)
	153 ± 20	L(B)			
MCG-6-30-15	11 ± 4	J(B)	2006-2011	Lira et al.(2015)	
	17 ± 4	H(B)			
	19 ± 4	K(B)			
Ark 120	315	U(L)	1986-2001	Glass (2004)	
	95 ± 30	JHKL(B)		This work	Glass (2004) Doroshenko & Lyuty(1999)

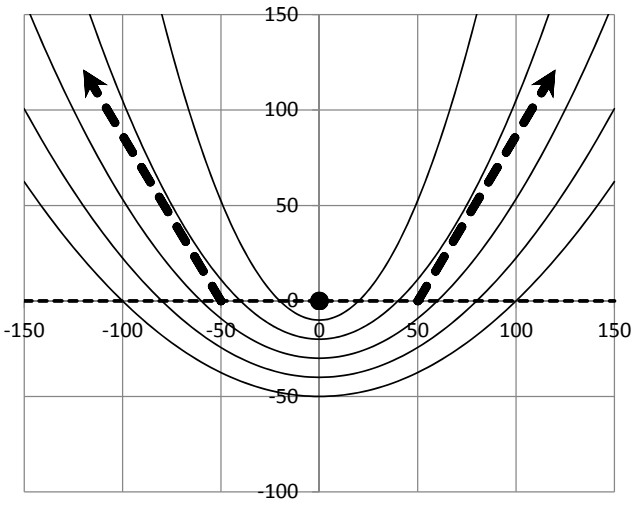

Figure 2: Cross section (in light days) of the inner wall of the near side of a hollow, bi-conical outflow (thick dashed arrows). Iso-delay paraboloids are shown at 20 day intervals. The horizontal dashed line shows the location of the optically-thick mid plane which obscures our view of the other side of the bi-cone (not shown).

material in the equatorial plane (what will be come the accretion disc) is optically thick, the response of the far side of the cone is probably not seen. We show the inner wall of the near side of the hollow bi-cone in Fig.3.

IR and optical light curves of an object are connected through a response function $\Psi(\tau)$ that depends on geometry and physical properties of the emitting medium:

$$F_{IR}(t) \sim const + \int_{-\infty}^{\infty} \Psi(\tau) F_{opt}(\tau - t) d\tau \qquad (1)$$

$\Psi(\tau)$ can be explained as a response of the medium to a central source's UV impulse in the form of the δ-function. We assume that the optical and UV variability occurs almost simultaneously. We can obtain $\Psi(\tau)$ from a model or we can try to estimate it from the real data using some methods for solving ill-posed inverse problems (see the next paragraph). Then we can investigate the structure and physical properties of the emitting medium through comparison of response functions, obtained from observational data, with ones, predicted by different models.

We have calculated $\Psi(\tau)$ directly for our model *via* Monte-Carlo simulations with 10000 dust cloudlets distributed randomly within the hollow bi-conical space given by parameters H, R_{min}, R_{max}, β, α, $\Delta\alpha$ (see Fig. 3). We also take into account the dependence of the UV flux on distance to the central source S and the anisotropy of the UV radiation. To get the $\Psi(\tau)$, we consider a short δ-function UV pulse at $t = 0$ and treat each cloud as a point-like object which

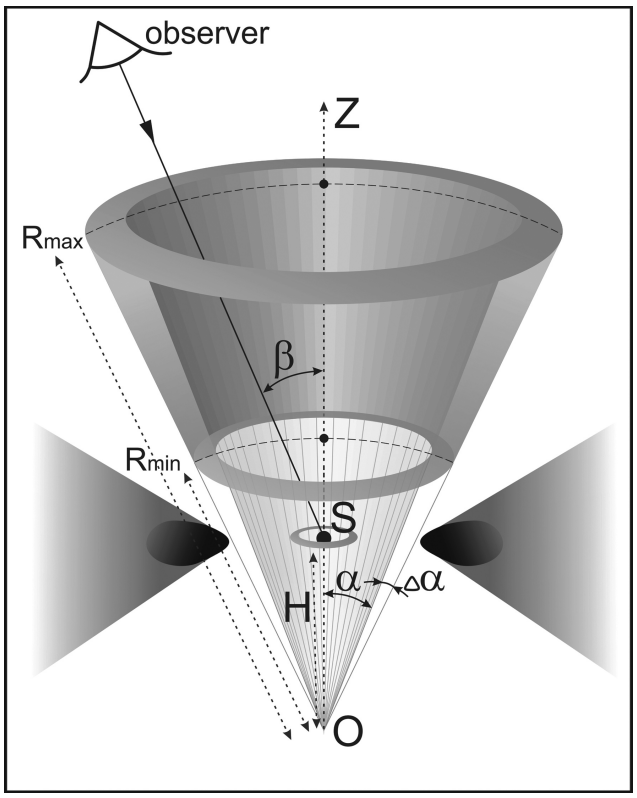

Figure 3: Geometry of the near side of the proposed hollow bi-conical dust distribution.

re-radiates in the IR only when it receives the UV pulse at a time lag τ. The lag is simply due to light travel effects. We obtain two response functions for two different regions: one close and one further away from S (see Fig. 4).

4. Reconstruction of response functions from real data

Unfortunately, we cannot obtain $\Psi(\tau)$ directly from (1), because the observational data are unevenly spaced and have long gaps. So we propose a new approach for recovery of the response function that combines the cross-correlation analysis of observational unevenly spaced time series and Tikhonov regularization.

As can be easily shown, the cross-correlation function $CCF_{F_{IR}F_{opt}}$ is a convolution of the auto-correlation function $ACF_{F_{opt}}$ with $\Psi(\tau)$:

$$CCF_{F_{IR}F_{opt}} \sim \int_{-\infty}^{\infty} \Psi(\tau) ACF_{F_{opt}}(\tau - t) d\tau \qquad (2)$$

There are several methods of cross-correlation analysis which allow obtaining cross-correlation function for unevenly spaced time series. We use the MCCF method (see details and references at Oknyansky et al. 1999, 2014a). The advantage of the MCCF method is that it imposes a limit on the interpolation which is

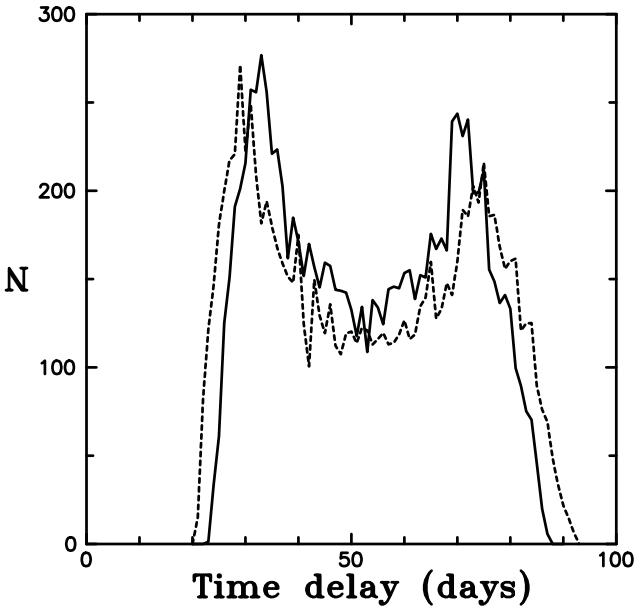

Figure 4: Monte Carlo simulations (using 10,000 clouds) of response functions for thin conical shells. H = 90 ld, $\beta = 20°$, $\alpha = 30°$, $\Delta\alpha = 5°$, $F_{UV} \sim 1/R^2$, axial anisotropy of the UV radiation is given by $F_{UV} \sim [cos(\gamma)(1 + 2cos(\gamma)/3)]^{1/2}$ (Netzer 2015). Solid line: R_{min} = 120 ld, R_{max} = 140 ld; dashed line: R_{min} = 140 ld, R_{max} = 160 ld. N is the number of clouds responding per day.

necessary for unevenly spaced data. For our purposes we used only the central part of the MCCF peak with the length 80 days (±40 days from the peak delay).

The eq. (2) is a Fredholm integral equation of the first kind with the convolution kernel. This is an ill-posed problem. Such problems can be solved using the Tikhonov regularization approach (Tikhonov et al. 1995) that allows one to find approximate solution, taking into account *a priori* information about the function sought, e.g., the smoothness of the solution or its closeness to some model (Koptelova et al. 2005).

Assuming that $\Psi(\tau)$ is a square integrable function, we compose the Tikhonov smoothing function:

$$M^{\alpha}[\Psi] = \|CCF_{F_{IR}F_{opt}} - ACF_{F_{opt}} * \Psi\|^2_{L_2} + \alpha\|\Psi\|^2_{L_2} \quad (3)$$

Provided that the regularization parameter α is chosen according to the discrepancy principle, the solution Ψ^{α} of the minimization problem for $M^{\alpha}[\Psi]$ can be considered as an approximate solution of (2).

Results of the reconstruction of the response function for the Seyfert galaxy NGC 7469 with the suggested approach based on observational K and V light curves in 2002 (Suganuma et al. 2006) are presented in Fig. 5. The reconstructed response function has two peaks. Two peaks are also observed in the theoretical response function in Fig. 4. Perhaps this is a characteristic feature of our proposed model. It will be of interest to investigate this in other objects.

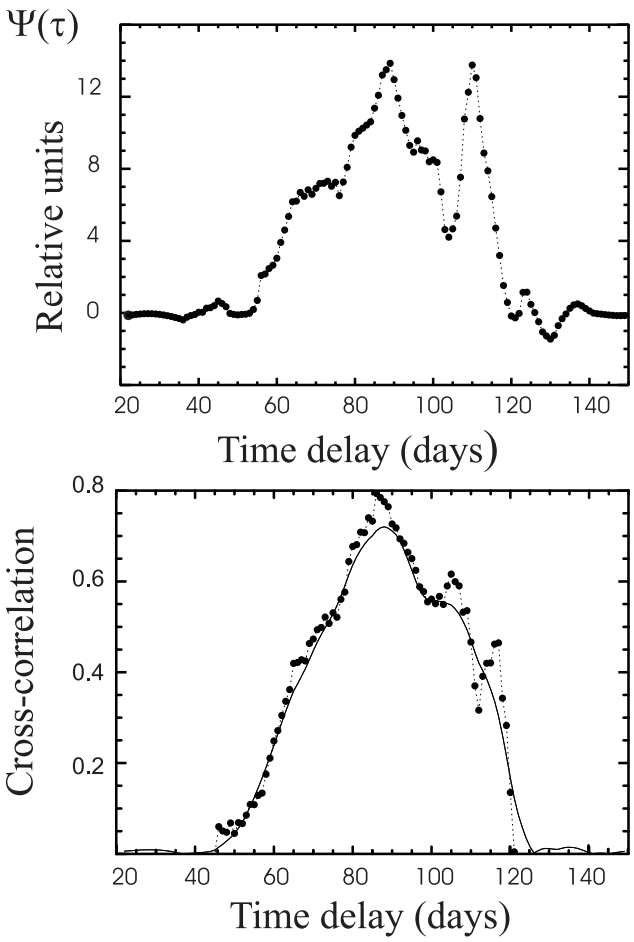

Figure 5: Upper: the reconstructed response function $\Psi(\tau)$ for the Seyfert galaxy NGC 7469. Lower: $CCF_{F_K F_V}(t)$, calculated from K and V band lightcurves (dotted line), and $ACF_{F_V} * \Psi$ for the reconstructed response function (solid line).

5. Cosmological applications

The ability to measure cosmological constants using the time delays of the near-infrared variability relative to the optical one was first mentioned by Kobayashi et al. (1998) and independently by Oknyanskij (1999, 2002). At the same time it was first shown (Oknyanskij 1999, 2002; Oknyanskij & Horne 2001) that for a number of AGNs the time delay of variability (in the K band) depends on the UV luminosity as $\tau \propto L_{UV}^{1/2}$ in accordance with the theoretical result of Barvainis (1987, 1992). In the recent publications Yoshii et al. (2014) and Hönig (2014) considered in detail the possibility of estimating cosmological parameters on the basis of measuring the dust sublimation radii in AGNs. Of particular interest is the ability to measure distances to objects with large redshifts, z.

For large z it is necessary to take into account the possible dependence of the delays on wavelength in the IR range and to make any appropriate correction. The equation for such a correction was derived by Oknyansky & Horne (2001) on the basis of the theory (Barvanis 1987) and observational data available at that time. However, as we have found now, the IR delays do *not* depend significantly on wavelength for most AGNs. The significant difference in IR lags with wavelengths can be just a temporary, rare situation in particular objects, as happened in the case of NGC 4151 just when it was in its very high state. Therefore for most of cases for a wide range of z the IR lags can be easy corrected to the rest frame just by allowing for the time dilation (i.e., dividing by $(1 + z)$).

6. Conclusions

We find that most AGNs show at best only a small increase of lags in the J, H, K, and L bands. Just one object, GQ Comae (which is a high-luminosity AGN), probably has big differences in the IR lags (lag for L is about 3 times bigger than for K). A similar difference in IR lags was observed temporarily in NGC 4151 when it was in a very high state. Probably this big difference in IR lags is at epochs when the dust is intensively sublimated. During more normal times when the dust region is located much farther out than the sublimation distance, the time lags are about the same.

Our model with hollow bi-conical outflow of the dust clouds does not contradict to the existence of the dust torus. Moreover, the torus and accretion disc in the model are needed to block the IR light from farther part of the conical outflow. Also the torus can be a reservoir for the dust in the outflow.

In the Table 1, a significant number of the objects (5 out of 11) with similar IR lags have been observed to change their Seyfert type. This could just be the result of these objects having been studied particularly well. At the same time our model can explain cases of changing Seyfert type. In the very low luminosity states of some objects, when they look like Seyfert 2s, dust creation can commence in the gas clouds in the hollow of the conical outflow. So the thickness of the conical shell with dust clouds will be bigger and some of the dust clouds can be on the line of sight and block the broad line region from view and the object will be classified as a type 2 (see the same idea for the torus model in Mason 2015).

Our model can explain not only the similar IR lags at different wavelengths but also the high correlation values for IR and optical variations. Furthermore, the model can better explain the observed luminosity in IR since the IR-emitting region (i.e., the dust cone) has a higher covering factor and hence is getting more UV radiation than in the case of the flat compact IR-emitting region.

Finally, we note that the relative wavelength independence of time lags in the IR simplifies the use of these time delays to estimate luminosities and hence estimate cosmological parameters.

Acknowledgements. We are thankful to Sebastian Hönig for useful comments, to Boris Artamonov for fruitful discussions, and to graphic designer Natalia Sinugina for producing Figure 3. This work has been supported by the Russian Foundation for Basic Research through grant no. 14-02-01274.

References

Barvainis R.: 1987, *Ap.J.*, **320**, 537.
Barvainis R.: 1992, *Ap.J.*, **400**, 502.
Clavel J. et al.: 1989, *Ap.J.*, **337**, 236.
Chuvaev K.K. et al.: 1997, *Astron. Lett.*, **23**, 355.
Doroshenko V.G., Lyuty V.M.: 1999, *Astron. Lett.*, **25**, 771.
Glass I.: 1998, *MNRAS*, **297**, 18.
Glass I.: 2004, *MNRAS*, **350**, 1049.
Hönig S.F., Kishimoto M.: 2011. *A&A*, **524**, A121.
Hönig S.F. et al.: 2013, *Ap.J.*, **771**, 87.
Hönig S.F.: 2014, *Ap.J. Lett.*, **774**, L4.
Kobayashi Y. et. al.: 1998, *Proc. SPIE*, **3352**, 120.
Koptelova E. et al.: 2005, *MNRAS*, **356**, 323.
Lira P. et al.: 2011, *MNRAS*, **415**, 1290.
Lira P. et al.: 2015, *MNRAS*, **454**, 368.
Lyutyi V.M. et al.: 1995, *Astron. Lett.*, **21**, 581.
Mason R.E.: 2015, *P&SS*, **116**, 97.
Netzer H.: 2015, *ARA&A*, **53**, 365.
Oknyanskij V.L: 1993 *Astron. Lett.*, **19**, 416.
Oknyanskij V.L.: 1999, *Odessa Astron. Publ.*, **12**, 99.
Oknyanskij V.L. et al.: 1999, *Astron. Lett.*, **25**, 483.
Oknyanskij V.L., Horne K.: 2001, *ASP Conf. Proc.*, **224**, 149.
Oknyanskij V.L. et al.: 2006, *ASP Conf. Ser.*, **360**, 75.
Oknyanskij V.L. et al.: 2008, *Odessa Astron. Publ.*, **21**, 79.
Oknyanskij V.L.: 2002, *ASP Conf. Proc.*, **282**, 330.
Oknyanskij V.L. et al.: 2013, *Odessa Astron. Publ.*, **26**, 212.
Oknyansky V.L. et al.: 2014a, *Astron. Lett.*, **40**, 527.
Oknyansky V.L. et al.: 2014b, *Odessa Astron. Publ.*, **27**, 47.
Pozo Nuñez et al.: 2014, *A&Ap*, **561**, L8.
Pozo Nuñez et al.: 2015, *A&Ap*, **576**, 73.
Sitko M.L. et al.: 1993, *Ap.J.*, **409**, 139.
Suganuma M. et al.: 2006, *Ap.J.*, *639*, 46.
Tikhonov A.N., Goncharsky A.V., Stepanov V.V., Yagola A.G.: 1995, *Numerical Methods for the Solution of Ill-Posed Problems*. Kluwer Academic Press, Dordrecht.
Vazquez B. et al.: 2015, *Ap.J.*, **801**, 127.
Yoshii Y. et al.: 2014, *Ap.J. Lett.*., **784**, L11.

REVISION OF THE PHENOMENOLOGICAL CHARACTERISTICS OF THE ALGOL-TYPE STARS USING THE NAV ALGORITHM

M.G.Tkachenko[1], I.L.Andronov[1], L.L.Chinarova[2]

[1] Department "High and Applied Mathematics", Odessa National Maritime University, Mechnikova st., 34, 65029, Odessa, Ukraine, *masha.vodn@yandex.ua, tt_ari@ukr.net*

[2] Astronomical Observatory, Odessa National University, Shevchenko Park, 65014, Odessa, Ukraine, *lidia_chinarova@mail.ru*

ABSTRACT. Phenomenological characteristics of the sample of the Algol – type stars are revised using a recently developed NAV ("New Algol Variable") algorithm (2012Ap.....55..536A, 2012arXiv 1212.6707A) and compared to that obtained using common methods of Trigonometric Polynomial Fit (TP) or local Algebraic Polynomial (A) fit of a fixed or (alternately) statistically optimal degree (1994OAP.....7...49A, 2003ASPC..292..391A).

The computer program NAV is introduced, which allows to determine the best fit with 7 "linear" and 5 "nonlinear" parameters and their error estimates. The number of parameters is much smaller than for the TP fit (typically 20 – 40, depending on the width of the eclipse, and is much smaller (5 – 20) for the W UMa and β Lyrae – type stars. This causes more smooth approximation taking into account the reflection and ellipsoidal effects (TP2) and generally different shapes of the primary and secondary eclipses. An application of the method to two – color CCD photometry to the recently discovered eclipsing variable 2MASS J18024395 + 4003309 = VSX J180243.9 +400331 (2015JASS...32..101A) allowed to make estimates of the physical parameters of the binary system based on the phenomenological parameters of the light curve. The phenomenological parameters of the light curves were determined for the sample of newly discovered EA and EW – type stars (VSX J223429.3+552903, VSX J223421.4+553013, VSX J223416.2+553424, USNO-B1.0 1347-0483658, UCAC3-191-085589, VSX J180755.6+074711= UCAC3 196-166827). Despite we have used original observations published by the discoverers, the accuracy estimates of the period using the NAV method are typically better than the original ones.

Keywords: Stars: variable – stars: eclipsing

1. Introduction

Phenomenological modeling is an effective tools to study newly discovered or poorly studied eclipsing binary stars, for which there is no sufficient information on spectra/temperatures and mass ratio. This additional information is needed for physical modeling using the algorithm of Wilson and Devinney (1971) also discussed by Wilson (1994). This method is implemented in some different programs, like BinaryMaker (Bradstreet, 2005), PHOEBE (Prsa A. et al., 2011), series of programs written in the Fortran language (Zoła et al. 1997, 2010).

The physical modeling of close binary stars is discussed in detail by Kopal (1957), Tsessevich (1971), Kallrath and Milone (2009).

The phenomenological modeling of variable stars has a long history starting from hand-drawing of the light curve and further algebraic polynomial fits of the parts of the light curve or trigonometric polynomial (TP) fits.

The statistically optimal degree of the polynomial (or other more complicated model) may be determined using at least three criteria and their modifications (see Andronov 1994, 2003 for reviews).

2. Approximations of Minima

The "local" approximations of the extrema including polynomials, splines, asymptotic parabolae, asymmetric hyperbolae, running parabolae and sines were discussed by Andronov (2005). The Gaussian shape was an usual approximation for spectral lines in the era preceding synthetic spectra, and, besides measuring Doppler shifts, was used also for minima determination of eclipsing variables and, in a modified form, by Mikulášek et al. (2012). However, the Gaussian function has no abrupt switch from zero to the zero profile, thus it is not possible to determine from the fit the value of the eclipse duration – one of the main parameters needed for the General Catalogue of Variable Stars (Samus' et al., 2015).

Andronov (2012ab) compared few limited – width approximations and proposed the following approximation:

$$x_C = C_1 + C_2\cos(2\pi\phi) + C_3\sin(2\pi\phi) + C_4\cos(4\pi\phi) + C_5\sin(4\pi\phi) + C_6 H(\phi / C_8, C_9) + C_7 H((\phi - 0.5)/C_8, C_{10}) \quad (1)$$

Here the shape of the eclipse is described as

$$H(z,\alpha)=\begin{cases}(1-|z|^{\alpha})^{3/2}, & \text{if } |z|\le 1\\ 0, & \text{if } |z|>1\end{cases} \quad (2)$$

The usual determination of phase is $\phi=\zeta-\mathrm{int}(\zeta-\zeta_0)$, where $\zeta=(t-T_{00})/P_0$, T_{00} is the initial epoch, P_0 is period, and ζ_0 is the minimal limit of the interval $(\zeta_0\le\phi<\zeta_0+1)$ of possible values of ϕ. Classical approach is the interval of phases $[0,1)$, i.e. $\zeta_0=0$, with an additional notification that one may extend the main interval by adding any integer number E to the phase, as the light curve is suggested to be periodic: $m(\phi+E)=m(\phi)$. This obvious extension may be realized at computer programs either by doubling the data with a shift of $E=1$, or by using suitable values of ζ_0 for different parts of the light curve. As typically the initial epoch and period are defined so that the primary minimum corresponds to $\phi=0$ (or close to 0) and the secondary minimum – to $\phi=0.5$. Thus for Eq. (1) it is suitable to choose $\zeta_0=-0.25$.

In previous papers, we have used the values T_{00} and P_0, which were determined by other methods (e.g. trigonometric polynomial). Andronov et al. (2015b) improved the method NAV to make possible differential corrections

$$\phi=\zeta-\mathrm{int}(\zeta-\zeta_0)+C_{11}+C_{12}\cdot(t-T_1), \quad (3)$$

where T_1 is some moment of time, which is recommended to be close to the mean time $\bar{t}$ for partial orthogonalization of basic functions (Andronov, 1994, 2003). The corrected values of the light elements are (Andronov et al. 2015b):

$$T_{01}=\frac{T_{00}+C_{11}P_0-C_{12}P_0T_1}{1-C_{12}P_0} \quad (4)$$

$$P_1=\frac{P_0}{1-C_{12}P_0} \quad (5)$$

We also use additional parameters (the relative depths of the primary and secondary minima, respectively) $d_1=1-10^{-0.4C_6}$, $d_2=1-10^{-0.4C_7}$ and their combinations $Y=d_1+d_2$ and $\xi=d_1/d_2=F_1/F_2$. Here F_1 and F_2 are relative values of the mean brightness of the eclipsed part of star. The value of Y varies from 0 (no eclipses) to 1 (both full eclipses).

Assuming a simplified model of uniform brightness distribution and spherical symmetry of components (Tsessevich 1971, Shulberg 1971, Andronov 1991, Malkov et al. 2007, Andronov and Tkachenko 2013), one may estimate physical parameters.

As generally the primary minimum is defined to be more deep than the secondary one (however, it may be not the case, if the minima are of the same depth within error estimates), it corresponds to the case, when the star with larger surface brightness (and so temperature) is eclipsed by a cooler component.

Papageorgiou et al. (2014) proposed the simplest parabolic approximation of the light curve in four fixed phase intervals, which has the simplest program realization. The number of parameters (12) is the same as in our NAV approximation, but the NAV approximations are continuous, allow to determine the width and corrections to the initial epoch and period. However, the NAV approximation needs more computational time.

Mikulášek (2015) proposed another special shape for the eclipse as

$$F_e=A\left(1+C\frac{\phi^2}{D^2}+K\frac{\phi^4}{D^4}\right)\left\{1-\left\{1-\exp\left[1-\cosh\left(\frac{\phi}{D}\right)\right]\right\}^r\right\} \quad (6)$$

from which some are similar to that we used in the NAV approximation, i.e. the characteristic width D is proportional to the eclipse half - width C_8, $A=C_6$ (for a primary minimum) or $A=C_7$ (for a secondary minimum), and, for small phases $\phi\to 0$, $\alpha\to 2r$ for "sharp" eclipses $r\le 1$ and else $\alpha\to 2$. Two additional parameters C, K should generally produce closer coincidence of the approximation to the observations, but also larger statistical errors of the parameters. Obviously, the number of parameters may also be increased in the NAV algorithm, as was discussed by Andronov (2012ab), but currently we try to make studies using small modifications of the initial algorithm.

3. Application to Concrete Stars

For the analysis, we have used photometric observations of 6 newly discovered eclipsing binary stars of different types, which were published in the "Open European Journal on Variable Stars" (OEJV).

The phase light curves and their best fit appoximations (including non-linear optimization for the parameters C_8 …C_{12}) are shown in Fig. 1 – Fig. 6. For the preparation of figures, the program MCV (Andronov and Baklanov 2004) was used. The parameters are listed in Table 1.

The analysis shows that the corrections of the period related to the parameter C_{12} range typically from 1σ to 7σ, so sometimes are statistically significant. The error estimates for the period using our method are typically better than the original ones, for two stars from 6 by a factor of 10-12. Similar situation is present for the initial epochs. We conclude that the current improvement of the method by adding parameters C_{11} and C_{12} is efficient for the determination of the initial epoch and the photometric period.

Among the coefficients C_2 …C_5 for this sample of stars, the largest value for a given star is typically of C_4, which corresponds to a "double frequency wave" due to the ellipticity effect.

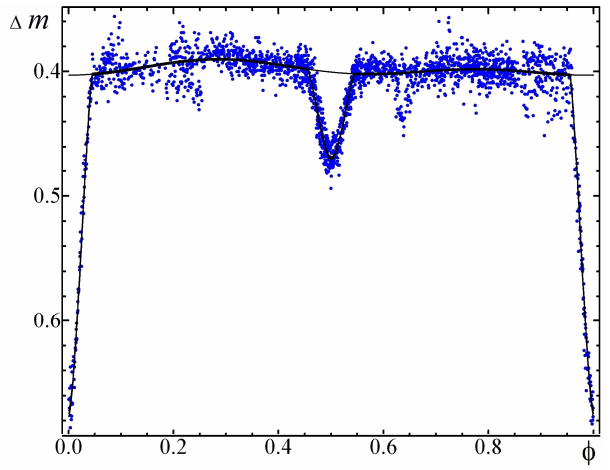

Figure 1: The phase light curve for the star VSXJ223421.4+553013. The observations are shown as blue dots, the black lines show the NAV approximation and ±1σ error corridors.

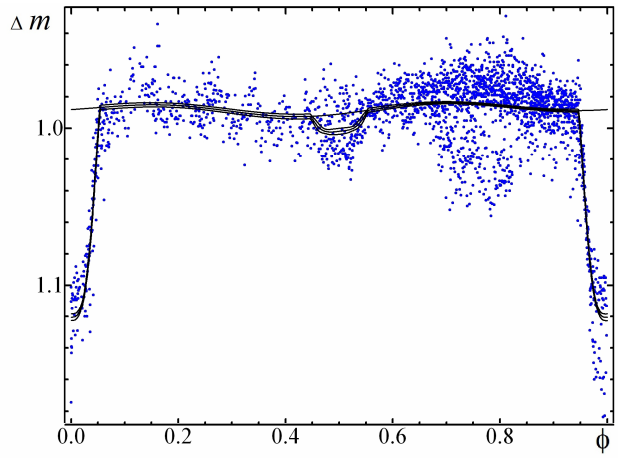

Figure 2: The phase light curve for the star VSXJ223416.2+553424. The observations are shown as blue dots, the black lines show the NAV approximation and ±1σ error corridors.

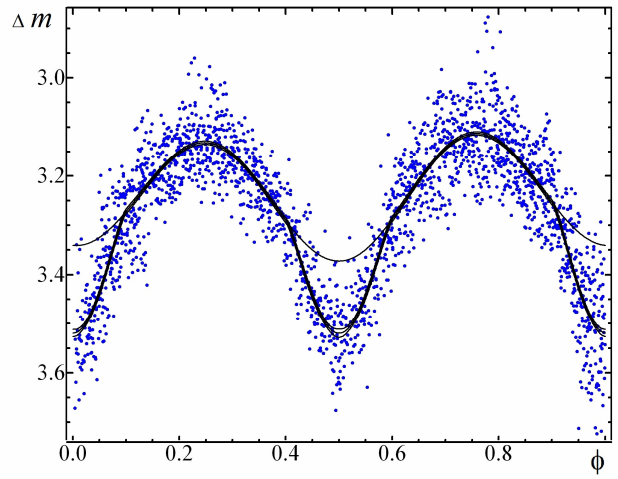

Figure 3: The phase light curve for the star VSXJ223429.3+552903. The observations are shown as blue dots, the black lines show the NAV approximation and ±1σ error corridors.

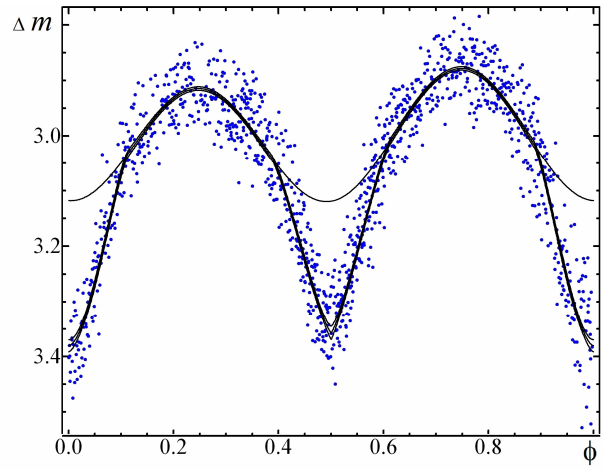

Figure 4: The phase light curve for the star USNO-B1.0 1347-0483658. The observations are shown as blue dots, the black lines show the NAV approximation and ±1σ error corridors.

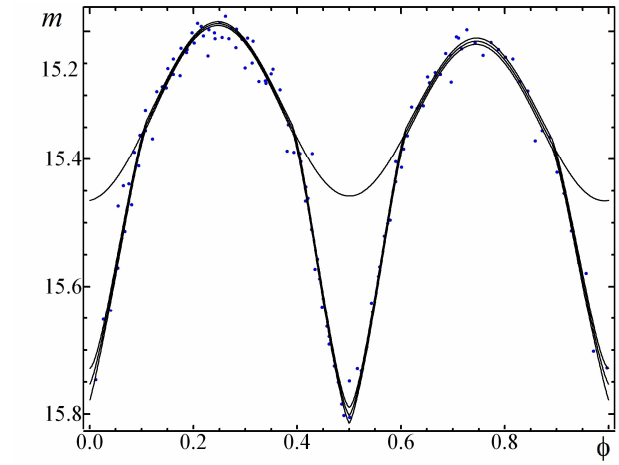

Figure 5: The phase light curve for the star UCAC3 191-085589. The observations are shown as blue dots, the black lines show the NAV approximation and ±1σ error corridors.

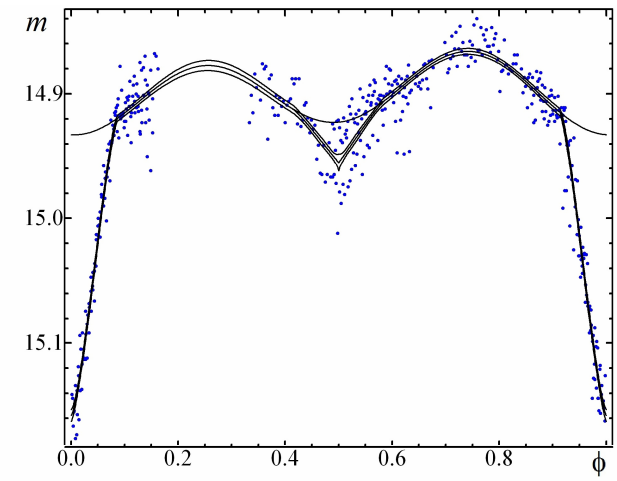

Figure 6: The phase light curve for the star UCAC3 196-166827=VSX J180755.6+074711. The observations are shown as blue dots, the black lines show the NAV approximation and ±1σ error corridors.

Table 1. Characteristics of the NAV approximations

	VSX J223421.4+553013 (Lehký 2009a, OEJV 99, #3)	VSX J223416.2+553424 (Lehký 2009a, , OEJV 99, #2)	VSX J223429.3+552903 (Lehký 2009a, OEJV 99, #1)
C_1	0.3980±0.0003	0.9876±0.0006	3.2393± 0.0027
C_2	0.0013±0.0004	-0.0014±0.0009	-0.0159±0.0032
C_3	-0.0038±0.0004	0.0014±0.0007	0.0092±0.0020
C_4	0.0036±0.0004	0.0019±0.0007	0.1170±0.042
C_5	0.0015±0.0004	-0.0024±0.0007	0.0040±0.0038
C_6	0.2714±0.0026	0.1325±0.0025	0.1786±0.0103
C_7	0.0695±0.0015	0.0109±0.0023	0.1475±0.0109
C_8	0.0456±0.0004	0.0546±0.0008	0.0985±0.0042
C_9	1.56±0.04	3.19±0.19	1.93±0.24
C_{10}	1.69±0.08	3.97±2.33	1.96±0.30
C_{11}	-0.0002±0.0001	0.0010±0.0003	-0.0067±0.0014
C_{12}	$(-1.89\pm0.93)\cdot10^{-6}$	$(4.08\pm1.93)\cdot10^{-6}$	$(-3.35\pm0.50)\cdot10^{-5}$
T_{00}	54373.28108±0.00035	54387.58563±0.00040	54387.35274±0.00040
P_0	1.324325±0.000150	1.105815±0.000009	0.387245±0.000009
T_{01}	54442.14572±0.00017	54466.09957±0.00035	54462.47568±0.00056
P_1	1.3243217±0.0000012	1.1058209±0.0000021	0.3872400±0.0000020
d_1	0.2212±0.0018	0.1148±0.0020	0.1517±0.0080
d_2	0.0620±0.0013	0.0100±0.0021	0.1270±0.0087
Y	0.2832±0.0024	0.1248±0.0030	0.2787±0.0140
γ	3.5662±0.0759	11.4929±2.4366	1.1941±0.08260
Min I	0.674 ±0.002	1.121±0.002	3.519 ±0.007
Max I	0.390 ±0.001	0.984±0.001	3.112 ±0.003
	USNO-B1.0 1347-0483658 (Lehký 2009b, OEJV 115, #1)	UCAC3 191-085589 (Moos et al. 2013, OEJV 156, #6)	VSX J180755.6+074711 (Franco et al. 2010, OEJV 135, #1)
C_1	3.0073±0.0033	15.3314±0.0035	14.8996±0.0012
C_2	-0.0005±0.0033	0.0034±0.0040	0.0050±0.0017
C_3	0.0180±0.0018	-0.0139±0.0025	0.0056±0.0018
C_4	0.1109±0.0047	0.1301±0.0051	0.0278±0.0026
C_5	-0.0035±0.0034	-0.0066±0.0038	-0.0006±0.0014
C_6	0.2627±0.0142	0.2882±0.0256	0.2250±0.0061
C_7	0.2383±0.0140	0.3432±0.0153	0.0324±0.0071
C_8	0.1124±0.0042	0.1095±0.0037	0.0866±0.0023
C_9	1.65±0.18	1.24±0.18	1.41±0.08
C_{10}	1.23±0.13	1.38±0.11	0.41±0.63
C_{11}	0.0012±0.0012	0.0022±0.0011	-0.0011±0.0007
C_{12}	$(3.64\pm3.94)\cdot10^{-6}$	0.0048±0.0014	0.0004±0.0002
T_{00}	55068.50679± 0.00075	55948.67692±0.00405	55381.44874±0.00344
P_0	0.2576355± 0.0000009	0.27448±0.00107	0.861209±0.00013
T_{01}	54881.46373± 0.00030	55949.22649±0.00029	55387.47629±0.00058
P_1	0.2576357±0.0000010	0.27484 ±0.00038	0.86154±0.00014
d_1	0.2149±0.0103	0.2331±0.0181	0.1879±0.0055
d_2	0.1971±0.0104	0.2710±0.0103	0.0294±0.0064
Y	0.4120±0.0171	0.5041±0.0227	0.2165±0.0083
γ	1.0906±0.0613	0.8602±0.0674	6.3740±1.3713
Min I	3.380± 0.011	15.753±0.025	15.157±0,004
Max I	2.878± 0.003	15.187±0.003	14.866±0.002

The stars USNO-B1.0 1347-0483658 and UCAC3 191-085589 show unequal maxima (O'Connell (1951) effect). This effect is more pronounced in the coefficient C_3 than C_5. This is in a good agreement with theoretical expectations (cf. Davidge and Milone, 1984).

In future, possibly it will have sense to exclude the term with C_5 from the mathematical model (1), if still being within the error estimates. This will be decided after analyzing a larger sample of stars.

The parameter α (Eq. (2)) (i.e. C_9, C_{10} for the primary and secondary minimum, respectively) is typically seen in the range from 1 to 2. The outstandingly small value of C_{10}=0.41±0.63 for VSX J180755.6+074711 also does not differ from this range within error estimates.

In our sample, the exception for both minima is present in VSX J223416.2+553424. The secondary eclipse is very shallow, but is still seen in the noisy observations,

Large values α>>2 typically correspond to a total eclipse or a transit and a large difference in radii. For this case, Andronov (2012a) proposed a possible extension for the expression (2) assuming that the eclipse starts at some non-zero value z_0, so

$$0 \le z_0 \le z \le 1. \qquad (7)$$

For the present noisy observations, such a complication due to using an additional parameter z_0 seems not to be effective. This object is also extreme in our sample due to a very large brightness ratio γ=11.5±2.5 and thus large relative temperature difference. Multi-color are needed for a more detailed study similar to that described by Andronov et al. (2015a) for the object 2MASS J18024395 + 4003309 = VSX J180243.9 +400331.

4. Conclusions

Parameters of the phenomenological modeling are determined for 6 newly discovered eclipsing binary stars of different types.

The initial algorithm (Andronov, 2012ab) was improved by adding two parameters allowing to make corrections to the initial epoch and period. The corresponding error estimates are typically significantly better than that obtained using other methods. This improvement of accuracy is more efficient for the EA – type stars, i.e. relatively short eclipses.

In our sample, there are 3 stars of the W UMa – type. They all show distinct eclipses, contrary to the GCVS statement that EB and EW – type objects are systems "having light curves for which it is impossible to specify the exact times of onset and end of eclipses" (Samus' et al. 2015). We propose to correct this definition.

The presence of eclipses is to be justified by statistical significance of the parameters C_6 and C_7 (eclipse depth), otherwise should be classified as "elliptic" (ELL).

For a fixed declination *i*, one may expect an increase with relative radii of the components (and thus from EA to EW types) of the parameters C_8 (eclipse half-width), C_2, C_4 (proximity effects), C_6 and C_7 (eclipse depth).

Acknowledgements. The authors are thankful to Professors S. Zoła and Z. Mikulášek for fruitful discussions over the years. This research is a part of the projects "Inter – Longitude Astronomy" (Andronov et al., 2010) and "Ukrainian Virtual Observatory" (Vavilova et al., 2012).

References

Andronov I.L.: 1991, Structure and Evolution of Stars. *Odessa Inst. Adv. Teachers*, 84p.
Andronov I.L.: 1994, *OAP*, **7**, 49.
Andronov I.L.: 2003, *ASP Conf. Ser.*, **292,** 391.
Andronov I.L.: 2005, *ASP Conf. Ser.*, **335,** 37.
Andronov I.L.: 2012a, *Astrophys.*, **55,** 536,
Andronov I.L.: 2012b, Częstochowski Kalendarz Astronomiczny – 2013, 133; 2012arXiv 1212.6707A.
Andronov I.L. et al.: 2010, *OAP*, **23**, 8.
Andronov I.L., Baklanov A.V.: 2004, *Astronomy School Reports*, **5**, 264.
Andronov I.L., Tkachenko M.G.: 2013, *OAP,* **26**, 204.
Andronov I.L. et al.: 2015a, *Journal of Astronomy and Space Science*, **32**, 127.
Andronov I.L, Tkachenko M.G., Chinarova L.L.: 2015b, *Physics Journal* (accepted); 2015arXiv151000333A
Bradstreet D.H.: 2005, *SASS*, **24**, 23.
Davidge T.J., Milone E.F.: 1984, *ApJS*, **55**, 571
Franco L., Marchini A., Papini R.: 2010, *OEJV,* **135**, 1.
Kallrath J., Milone E.F..: 2009, *Eclipsing Binary Stars: Modeling and Analysis*, Springer-Verlag New York, 444p.; 2009ebs..book.....K
Kopal Z. (1959). Close Binary Systems. *Chapman & Hall, London*, 558p.
Lehký M.: 2009a, *OEJV,* **99**, 1.
Lehký M.: 2009b, *OEJV,* **115**, 1.
Malkov Y. et al.: 2007, *A&A*, **465**, 549.
Mikulášek, Zdeněk; Zejda, Miloslav; Janík, Jan: 2012, Proc. IAU Symp., **282**, 391; 2012IAUS..282..391M
Mikulášek Z.: 2015, *A&A* **584**A, 8; 2015A&A...584A...8M.
Moos C., Hambsch F.-J., Krajci T.: 2013, *OEJV,* **156**, 1.
O'Connell D.J.K., 1951: *PRCO*, **2**, 85-100
Papageorgiou A., Kleftogiannis G., Christopoulou P.-E.: 2014, *Contrib. Astron. Obs. Skalnate Pleso*, **43**, 470.
Prsa A. et al.: 2011. PHOEBE: Physics Of Eclipsing Binaries. *Astrophysics Source Code Library*, (record ascl: 1106.002; 2011ascl.soft06002P).
Samus N.N. et al.: 2015, *General Catalogue of Variable Stars, CDS/ADC Collection of Electronic Catalogues*, 1, 2025, code 2009yCat....1.2025S, electronically available at http://www.sai.msu.su/gcvs/gcvs/
Shul'berg A.M.: 1971. *Close Binary Systems with Spherical Components,* Moscow, Nauka, 246
Tsessevich V.P. (ed.): 1971, *Eclipsing Variable Stars.* Moscow: Nauka, 350p.; 1971isme.conf.....T
Vavilova I.B. et al.: 2012, *KPCB*, **28**, 85.
Wilson R.E. 1994, *PASP*, **106**, 921-941.
Wilson R.E., Devinney E.J.: 1971, *ApJ*, **166**, 605-619.
Zoła S. et al.: 1997, *A&A*, **324**, 1010.
Zoła S. et al.: 2010, *MNRAS*, **408**, 464.

PHOTOMETRY AND MODULATION OF LIGHT CURVES IN THE BLAZHKO STAR V365 HER

S.N. Udovichenko

Astronomical Observatory of I.I.Mechnikov Odessa National University
T.G.Shevchenko Park, Odessa 65014, Ukraine, *udovich222@ukr.net*

ABSTRACT. The photometric CCD observations for the Blazhko RR Lyr type star V365 Her in Astronomical stations near Odessa (Ukraine) have been carried out. The light curves in V system were obtained and the frequency Fourier analyse was performed.The strong Blazhko effect and modulation of the light curves were detected. From Fourier spectra 15 frequencies were identified.

Key words: Stars: oscillations – stars; variables: RR Lyr – stars: individual: V365 Her.

1. Introduction

The variability of the star was found by C.Hoffmeister in 1936. The star thoroughly was investigated by V.P.Tsessevich, which determined the primary elements of period: Max. hel. J.D. = 2436047.522 + 0.6130535 · E, and discovered the sophisticated shape of light variation curves, known as Bllazhko effect (40.64 day) (Tsessevich, 1961, 1966). He mentioned, that the curve of maximum height shows considerable dispersion, and it seems, that the most part of time we observe the weakened maxima and only in some time intervals (short-term) we observe the maxima in the considerable heights. It indicates in modulation of a light curves by additional frequencies, and the star represents the scientific interest for observations. Visual observations in 20 century were carried out by Hoffmeister and Tsessevich. Now V365 Her is known as RR Lyr-star type (RRab) with amplitude $12.^m7 - 14.^m0$ (P), has period $0.^d613138$, Kholopov et al. (1985).

2. Observations

The photometric CCD observations of V365 Her in Astronomical stations near Odessa in observation season 2009-15 have been carried out. Two stars were chosen as comparison and check stars (comp=UCAC4-558-060233, check=UCAC4-558-060246). The 48 cm reflector AZT-3 with the f/4.5 Newtonian focus and CCD photometer with chip Sony ICX429ALL (600x800 pixels), equipped with V filter, Peltier cooler were used (Udovichenko, 2012). The hermetic housing and thermoelectric (Peltier) cooler provide a temperature difference between the crystal and the environment of about -40^{o}C, and the temperature was supported by a constant. The exposure time for variable and comparison stars for the most part were chosen to except a saturation of frame and consist 90 sec. More then 5600 CCD frames were gathered during 55 nights. The reductions of the CCD frames were carried out using the MUNIPACK (Motl) software. The procedures for the aperture photometry are composed of the dark-level and flat-field corrections and determination of the instrumental magnitude and precision. The all set of observations are shown in fig.1. The errors on individual data points vary between 0.005 mag to 0.01 mag.

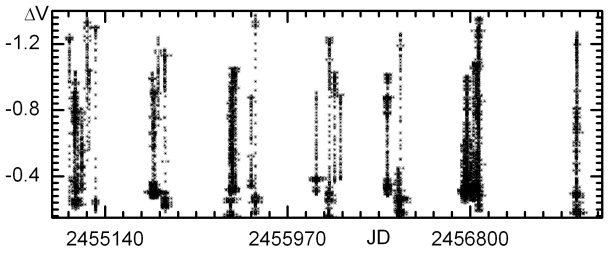

Figure 1: The all data set of observations V365 Her.

3. Frequency analysis

For all observations of V365 Her were determined the magnitudes comparatively of comparison star.

The frequency analyses were performed using a package of computer programs with single-frequency and multiple-frequency techniques by using utilize Fourier as well as multiple-least-squares algorithms (program Period04, Lenz and Breger, 2004). The pulsation period was determined with this package as the highest peak on the Fourier amplitude spectra. The all light curves V365 Her with pulsating period are shown on fig. 2. These phase curves were computed from elements:

$$MaxHJD = 2454978.403 + 0.613182 \cdot E.$$

Table 1: Identified Fourier amplitude and phases of the pulsation and modulation frequencies in light curves of V365 Her.

Identif.	Frequency	Amplitude	Phase	S/N
f0	1.630835	0.346	0.15	6.6
2f0	3.26168	0.127	0.86	26.7
3f0	4.89255	0.086	0.89	20.2
4f0	6.52330	0.061	0.22	13.1
5f0	8.15355	0.052	0.15	11.7
6f0	9.78498	0.021	0.43	6.1
7f0	11.41402	0.021	0.68	4.6
f0+fm	1.65552	0.085	0.33	17.2
f0- fm	1.60613	0.054	0.54	11.7
2f0-fm	3.22425	0.034	0.74	6.6
3f0+fm	4.91979	0.034	0.83	7.1
3f0-fm	4.85806	0.026	0.85	7.0
4f0+fm	6.5530	0.034	0.26	7.6
5f0+fm	8.1788	0.038	0.80	6.7
6f0-fm	9.74763	0.024	0.47	6.1

Table 2: Time of maxima V365 Her.

Time J.D.	Time J.D.	Time J.D.
2454978.406	2455718.538	2456425.517
2455000.510	2455720.377	2456785.478
2455002.334	2455734.480	2456815.517
2455005.391	2455804.382	2456828.398
2455059.338	2455823.383	2456836.361
2455067.319	2456159.387	2456839.427
2455097.367	2456183.311	2457283.362
2455355.527	2456210.284	
2455411.336	2456422.466	

The maximum of the light curves amplitude variation is 1.3 mag, minimum 0.8 mag, and strong Blazhko modulation of amplitude reach about 0.5 mag and phase modulations up to 0.05. The power spectra of basic frequency and after prewhitening is shown in Fig. 3.

After prewhitening of basic frequency the harmonics of basic frequency kf0 and triplet of frequencies $kf_0 \pm f_m$, responsible for modulation of light curves was found. The Fourier amplitude and phases of the pulsation component identified in the spectra of the light curves of V365 Her are presented in Table 1. The basic frequency denoted as f_0, the modulation frequency of Blazhko effect denote as f_m. We find triplet of frequencies $f_0 \pm f_B$, but, perhaps, there are more frequencies in the pulsation spectra of V365 Her. From obtained data the mean period of Blazhko effect amount $14^d.6$.

The time of maxima V365 Her presents in Table 2.

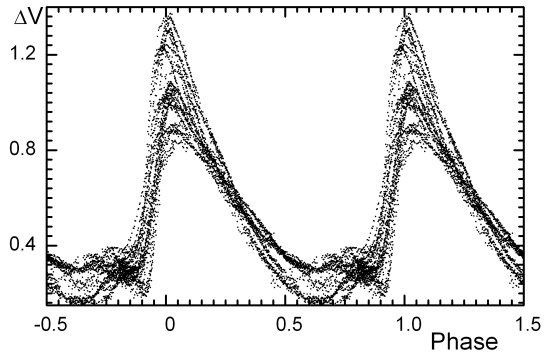

Figure 2: The light curves V365 Her with phase of basic period. The strong Blazhko modulation of amplitude reach about 0.5 mag and phase modulations up to 0.05.

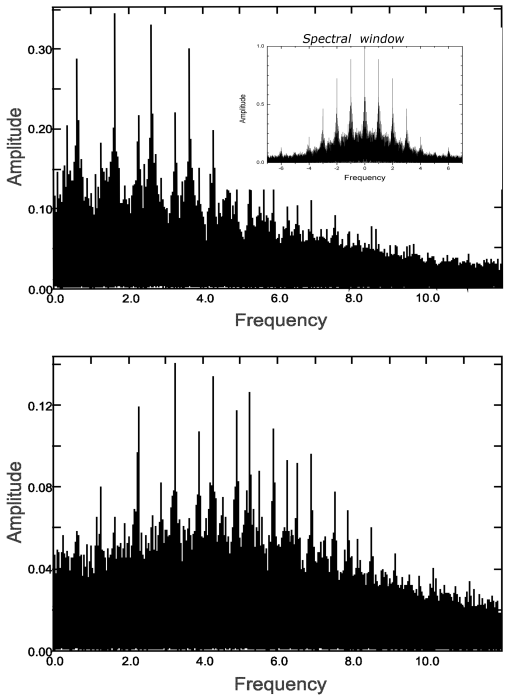

Figure 3: The Fourier amplitude spectrum of basic frequency and after prewhitening. The spectral window shows inside first picture.

References

Hoffmeister C.: 1936, *Astron. Nachrichten.*, **259**, 37.

Lenz P., Breger M.: 2004, *Comm.in Asteroseismology*, **144**, 41.

Motl D.: *http://sourceforge.net/projects/c-munipack/files.*

Samus N.N., Durlevich O.V., Kazarovets E.V., Kireeva N.N., Pastukhova E.N., Zharova A.V. et al.: 2011, *General Catalogue of Variable Stars* (GCVS database, Version 2011Jan).

Tsessevich V.P.: 1980, *Sov. Astron.Jurn.*, **38**, 293.

Tsessevich V.P.: 1966, RR Lyrae-type variable stars, Naukova Dumka, Kiev.

Udovichenko S.N.: 2012, *Odessa Astron. Publ.*, **25**, 32.

Subsection Virtual observatories and intensive data

COMPARISON OF ZERO ZONE CATALOGUES OF THE FON PROGRAM BASED ON THE KYIV AND KITAB OBSERVATIONS

V.M.Andruk [1], H.Relke [2], Yu.I.Protsyuk [3], M.M.Muminov [4], Sh.A.Ehgamberdiev [4], Q.X.Yuldoshev [4], V.V.Golovnia[1]

[1] Main Astronomical Observatory of National Academy of Sciences, 27 Akad. Zabolotnogo St., 03680, Kyiv, Ukraine, *andruk@mao.kiev.ua*
[2] Walter Hohmann Observatory, Wallneyer St.159, 45133 Essen, Germany, *helena_relke@yahoo.com*
[3] Research Institute "Nikolaev Astronomical Observatory", 1 Observatornaya St., 54030, Mykolaiv, Ukraine, *yuri@nao.nikolaev.ua*
[4] Ulugh Beg Astronomical Institute of the Uzbek Academy of Sciences, 33 Astronomicheskaya St., 100052, Tashkent, Uzbekistan, *muminov_mm@mail.ru*

ABSTRACT. The two new catalogues for the zero zone of the FON project were created after the processing of two different collections of digitized photographic plates. The photographic plates were received at the DAZ and DWA telescopes of the Kitab observatory of the Republic of Uzbekistan (KO UAS) and of the Main astronomical observatory in Kyiv (MAO NASU) in the number of 90 and 120 plates, respectively. The digitization of these photographic plates in the frame of the Ukrainian Virtual Observatory project was performed by means of the Epson Expression 10000XL scanner with the scanning resolution of 1200 dpi. The coordinates of stars and galaxies for the both catalogues are determined in the system of the Tycho2 catalogue. The stellar magnitudes of all objects are done in B-magnitudes of the photoelectric standard system. The difference between the calculated and the reference positions is equal $\sigma_{\alpha\delta}$ = ±0.06–0.07". The internal accuracy of the both catalogues for all objects is $\sigma_{\alpha\delta}$ = ±0.20", σ_B = ±0.18^m and $\sigma_{\alpha\delta}$ = ±0.27", σ_B = ±0.17^m, respectively. We present the comparison of these both catalogues with each other and with the Tycho2, UCAC4 as well as PPMX catalogues and discuss the results.

Keywords: photometric – methods: data analysis – catalogs, virtual observatory tools – astrometry - techniques

1. Introduction

On the basis of the processing of different sets of observational data of the FON project (Kislyuk et al., 2000, Yatsenko et al., 2011) for the zero zone were created two star catalogues of the positions and stellar magnitudes. This work was done by the using of the resources of the Ukrainian Virtual Observatory UkrVO (Vavilova et al., 2012, Vavilova et al., 2012). The sets of observational data consist of the photographic plates exposed with the Double Wide Angle Astrograph (**DWA**, 40/200, 103"/cm, Goloseevo, h=186m) and the Zeiss Double Astrograph (**DAZ**, 40/300, 76"/cm, Kitab, h=657m). The catalogues were created on the basis of photographic plates digitized by the using of the Epson Expression 10000XL scanner (Andruk et al., 2010, Golovnya et al., 2010, Protsyuk et al., 2014, Protsyuk et al., 2014, Protsyuk et al., 2014). The reduction procedure was done with the software that was previously used in the series of works (Andruk et al., 2014, Muminov et al., 2014, Yizhakevych et al., 2014, Protsyuk et al., 2014, Kazantseva et al., 2015) and is described in detail in the following publications (Muminov et al., 2015, Andruk et al., 2015, Andruk et al., 2016). The photographic plates were scanned with a spatial resolution of 1200 dpi, the size of each plate is 30 x 30 cm (13000 x 13000 pixels). The working areas (see Figure 1) are 7.8° x 7.8° (1 px = 2.17 ") and 5.2° x 5.2° (1 px = 1.45") for the DWA and DAZ telescopes respectively. The versions of both catalogues were obtained by the processing of single scans without the rotation of the plates on the 90°. This approach allows to save resources for the storing and processing information more than twice times without the loss of accuracy of the results. The software concept and the steps of the processing of digitized photographic plates

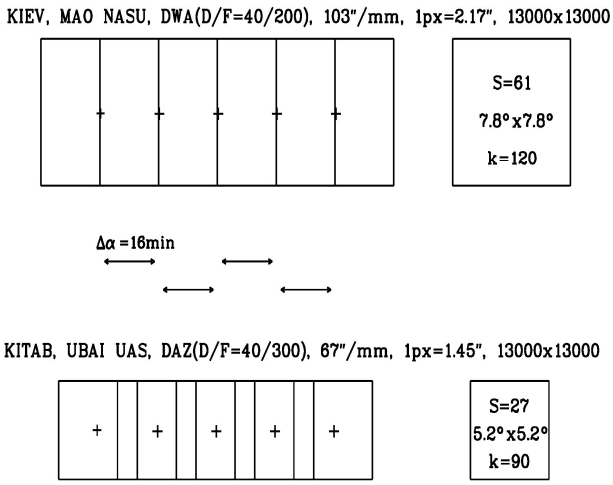

Figure 1: Scheme and the relative size of the overlapping zones for the MAO NASU and KO UAS.

for the zero zone will be then applied for all photographic plates of the FON project exposed as in Kyiv (sky area from 0 to 90 degrees) and as well as in Kitab (sky area from 0 to -20 degrees) respectively.

2. The processing of the digitized photographic plates and creating of the catalogues

The processing of these two digitized sets of photographic plates exposed with the DWA (120 plates) and DAZ (90 plates) telescopes was performed on the base of the common method which was developed and has been applied in practice in the MAO NASU. The steps of the processing of the scanned photographic plates are:

1. Conversion of the tiff-format files to the fit-format files using the GIMP package.
2. The processing of the scans using the MIDAS/ROMAFOT package to obtain the rectangular coordinates X, Y and instrumental magnitudes of registered objects.
3. The dividing of the registered objects into two exposures for each digitized plate.
4. The creating of the files with the reference stars for each digitized plate using the Tycho2 catalogue.
5. The creating of the files for the relationship between the rectangular and equatorial coordinate systems of reference stars.
6. Correction of the rectangular coordinates of registered objects for systematic errors.
7. Reduction of the rectangular coordinates X, Y of registered objects in the system of equatorial coordinates α, δ of the Tycho2 catalogue.
8. Conversion of the instrumental photometric values of objects to the system of photoelectric B_{pe} stellar magnitudes of the Johnson's system.

For the calibration of the characteristic curves of the photographic plates, the recording photometric field errors and the conversion of the instrumental photometric values to the system of photoelectric Bpe stellar magnitudes of the Johnson system were used data from the catalogues (Kornilov et al., 1991, Mermilliod, 1991, Andruk et al., 1995, 1996, Relke, et al., 2015). For the plotting of the characteristic curves of photographic plates was used the photometric information of both exposures.

The process of the creating of the CAT1 and CAT2 catalogues for the two sets of observations at the DWA and DAZ telescopes was as follows. In the overlapping zones of the photographic plates the identification and selection of candidates in stars and galaxies was carried out according to the following criteria:

1) the difference between equatorial coordinates should not be greater than the size of the one pixel
2) the difference between stellar magnitudes should not exceed ± 2 mag (because of the accounting of variable stars).

If the found candidate meets the selection criteria at least on two plates, it was included in the list of the objects for the catalogues. For the non-overlapping areas of the plates of DAZ telescope the candidates in stars and galaxies were implemented by the direct identification with the objects from the UCAC4 catalogue (Zacharias et al., 2013). The CAT1 and CAT2 catalogues contain 1320108 and 1795840 stars and galaxies up to Bph ≤ 16.5^m (the photographic magnitudes of the Johnson system) for the epoch of 1990.35 and 1983.29 respectively. The CAT1 and CAT2 catalogues cover the zones of width up to 8° (from -4° to +4°) and of width up to 5.2° (from -2.6º to + 2.6°), respectively. As the result of the comparing CAT1 and CAT2 catalogues was received a third MCAT catalogue, which contains the averaged data for the 669480 stars and galaxies.

3. Internal errors of the catalogues

The distribution of internal errors of defined equatorial coordinates σα, σδ and photometric magnitudes σBph of stars and galaxies on the intervals of stellar magnitudes of the three catalogues are given in the table 1. The average errors are provided at the top of the table 1 and their corresponding values for three catalogues are equal:

σ_α = ±0.279", ±0.208", ±0.105"; σ_δ = ±0.273", ±0.201", ±0.157"; σ_{Bph} = $\pm0.168^m$, $\pm0.176^m$, $\pm0.140^m$.

Table 1. The errors of the defined equatorial coordinates and stellar magnitudes for the three catalogues

B_{ph} mag	σ_α, σ_δ, arcsec		σ_{Bph} mag
	CAT1		
6.6	±0.286	±0.249	±0.204
7.6	0.218	0.178	0.155
8.6	0.138	0.119	0.116
9.6	0.086	0.082	0.081
10.6	0.066	0.066	0.061
11.6	0.062	0.064	0.068
12.6	0.106	0.108	0.094
13.6	0.190	0.192	0.119
14.6	0.285	0.278	0.162
15.3	0.355	0.346	0.212
16.3	0.395	0.396	0.262
17.1	0.455	0.416	0.156
	CAT2		
6.6	±0.203	±0.356	±0.296
7.6	0.264	0.224	0.264
8.6	0.148	0.143	0.231
9.6	0.097	0.094	0.175
10.6	0.064	0.064	0.134
11.6	0.057	0.059	0.086
12.6	0.106	0.107	0.093
13.6	0.162	0.159	0.116
14.6	0.179	0.177	0.144
15.5	0.218	0.215	0.201
16.2	0.263	0.253	0.193
17.1	0.258	0.289	0.278
	MCAT		
6.7	±0.173	±0.203	±0.333
7.6	0.139	0.142	0.209
8.6	0.093	0.095	0.160
9.6	0.070	0.061	0.110
10.6	0.056	0.046	0.077
11.6	0.050	0.045	0.067
12.6	0.062	0.078	0.087
13.6	0.090	0.133	0.103
14.6	0.111	0.167	0.148
15.3	0.123	0.191	0.170
16.2	0.132	0.207	0.182
17.1	0.132	0.187	0.491

4. Actual accuracy (external errors) of the catalogues

The results of the comparison of the three catalogues with the reference Tycho2 catalogue are presented in the second part of the table 2 as well as on the figure 2.

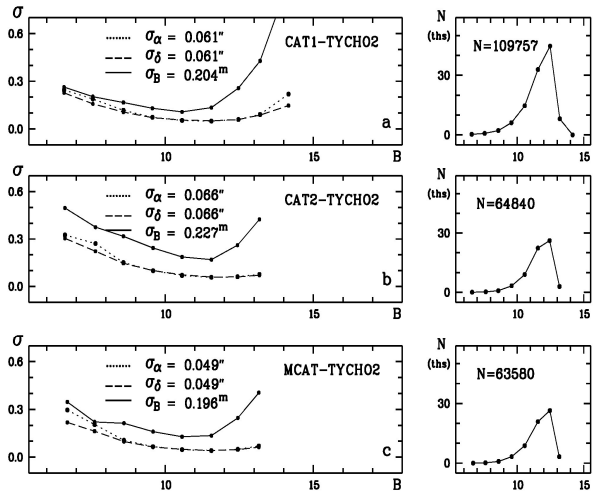

Figure 2: The trend of the errors of astrometric reduction with the B-magnitude for the three catalogues relative to the reference Tycho-2 catalogue.

We point out that the errors of astrometric reduction for the reference stars of the Tycho2 catalogue do not exceed the value of $\sigma_{\alpha\delta} = \pm 0.07$". The comparison of the calculated equatorial coordinates of the created catalogues was also made with the equatorial coordinates of the UCAC4 (Zacharias et al., 2013) and PPMX (Roeser et al., 2008) catalogues. The results of the comparison are given in the third and fourth parts of the table 2 as well as on the figures 3 and 4.

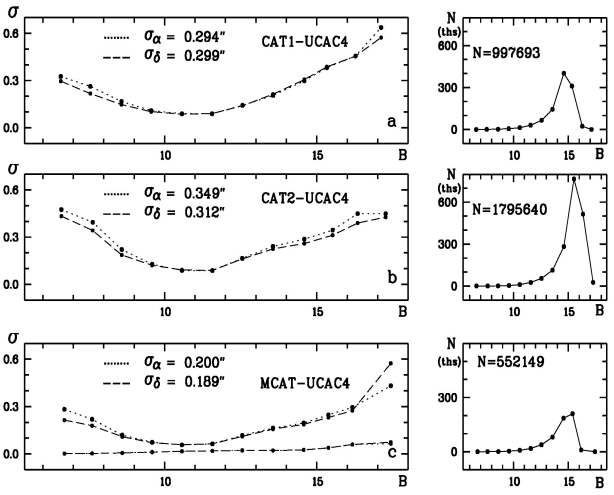

Figure 3: The trend of the errors of differences in equatorial coordinates with the B-magnitude for the three catalogues relative to the UCAC4 catalogue.

The astrometric errors of the created catalogues relative to the UCAC4 catalogue are: $\sigma_\alpha = \pm 0.294$", ± 0.349", ± 0.200"; $\sigma_\delta = \pm 0.299$", ± 0.312", ± 0.189". The error values relative to the PPMX catalogue are: $\sigma_\alpha = \pm 0.260$", ± 0.274", ± 0.186"; $\sigma_\delta = \pm 0.273$", ± 0.261", ± 0.188".

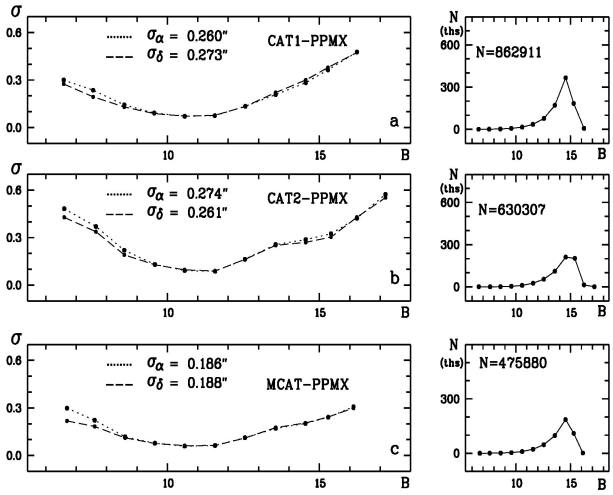

Figure 4: The trend of the errors of differences in equatorial coordinates with the B-magnitude for the three catalogues relative to the PPMX catalogue.

The photometric errors for the new three catalogues are presented on the figure 5.

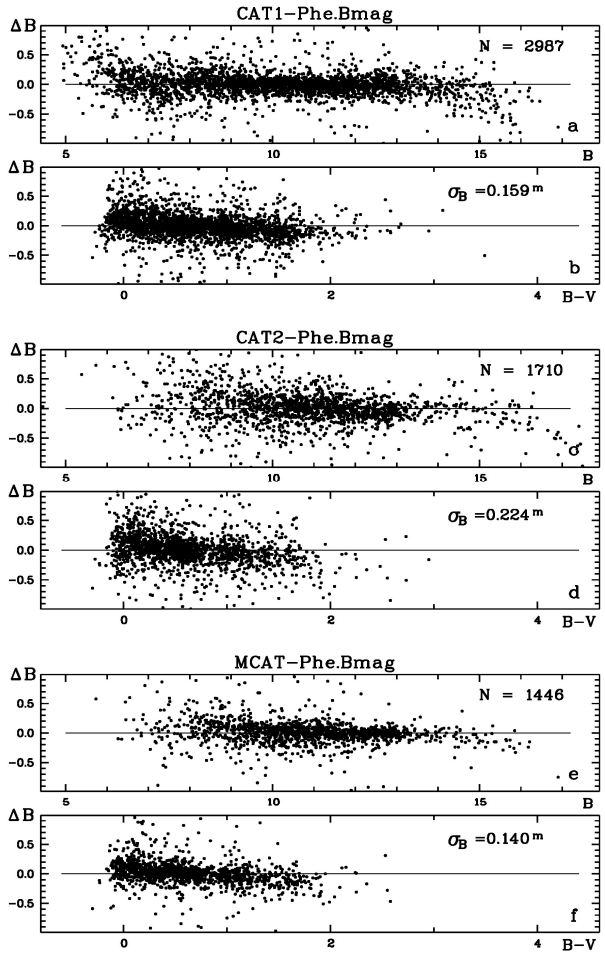

Figure 5: The trend of the errors of differences in magnitudes with the B-magnitude for the three catalogues relative to the photo electrical B-magnitudes.

The photometric errors were determined by the comparing of the stellar magnitudes of our three catalogues

with the photoelectric values of reference photometric catalogues. The calculated results are presented at the bottom of the table 2. For the three catalogues the error values are as follows: $\sigma_{Bph} = \pm 0.159^m, \pm 0.224^m, \pm 0.140^m$.

Table 2. The external errors of the three catalogues

	CAT1	CAT2	MCAT
N	320108	1795840	669480
σ_α	0.279"	0.208"	0.105"
σ_δ	0.273"	0.201"	0.157"
σ_{Bph}	0.168^m	0.176^m	0.140^m
TYCHO2			
	109757	64810	63580
	0.061"	0.066"	0.049"
	0.061"	0.066"	0.049"
	0.204^m	0.227^m	0.196^m
UCAC4			
	997693	1795840	552149
	0.294"	0.349"	0.200"
	0.299"	0.312"	0.189"
PPMX			
	862911	630307	475880
	0.260"	0.274"	0.186"
	0.273"	0.261"	0.188"
Pe.Bmag			
	2987	1710	1448
	0.159^m	0.224^m	0.140^m

5. Some remarks

The "Photographic Survey of the Northern Sky" (FON project) was proposed by the Main astronomical observatory Academy of Sciences of Ukraine, Kyiv (MAO NASU) (Kolchinsky et al., 1977; Kolchinsky et al., 1979). The idea of this project was due by the situation in the field of photographic astrometry in the early seventies of the twenties century. Some observatories of the former Soviet Union (Goloseevo, Zvenigorod, Dushanbe, Abastumani and Kitab) equipped with identical astrographs produced by the "Carl Zeiss Jena" (DDR) took part in this project. The observatories finished the observations at the end of the 90s of the XX century and have in their archives thousands of the photographic plates waiting for the reduction. The archive of the Kitab observatory (zone from -20° to +30°) contains about 2600 photographic plates. Now the staff members of the Kitab observatory have organized the digitalization of the photographic plates of the "FON" project.

6. Conclusion

The created star catalogues of the positions and stellar magnitudes (Bph) of the zero zone of the Kyiv and Kitab parts of the FON project will be posted on the web pages of the MAO NASU and the Astronomical Institute of the Uzbek Academy of Sciences. The catalogues contain the equatorial coordinates of stars (α, δ) on the equinox 2000.0 as well as the stellar magnitudes (Bph). We provide the errors definitions of these values and number of determinations as well as an additional information in the form of the average values for the diameters of star images f (FWHM) and the values of the maximal intensity in the center of object images (cInt).

Acknowledgements. The authors are thankful to anybody who has read this contribution to the end. This work was partially supported by the Ukrainian Astronomical Association.

References

Andruk V.M. et al.: 1995, *Astron. Nachr.*, **316, N4,** 225.
Andruk V.N. 1996, *Kinem. Phys. Cel. Bodies*, **12, N4,** 60.
Andruk V.M. et al.: 2010, *Kinem. Phys. Cel. Bodies*, **26, N3,** 146.
Andruk V.M. et al.: 2014, *Odessa Astron. Publ.*, **27/1,** 53.
Andruk V.M. et al.: 2015 ArXiv (in press).
Andruk V.M. et al.: 2016, *Kinem. Phys. Cel. Bodies*, **32, N1**, 56.
Golovnya V. et al.: 2010, *J. of Phys. Studies*, **14, N2**, 2902.
Kazantseva L.V. et al.: 2015, *Kinem. Phys. Cel. Bodies*, **31, N1,** 58.
Kislyuk. V.S. et al.: 2000, *Kinem. Phys. Cel. Bodies*, **16, N6,** 483.
Kolchinsky I.G., Onegina A.B.: 1977*, Astrometry and Astrophysics,* **N33**, 11.
Kolchinsky I.G., Onegina A.B.: 1979, *Astrometry and Astrophysics*, **N39,** 57.
Kornilov V.G. et al.: 1991, *Trudy GAIS*, **63,** 1.
Mermilliod J.C.: 1991, *Homogeneous means in the UBV system*.
Muminov M.M. et al.: 2014, *Odessa Astron. Publ.*, **27/1,** 57.
Muminov M.M. et al.: *Izvestija GAO*, Pulkovo, 2016 (in press).
Protsyuk Yu.I. et al.: 2014, *Odessa Astron. Publ.*, **27/1,** 59.
Protsyuk Yu.I. et al.: 2014, *Odessa Astron. Publ.*, **27/1,** 61.
Protsyuk Yu.I. et al.: 2014,*Odessa Astron. Publ.*, **27/1,** 63.
Protsyuk Yu.I. et al.: 2014, *Kinem. Phys. Cel. Bodies*, **30, N6,** 54.
Relke H. et al.: 2015, *Odessa Astron. Publ.*, **28, N1.**
Roeser S. et al.: 2008, *A&A*, **488**, 401.
Vavilova I.B. et al.: 2012, *Kinem. Phys. Cel. Bodies*, **28, N2,** 85.
Vavilova I.B. et al.: 2012, *Baltic Ast.*, **21, N3**, 356.
Yatsenko A.I. et al.: 2011, *Kinem. Phys. Cel. Bodies*, **27, N5,** 249.
Yizhakevych O. et al.: 2014, *Odessa Astron. Publ.*, **27/1,** 67.
Zacharias N. et al.: 2013, *Astron. J.*, **145.** 44.

CATALOG OF POSITIONS AND B MAGNITUDES OF STARS IN THE CIRCUMPOLAR REGION OF NORTHEN SKY SURVEY (FON) PROJECT

V.M.Andruk[1], L.K.Pakuliak[1], V.V.Golovnia[1], G.A.Ivanov[1], O.M.Yizhakevych[1], Yu.I.Protsyuk[2], S.V.Shatokhina[1]

[1] Main Astronomical Observatory of National Academy of Sciences, 27 Akad. Zabolotnogo St., 03680, Kyiv, Ukraine, *andruk@mao.kiev.ua*
[2] Research Institute *"*Nikolaev Astronomical Observatory*"*, 1 Observatornaya St*.*, 54030*,* Mykolaiv*,* Ukraine*, yuri@nao.nikolaev.ua*

ABSTRACT. The catalog of star positions and B-magnitudes for the circumpolar region (from 58º to 90º in declination) of Northern Sky Survey project has been created under the motto of the rational use of resources accumulated in UkrVO JDA (Joint Digital Archive) in MAO NASU. The total amount of processed plates is 477. Digitizing of astronegatives has been carried out using Microtek ScanMaker 9800XL TMA and Epson Expression 10000XL scanners, with the scanning mode – 1200 dpi, the linear size of the plates – 30x30 cm or 13000x13000 px. The catalog contains 1 975 967 stars and galaxies with $B \leq 16.5^m$ for the epoch of 1985.28. The coordinates of stars and galaxies were obtained in the Tycho-2 reference system, and B-value in the system of photoelectric standards. The internal accuracy of the catalog for all the objects is $\sigma_{\alpha\delta} = \pm 0.23$ "and $\sigma_B = \pm 0.12^m$ (for stars in the range of $B = 8^m$ -14^m errors are $\sigma_{\alpha\delta} = \pm 0.11$" and $\sigma_B = \pm 0.06^m$). Convergence between the calculated and reference positions is $\sigma_{\alpha\delta} = \pm 0.06$ "(for 171 124 stars from Tycho-2), and the convergence with photoelectric stellar B-magnitudes is $\sigma_B = \pm 0.15^m$ (for 5130 stars). External accuracy from the comparison with UCAC-4 is $\sigma_{\alpha\delta} = \pm 0.33$ "(1 928 367 stars and galaxies were cross identified).

Keywords: virtual observatory tools – astrometry – techniques: photometric – methods: data analysis – catalogs

1. Introduction

For the creation of the circumpolar region star catalogue 477 plates of the FON project (Kislyuk, 2000; Yatsenko, 2011) were digitized and processed. The catalogue covers the region from 58º to 90º in declination and includes positions and B-magnitudes of stars. The work is done with the involvment of collected resources of UkrVO JDA (Joint Digital Archive) (Vavilova, 2012; Vavilova, 2012).

The process of digitizing the UkrVO archives was not limited to photographic surveys relatively homogeneous in quality. Plates, obtained in a variety of observational programs and received on different instruments with different methods, different structures of object images, digitized with different models of scanners were taken into processing. The variety of digitized material required constant upgrading of software and finding new approaches to its solution. The algorithms and methods developed in this investigation permit to resolve many problems of plates processing from different observational archives.

The FON plates were obtained with four-fold overlapping on both coordinates. For this catalogue in some areas with distances ±2º from the centers of plates on the declination the two-fold overlapping was used. The overlapping along the strips on the right ascension is made with 4º/cosδ shift of plate centers. The centers of adjacent strips are spaced apart from each other by 4º on declination. The number of plates in the RA stripes shown in the Table 1.

All the plates were obtained with MAO NASU DWA (Double Wide-angle Astrograph, D/F=40/200, 103"/mm, h=186m). The linear dimensions of the most plates are 30x30 sm (8x8°).

Table 1. Number of plates in each RA stripe.

DEC	N	DEC	N	DEC	N
88º	8	76º	53	64º	50
84º	25	72º	51	60º	102
80º	24	68º	58	56º	106

The plates were digitized using Microtek ScanMaker 9800XL TMA and Epson Expression 10000XL commercial scanners with the resolution 1200 dpi. The dimensions of the digital image fields are up to 13000x13000 px (1px = 2.17"). This version of the catalogue is obtaines from the processing of single scans without turning the plate by 90°. This permits to save resources for storage and processing the data in half without losses in accuracy (Andruk, 2016). The results of scanners' testing, principles and stages of astronegative digital image processing are stated in the series of publications (Andruk, 2005, Andruk, 2007, Andruk, 2010, Golovnya, 2010, Protsyuk, 2014, Protsyuk, 2014, Protsyuk, 2014). The results of the software testing arer described in (Kazantseva, 2015; Protsyuk, 2014; Andruk, 2014; Muminov, 2014; Vavilova, 2014; Yizhakevych, 2014).

2. Separation of stars into two exposition sets

The FON plates were obtained with two expositions: the long and short of 16-20 minutes and 30-60 second respectively. For astrometric catalogue star images of short expo-

sition are not used and should be excluded at the initial step before the astrometric solution. Stages and functional dependences of different parameters in the separation of detected objects into two sets are shown on Fig.1. Upper panels demonstrate the correlation between instrumental photometric values of long and short expositions m_2 и m_1 at initial and final stages of separation on the left and right sides of the figure correspondingly. Differences of magnitudes Δm reduced to the mean value are given on the panels **b, d** in relation to m_1 and the distance from the center of the plate R. The differences of distances between centers of images Δr are given on the panel **c** in relation to m_1. The differences of rectangular coordinates ΔX, ΔY are presented on the panels **e, f** relative to the rectangular coordinates Y, X. The lower panels (**g, h, j**) show the real and pre-calculated histograms of distribution Δm, ΔX, ΔY, shown with solid and dashed lines, respectively. It will be recalled that the value of the ΔX, ΔY differences' rotation in relation to the center of rectangular coordinates Y, X depends on the declination of the plate. The mutual rotation of two frames is absent at the equator.

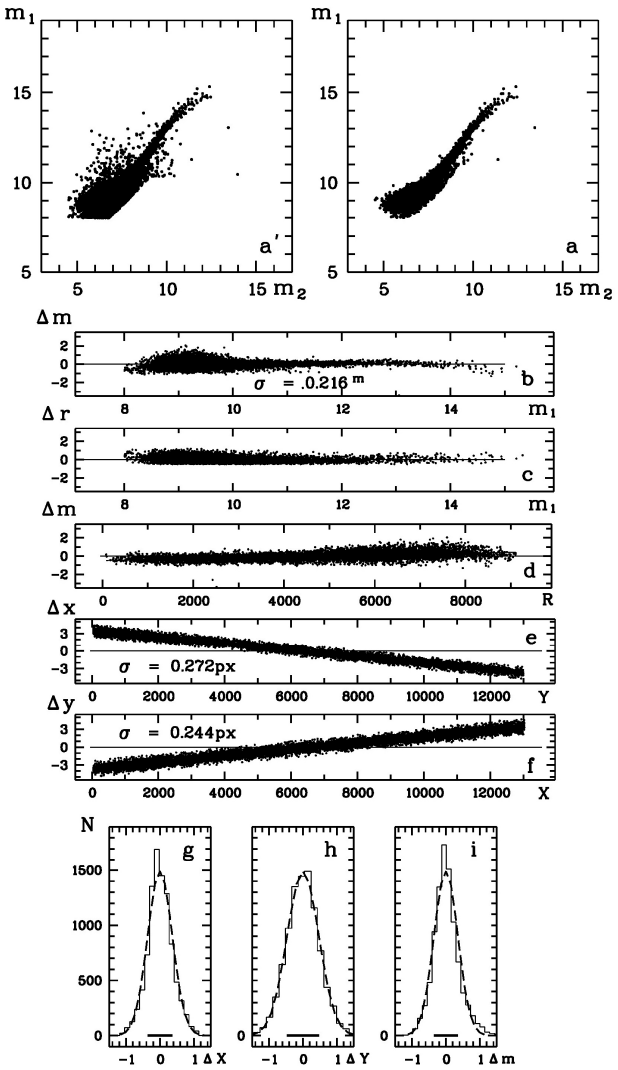

Figure 1: Stages of processing and functional dependences of different parameters in separation of star images into two exposition sets on the example of the test plate.

3. The magnitude equation

When calculating the tangential coordinates the special attention is given to the accounting of the magnitude equation mdtX and mdtY. It was found that for the plates exposed on astrographs the magnitude equation becomes significant for stars from $B \approx 11^m$ and its influence increases with the brightness of stars.

Fig. 2 shows the magnitude equation for the long exposition of the test plate with two expositions and Fig.3 presents the residual differences after its elimination. Fig.2 demonstrates the differences Δα, Δδ between observed and catalogue positions in relation to star image diameters $f_{½}$, instrumental photometric values m_1, magnitudes B and color indices B-V of Tycho-2 before the corrections for systematic errors of the scanner. From plots it is obvious that the magnitude equation is linear on all sections of $f_{½}$ and B and there the quadratic dependence on instrumental photometric values m_1 exists. Fig.3 shows the trend of residual differences in coordinates after the correction for the magnitude equation and the errors of the scanner.

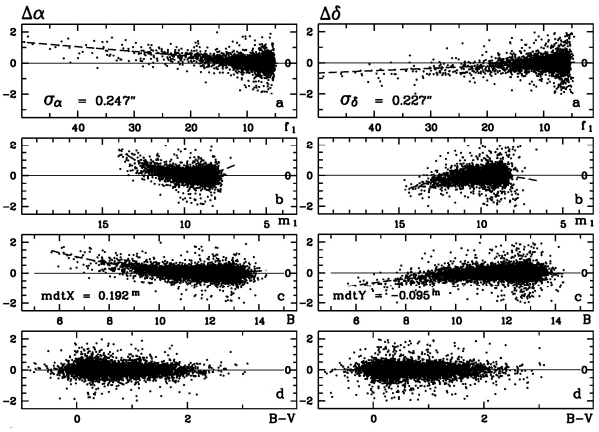

Figure 2: The magnitude equation for the long exposition detected on the plates with two expositions of the FON project.

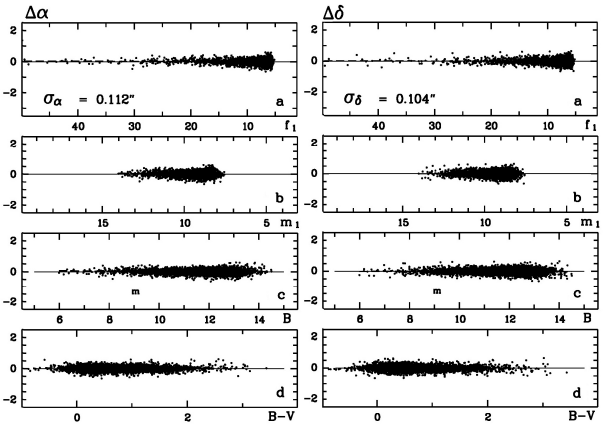

Figure 3: The residual differences in coordinates after the corrections for the magnitude equation and the scanner errors.

4. Astrometric solution in the Tycho-2 reference system

In each step of catalogue creation the star catalogue TYCHO-2 was taken as reference. The accuracy of it is $\boldsymbol{\sigma_{RA,DEC}} = \pm 0.060''$, $\boldsymbol{\sigma_{\mu}} = \pm 0.0025''$/yr, $\boldsymbol{\sigma_{m}} = \pm 0.10^{m}$ for its all 2 539 913 stars.

For all scans of plates with the field dimensions up to 8x8° the tangential coordinates ξ, η were calculated by equations (1). The same formulae were used on the stage of scanner systematic errors Δα, Δδ studying.

$$\xi_i = a_1+a_2X_if_{½i}+a_3Y_if_i+ a_4R_im_i+a_5f_{½i} + \sum b_{lm}X_i^lY_i^m,$$
$$(l=0\div6,\ m=0\div6,\ l+m=n,\ n=1\div6) \qquad (1)$$
$$\eta_i = c_1+c_2X_if_{½i}+c_3Y_if_i+ c_4R_im_i+c_5f_{½i} + \sum d_{lm}X_i^lY_i^m,$$
$$(l=0\div6,\ m=0\div6,\ l+m=n,\ n=1\div6)$$

Here, i = 1,2,…n – number of reference stars; X_i, Y_i and R_i – rectangular coordinates and distances of stars from the centers of plates; m_i – photometric measured data of stars; $f_{½i}$ – diameters of star images (FWHM); coefficients a_2, a_3, a_4 and c_2, c_3, c_4 define coma affects, coefficients a_5, c_5 – taking into account the magnitude equation, which is calculated separately; coefficients of the full sixth-order polynomial b_{lm} и d_{lm} (27 terms) in the generalized case describe the aberrations of telescope optics with the systematic errors of the scanner included. A step-by-step description of scanner systematic errors exclusion is set out in (Andruk, 2015).

Fig. 4 shows the results of the test plate processing. On the left side the trend of telescope systematic errors σ_α, σ_δ over the plate field is shown. Right panels demonstrate the trend of the residual differences Δα, Δδ. Negative and positive values of differences are shown by horizontal and vertical strokes which have linear dimensions according to the scale of values presented on the figure. Errors are obtained by averaging within 250x250 px cells.

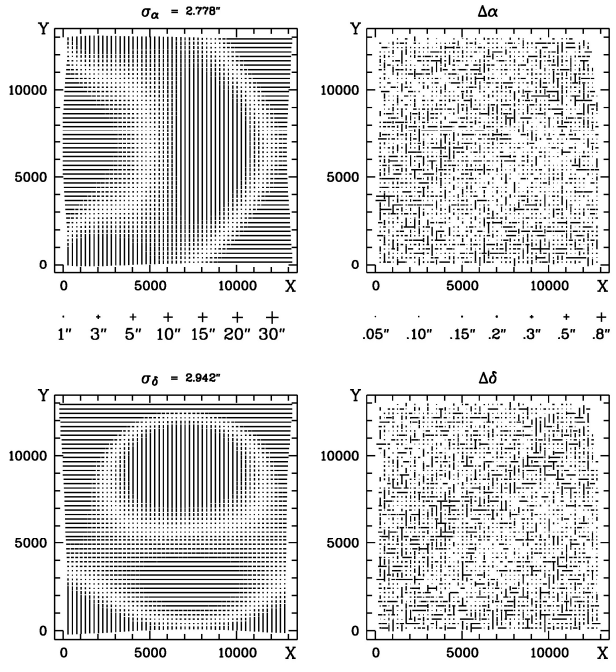

Figure 4: The distribution of errors and residual differences over the plate field as a result of the astrometric solution.

5. Photometric reduction into the system of photoelectric B-magnitudes

The reference system for the photometric solution is based on the photoelectric B_{pe}-values from catalogues (Kornilov, 1991, Mermilliod, 1991). The stages and principles of astronegative characteristic curve restoration accounting the field photometric equation and the data of two expositions are described in (Andruk, 2012). The approximation of the characteristic curve and determination of photographic B-magnitudes B_{ph} for all 477 plates were carried out by the least square method solution of the set of equation (2):

$$B_i = e_1 + e_2X_i + e_3Y_i + e_4R_i + e_5R_i^2 + e_6R_i^4 + \sum f_nm_i^n$$
$$(n=1,2,\ldots5) \qquad (2)$$

Here, i = 1,2,…n is the number of photoelectric data for standard star on the plate; X_i, Y_i и R_i are the rectangular coordinates and the distances from the center of the plate; m_i – instrumental photometric evaluations; coefficients e_2, e_3, e_4, e_5, e_6 define the field photometric equation; f_1, f_2, f_3, f_4, f_5 describe the functional form of the characteristic curve. The equation (2) was chosen as minimizing the errors of the reduction into the reference B_{pe} system in the best way.

6. Catalogue creation

When creating the catalogue the next steps were undertaken:

1. Digitizing of astronegatives using Microtek ScanMaker 9800XL TMA and Epson Expression 10000XL scanners with 1200 dpi resolution.
2. Conversion of the tiff-format files to the fit-format files using the GIMP package.
3. Calculation of the rectangular coordinates X, Y, photometric instrumental evaluations m, $f_{½}$ and other parameters using the MIDAS/ROMAFOT package for all registered objects.
4. Astrometric reduction of all objects into Tycho-2 reference system to obtain their position α, δ at the epoch of plates' exposure.
5. Conversion of instrumental photometric evaluations m into the reference system of photoelectric B_{pe}-magnitudes.
6. Calculation of mean values of equatorial coordinates α, δ and stellar magnitudes B for stars and galaxies in the limits of RA-overlapping of scans for each RA stripe. Elimination of artefacts.
7. Averaging of α, δ, B values in the overlapping areas between RA stripes.
8. Preparation of the catalogue of positions α, δ and stellar magnitudes B and its supplementation with proper motions data μ_α, μ_δ from UCAC4 (Zacharias, 2013).

The processing of scans was carried out using MIDAS/ROMAFOT software package. The photometric equalization of scans was made by taking into account the individual flat-field calculated for each plate separately (Andruk, 2005). The number of registered objects on the astronegatives, exposured in the areas of Milky Way reaches 300 000. The total number of objects found on the

whole set of 477 plates is around 25.933 million ones of different origin. Equatorial coordinates α, δ for all objects are obtained in the reference system of Tycho-2 at the epoch of exposition of each plate. As a rule, the reduction was made for full fields of plates with dimensions 8ºx8º, the exception was made for the high-latitude zones (84º and 88º) with a much smaller dimensions of processed fields. Photographic B_{ph}-magnitudes of objects were derived from equations (2) for characteristic curves of astronegatives calibrated with photoelectric B_{pe}-magnitudes.

The final positions and B-magnitudes of stars and galaxies as well as their errors were calculated by equations (3) and (4):

$$\begin{aligned} \alpha &= (\alpha_1/\sigma_{\alpha 1}^2 + \alpha_2/\sigma_{\alpha 2}^2) \;/\; (1/\sigma_{\alpha 1}^2 + 1/\sigma_{\alpha 2}^2) \\ \delta &= (\delta_1/\sigma_{\delta 1}^2 + \delta_2/\sigma_{\delta 2}^2) \;/\; (1/\sigma_{\delta 1}^2 + 1/\sigma_{\delta 2}^2) \\ B_{ph} &= (B_1/\sigma_{B1}^2 + B_2/\sigma_{B2}^2) \,/\, (1/\sigma_{B1}^2 + 1/\sigma_{B2}^2) \end{aligned} \qquad (3)$$

$$\begin{aligned} \sigma_\alpha &= (1 \,/\, (1/\sigma_{\alpha 1}^2 + 1/\sigma_{\alpha 2}^2))^{1/2} \\ \sigma_\delta &= (1 \,/\, (1/\sigma_{\delta 1}^2 + 1/\sigma_{\delta 2}^2))^{1/2} \\ \sigma_B &= (1 \,/\, (1/\sigma_{B1}^2 + 1/\sigma_{B2}^2))^{1/2} \end{aligned} \qquad (4)$$

7. The accuracy of the catalogue

The comparison of 171 124 reference stars of the catalogue with Tycho-2 gives the errors of the astrometric reduction $\sigma_{\alpha\delta} = \pm 0.06"$.

The errors of photometry were derived from comparison of calculated stellar magnitudes with the photoelectric values of 5130 stars from the photometric reference catalogues. The errors are $\sigma_B = \pm 0.12^m$.

The comparison of the catalogue with UCAC-4 gives the positional errors in relation to UCAC4 at the level of $\sigma_{\alpha\delta} = \pm 0.33"$ (1 928 367 stars and galaxies were cross-identified in both catalogues).

8. Conclusion

The comprehensive software was developed and implemented in the Department of the Astrometry MAO NASU to process the digitized astronomic negative plates as well as to obtain the final product in the form of a catalogue of positions and stellar magnitudes of stars and galaxies. The above version of the catalogue created in the circumpolar zone of FON project contains 1 975 967 stars and galaxies down to $B \le 16.5^m$ at the epoch 1985.28. The positions of objects are obtained in the reference system of Tycho-2. The stellar magnitudes B are in the system defined by photoelectric standards. The internal accuracy of the catalogue for all objects is $\sigma_{\alpha\delta} = \pm 0.23"$ and $\sigma_B = \pm 0.12^m$. For the stars in the interval of magnitudes $B = 8^m$ -13^m the errors are $\sigma_{\alpha\delta} = \pm 0.11"$ and $\sigma_B = \pm 0.06^m$.

The convergence of the coordinates with the Tycho-2 reference system obtained on 171 124 stars is $\sigma_{\alpha\delta} = \pm 0.06"$. The convergence of magnitudes with the photoelectric values B_{pe} for 5 130 stars is $\sigma_B = \pm 0.15^m$. The positional errors of the catalogue derived on 1 928 367 cross-identified stars in comparison to UCAC4 are $\sigma_{\alpha\delta} = \pm 0.33"$.

The algorithms and methods of plate digitizing and processing and the software developed in the Department of Astrometry MAO NASU is now applied for the total set of exposured plates of the FON project with the aim of creating the catalogue of positions and B-magnitudes of the whole northern sky from 0º to 90º on declination.

The created star catalogue of the positions and stellar magnitudes of the circumpolar zone of the FON project will be posted on the web pages of the MAO NASU and UkrVO. The catalogue contains the equatorial coordinates of 1 975 967 stars and galaxies (α, δ) on the equinox 2000.0 and the epoch 1985.28 as well as the stellar magnitudes (Bph). We provide the errors definitions of these values and number of determinations as well as an additional information in the form of the average values for the diameters of star images $f_{½}$ (FWHM) and the values of the maximal intensity in the center of object images (cInt).

Acknowledgements. The authors are grateful to the MAO NASU ACISS for the technical assistance. The authors thank Ph.D. P.F.Lasorenko for consultations. This work was partially supported by the Ukrainian Astronomical Association.

References

Andruk V.M. et al.: 2005, *Kinem. Phys. Cel. Bodies*, **21, N5**, 396.
Andruk V.M. et al.: 2005, *Kinem. Phys. Cel. Bodies. Supl.*, **N5**, 413.
Andruk V.M. et al.: 2007, *J. Phys. Studies*, **11, N3**, 329.
Andruk V.M. et al.: 2010, *Kinem. Phys. Cel. Bodies*, **26, N3**, 75.
Andruk V.M. et al.: 2012, *Visnyk KNU, Astronomy*, **N48**, 11 *(in ukraine)*.
Andruk V.M. et.al.: 2014, *Odessa Astron. Publ.*, **27/1,** 53.
Andruk V.M. et al.: 2015, 2015arXiv, in press.
Andruk V.M. et al.: 2016, *Kinem. Phys. Cel. Bodies*, **32, N1**, 56 (in press).
Golovnya V.V. et al.: 2010, *J. Phys. Studies*, **14, N2**, 2902.
Kazantseva L.V. et.al.: 2015, *Kinematics and Physics of Celestial Bodies*, **31, N1**, 58.
Kislyuk V.S. et al.: 2000, *Kinem. Phys. Cel. Bodies*, **16, N6**, 483.
Kornilov V.G. et al.: 1991, *Trudy GAIS*, **63**, 1.
Mermilliod J.C.: 1991, *Homogeneous means in the UBV system*.
Muminov M.M. et.al.: 2014, *Odessa Astron. Publ.*, **27/1,** 57.
Protsyuk Yu.I. et.al.: 2014, *Odessa Astron. Publ.*, **27/1,** 59.
Protsyuk Yu.I. et.al.: 2014, *Odessa Astron. Publ.*, **27/1,** 61.
Protsyuk Yu.I. et.al.: 2014, *Odessa Astron. Publ.*, **27/1,** 63.
Protsyuk Yu.I. et.al.: 2014, *Kinematics and Physics of Celestial Bodies*, **30, N6**, 54.
Vavilova I.B. et al.: 2012, *Kinem. Phys. Cel. Bodies*, **28 N2**, 85.
Vavilova I.B. et al.: 2012, *Baltic Ast*., **21, N3,** 356.
Vavilova I.B. et.al.: 2014, *Odessa Astron. Publ.*, **27/1,** 65.
Yatsenko A.I. et al.: 2011, *Kinem. Phys. Cel. Bodies*, **27, N5**, 249.
Yizhakevych O. et.al.: 2014, *Odessa Astron. Publ.*, **27/1,** 67.
Zacharias N. et al.: 2013, *AJ*, **145**, 44.

CATALOGUES OF THE FAINT OBJECTS IN THE AREAS WITH GAMMA-RAY BURSTS

V.V. Golovnia[1], Yu.I. Protsyuk[2], V.M. Andruk[1], I.B. Vavilova[1], L.K. Pakuliak[1], I.V. Kulyk[1], Ya.O. Romanyuk[1], O.R. Baransky[3]

[1] Main Astronomical Observatory NAS of Ukraine, Kyiv, Ukraine, *golov@mao.kiev.ua, andruk@mao.kiev.ua*,
[2] Nikolaev Astronomical Observatory, Mykolaiv, Ukraine, *yuri@nao.nikolaev.ua*
[3] Taras Shevchenko National University of Kyiv, Kyiv, Ukraine

ABSTRACT. The results of GRB observations are being published in the GCN Circulars in real-time. To study all the objects in the sky areas around the GRBs we identified them on the digitized MAO Double Wide angle Astrograph (DWA) plates (D/F=40/200) within a circle with the radius of dozens of arcminutes. We selected only GRBs with the positional accuracy between ±0.3" and ±7.5" and the range of magnitudes between 14^m and 20^m.

We used MIDAS/ROMAFOT package to obtain the catalogues of the faint objects in small areas in the GRBs vicinity. For the plates of DWA telescope the positional rms errors are ± 0.20" for RA and DEC, the photometric errors are ± 0.20^m. All positions were obtained in Tycho-2 system.

Keywords: gamma-ray burst, astronomical data base, methods: data analysis

1. Introduction

Gamma-ray bursts are the most powerful explosions known in the Universe. Now they are identified with the regions of formation of massive stars in galaxies and the parent short-lived explosions of massive stars, which have a random spatial distribution in the sky (Sokolov et al., 2009; Raikov et al., 2010; Kienlin.et al., 2014; Gerasim et al., 2015).

The astroplates give us an unique opportunity to identify the optical counterparts of the GRBs and study all the objects in the vicinity of the registered GRB (Golovnya et al., 2012, 2014; Pakuliak et al., 2013; Vavilova et al., 2014). With this aim we used MIDAS/ROMAFOT software package to obtain catalogues of the faint objects in small areas in the vicinity of the registered GRB. This software was developed at the MAO NAS of Ukraine for processing the scanned records to get a high precision astrometric and photometric data of objects (Andruk et al., 2005, 2007, 2010, 2014; Yatsenko et al., 2011; Golovnya et al., 2010).

2. Search of optical analogs of GRB

The results of GRB observations are being published in the GCN Circulars in real-time (Barthelmy, 2015). The Database of Joint Digital Archive (JDA) of Ukrainian Virtual Observatory (UkrVO), which contains observational data obtained at Ukrainian observatories, was used to search for optical analogs of GRBs on the astroplates (Sergeeva et al., 2004; Vavilova et al., 2010, 2012a, 2012; Pakuliak et al., 2012; Protsyuk et al., 2014).

Table 1 shows the optical coordinates of some GRBs and their precision (sigm) from GCN Circulars, for which the optical identifications were successful (Beardmore et al., 2015; Goad et al., 2015; Osborne et al., 2015; Evans et al., 2015). The table also lists numbers of the plates (N) from JDA UkrVO for the corresponding objects.

Table 1: The number of plates (N) in JDA UkrVO

GRB	RA, Dec, J2000 h m s deg ' "	Sigm ", ±	N
150728A	19:28:55.28+33:54:57.8	4.1	3
150626B	12:30:32.04+66:46:18.6	1.7	5
150607A	09:19:57.25+68:26:09.6	1.4	3
150530A	21:50:02.94+57:30:59.8	1.6	9
150527A	19:15:50.32+04:12:06.9	1.5	9
150423A	14:46:18.96+12:17:00.6	1.8	10
150323A	08:32:42.74+45:27:52.8	1.9	6

However, the identification process was not always successful. Let us give an example of the search for GRB 140419A (Osborne et al., 2014). At the first detection this object had a magnitude of ~13.5, then it was increased to 12.5 in ~70 sec and then the brightness decayed fast to ~14.3^m for about 350 sec (Guver et al., 2014). We found two plates obtained in 1978 and 1990 with the desired areas, but we could not find the optical analogue of this GRB. Also, no optical counterpart was found in the close vicinity of GRB 140818B (Beardmore et al., 2014). But inspecting larger area around this object, we found some images near GRB position on both selected plates. Brightness of the objects was estimated as V=15.0 and V=16.5 (Golovnya, 2014).

The five plates were found in JDA UkrVO for GRB 150212A and GRB 150213B, but they had no optical analogue (Evans et al., 2015, Golovnya, 2015, Osborne et al., 2015, Golovnya, 2015).

Three plates with the GRB150220A (Evans et al., 2015) were found with a limited magnitude of 16.4, 15.6 and 15.7 respectively. Two objects were found on plate GUA040C002183, EPOCH=1993.2192. Fig. 1 shows 13′x13′ area around GRB150220A with these two objects. The coordinates and B magnitudes were obtained in the system of TYCHO-2 catalogue with rms errors of 0.093", 0.099", 0.21^m for right ascension, declination, and magnitudes respectively (Golovnya & Andruk, 2015).

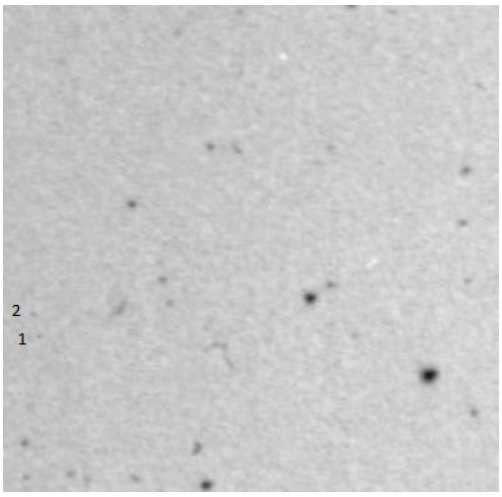

Figure 1: The area of GRB150220A with identified Obj1 and Obj2

We observed the same field around GRB 150220A with 0.7-m f/4 reflector of Kyiv comet station on Mar 10, 2015 during 18 days after the burst has been occurred. The telescope is equipped with CCD (1027x1056 pixels with a scale of 0.95"/px). We obtained 21 CCD frames with 60 sec expositions in R-filter (Romanyuk et al., 2015). The individual frames were summed in order to increase the signal. We did not find aforementioned images of Obj1 and Obj2 on the final CCD frame. However, we confirmed some of the positions of X-ray sources reported early by P.A. Evans. Table 2 contains the coordinates of X-ray sources given by Evans et al. (2015) and their optical identifications made with the CCD.

Table 2: Source's position as follows by P.A.Evans (GCN 17501) and Ya.O.Romanyuk (GCN 17645).

	GCN 17501		GCN 17645	
	h m s	° ' "	h m s	° ' "
1	9 01 31.65	-01 39 07.6	outside our field	
2	9 01 30.74	-01 38 27.0	outside our field	
3	9 02 08.55	-01 36 59.1	9 02 08.1	-01 36 35
4	9 02 08.90	-01 40 20.1	extremely faint	
5	9 01 28.27	-01 39 06.3	outside our field	
6	9 02 25.29	-01 41 14.9	9 02 25.3	-01 41 15
7	9 01 46.37	-01 38 13.9	9 01 46.4	-01 38 14

We detected the optical counterpart (18.3^m) of the GRB 151027A with 0.5-m telescope Mobitel KT-50 of the Nikolaev observatory with Alta-U9000 CCD with R-filter (Protsyuk & Kovalchuk, 2015).

3. Creation of catalogs of objects in the areas around GRBs

As it was shown above, the optical counterparts of some GRBs and X-ray sources can be identified with the plates from the JDA UkrVO. With this aim we decided to create the catalogues of faint stars in the vicinity of GRBs (the catalogues are under development). At the first step we scanned the plates with resolution of 1200 dpi, but in order to increase a positional accuracy, we shall rescan the plates with resolution of 1600 dpi.

Special tools were also developed, which allowed obtaining the positions and magnitudes of faint stars with accuracy of about ± 0.20" and ± 0.20^m respectively. Each catalogue covers the sky area of about 10-20 arcmin and contains the coordinates and magnitudes of about hundreds of stars. The TYCHO2 or UCAC4 catalogues are used as reference ones. The developed tools allow us the fast cross-identification between the lists of the obtained optical positions of the faint stars and GRB coordinates (Protsyuk et al., 2014a, 2014). The catalogues will be put on the UkrVO web-site after completing.

Acknowledgements. This work was partially supported by the Ukrainian Astronomical Association.

References

Andruk V.N. et al.: 2005, *Kinematika i Fizika Nebesnykh Tel*, **21**, N5, 396.
Andruk V. et al.: 2007, *J. Phys. Studies*, **11**, No3, 329.
Andruk V.M. et al.: 2010, *Kinem. Physics Celest. Bodies*, **26**, No3, 146.
Andruk V.N. et al.: 2014, *Odessa Astron. Publ.*, **27/1**, 53.
Barthelmy S.: 2015, *gcn.gsfc.nasa.gov.*
Beardmore A.P. et al.: 2014, *GCN 16712*.
Beardmore A.P. et al.: 2015, *GCN 18088*.
Evans P.A. et al.: 2015, *GCN 17879, GCN 17735*.
Evans P.A. et al.: 2015, *GCN 17452*.
Evans P.A.: 2015, *GCN 17501*.
Gerasim R.V. et al.: 2015, *Astrophys.*, **58/2**, 204.
Goad M.R. et al.: 2015, *GCN 17615*.
Goad M.R. et al.: 2015, *GCN 17968, GCN 17889*.
Golovnya V. et al.: 2010, *J. Phys. Studies*, **14**, No 2, 2902.
Golovnya V. et al.: 2012, *Kyiv Univ. Messenger. Astronomy*, **49**, 36 (in ukrainian).
Golovnya V.V.: 2014, *GCN 16757*.
Golovnya V. et al.: 2014, *www.astroplate.cz/wp-content/uploads/2014/01/Golovnya_UkrVO_new_life.pdf*
Golovnya V.V.: 2015, *GCN 17473*.
Golovnya V.V.: 2015, *GCN 17484*.
Golovnya V.V., Andruk V.M.: 2015, *GCN 17589*.
Guver T. et al.: 2014, *GCN 16120*.
Kienlin A. et al.: 2014, *Astroph. J. Suppl. S.*, **211**, 13.
Osborne J.P. et al.: 2014, *GCN 16124*.
Osborne J.P. et al.: 2015, *GCN 17475*.
Osborne J.P. et al.: 2015, *GCN 17905*.
Pakuliak L et al.: 2012, *IAUS*, **285**, 389.
Pakuliak L. et al.: 2013, *Odessa Astron. Publ.*, **26/2**, 236.
Protsyuk Yu., Kovalchuk O.: 2015, *GCN 18533*.
Protsyuk Yu.I. et al.: 2014, *Odessa Astron. Publ.*, **27/1**, 59.
Protsyuk Yu.I. et al.: 2014, *Kinemat. Physics Celest. Bodies*, **30**, N6, 54.
Raikov A.A. et al.: 2010, *Astrophys.*, 53, 3, p.396.
Romanyuk Ya. et al.: 2015, *GCN 17645*.
Sergeeva et al.: 2004, *Baltic Astronomy*, **13**, No 4, 677.
Sokolov V.V. et al.: 2009, Workshop "Many faces of GRB phenomena – optics vs high energy".
Vavilova I.B., Pakuliak L.K., Protsyuk Yu.I.: 2010, *Kosmichna Nauka i Tekhnologiya*, **16**, 62.
Vavilova I.B. et al.: 2012, *Kinem. Physics Celest. Bodies*, **28**, No2, 85.
Vavilova I.B. et al.: 2012, *Baltic Astronomy*, **21**, 356.
Vavilova I. et al.: 2014, *Odessa Astron. Publ.*, **27/1**, 65.
Yatsenko A.I. et al.: 2011, *Kinem. Physics Celest. Bodies*, **27**, No5, 249.

RESEARCH OF THE LONG-TERM BEHAVIOUR OF THE PLEIADES BY USING OF PHOTOGRAPHIC PLATES FROM UKRVO DIGITAL ARCHIVE AND BALDONE OBSERVATORY

L.V.Kazantseva[1], V.M.Andruk[2], S.V.Shatokhina[2], Yu.I.Protsyuk[3], I.Eglitis[4], M.Eglite[4]

[1]Astronomical Observatory of Kyiv Shevchenko National University, Observatorna St. 3, Kyiv, 04053, Ukraine, *likaz@observ.univ.kiev.ua*
[2] Main Astronomical Observatory of National Academy of Sciences, Akad. Zabolotnogo St. 27, Kyiv, 03680, Ukraine, *andruk@mao.kiev.ua, svetash@mao.kiev.ua*
[3] Research Institute Nikolaev Astronomical Observatory, Observatornaya St. 1, Mykolaiv, 54030, Ukraine, *yuri@nao.nikolaev.ua*
[4] Baldone Observatory, Institute of Astronomy, University of Latvia Baldones Riekstukalns, Rigas raj., LV 2125, Latvia, *ilgmars@latnet.lv*

ABSTRACT. The Pleiades Star Cluster (M45) is one of the most studied star clusters in the galaxy. At the same time as part of the Pleiades are many long-period variable stars, including flashing that need further study. Recent work on the processing of photographic images of the Pleiades obtained at different observatory revealed a number of star clusters with large variations in coordinates, the reason you want to understand. Collection of UkrVO unified digital archive contains a number of plates with images of the stars of the Pleiades obtained on different instruments. Processing of this material allows to test out standard programs for digital astronomical images processing. Also we will add information about variable stars and will improve the coordinates and proper motions of cluster stars. Selected material covers the period 1909 – 1999 years. The plates have different margins, scale, number of stars on images and obtained limiting magnitude. Exactly this diverse set of options lets you to be sure of results.

Keywords: virtual observatory tools – astrometry – techniques: data analysis: star cluster – M45.

1. Introduction

Pleiades Star Cluster (M45) is one of the most studied star clusters in the Galaxy, but still continues its active research: rotation, inflation, and lithium in the Pleiades (Somers, 2015); search for free-floating planetary-mass objects in the Pleiades (Zapatero Osorio, 2014); empirical isochrones, luminosity, and mass functions of the Pleiades cluster (Bouy, 2015).

The Pleiades became the object of interest for digitization: possible Cyclic Activity of the Pleiades' Star (Hambaryan, 2003); for studying the long-term behaviors of the Pleiades flare stars (Tsvetkov, 2002); search for extrasolar Planets in the Pleiades (Yamamoto, 2013).

We are considering two problems: testing of a comprehensive program digitized images processing (Andruk, 2010) and search for changes in the laws of time astrometric and photometric data for the stars of the Pleiades.

2. Plates with Pleiades Star Cluster in UkrVO archives and taken for processing

Now Joint Electronic Archive of UkrVO (Vavilova, 2012) has 339 M45 images in 16 particular archives, which were obtained in the 8 observation points.

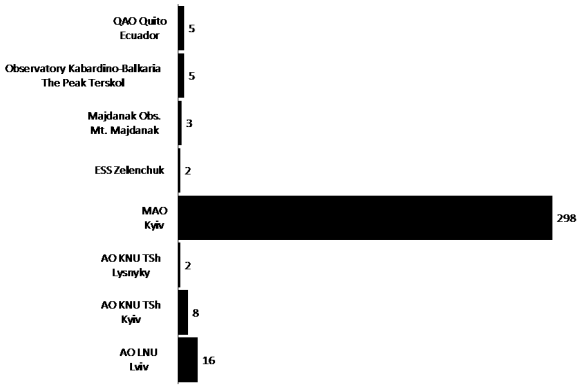

Figure 1: Distribution of observation points data

In addition, we have included in the processing 38 plates of Research Institute "Nikolayev Astronomical Observatory" and 60 plates of Baldone observatory of Institute of Astronomy, University of Latvia.

Photographic plates were scanned using different scanners. Digital images processing was carried out by one and the same comprehensive program. Already wear processed 36 plates for different instruments.

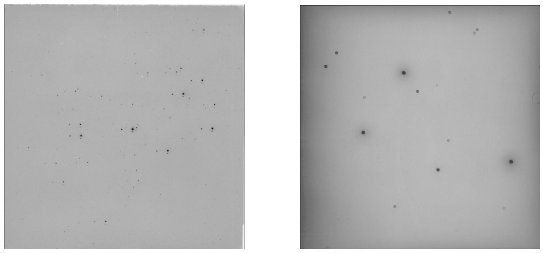

Figure 2: Scan images of plates with different scales.

Work began recently, made only its initial stage, was processed only 1/10 of the planned material, continues to develop a standard approach to the accurate identification of the stars in a large number of objects in an image, were obtained astrometric and photometric data.

Table 1. Number of plates for each telescope.

Instrument	AO	D m	F m	N
Zeiss Zonal Astrograph	NAO	0,1	2,0	10
Zeiss-600	Terskol	0,6	7,5	4
Double Astrograph Repsold	AOKNU	0,2	4,3	2
Double Long Focus Astrgraph	MAO	0,4	5,5	9
Double Wide Angle Astrograph	MAO	0,4	2,0	3
Baldone Schmidt Telescope	BAO	1,2	2,4	4
Three-Camera Astrograph	MAO	0,1	1,7	2
Unknown	AOKNU			2

3. Preliminary results

The scans processing was carried out using MIDAS/ROMAFOT software package, with the individual flat-field calculated for each plate separately (Andruk, 2005; Andruk, 2014).

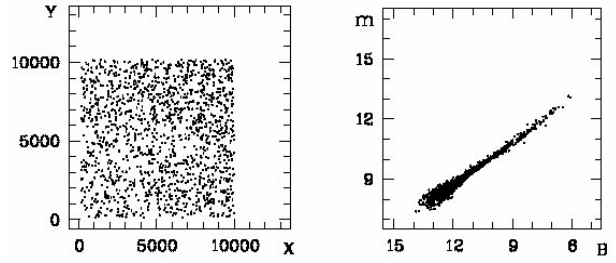

Figure 3: Digital image and the dependence of the magnitude for plate N0078.

The processing of digital images of various sources has been described repeatedly (Kazantseva, 2015; Protsyuk, 2014). We used the standard method of complex processing and compared the results virtually the same region of the sky for the various epochs and observation conditions.

Table 2. The internal accuracy for all objects on the coordinates.

Instrument	mean rmsRA	mean rmsDE
Zeiss Zonal Astrograph	0,135″	0,150″
Zeiss-600	0,283	0,090
Double Astrograph Repsold	0,089	0,093
Double Long Focus Astrograph	0,056	0,050
Double Wide Angle Astrograph	0,096	0,087
Baldone Schmidt Telescope	0,129	0,108
Three-Camera Astrograph	0,092	0,087
Unknown	0,541	0,493

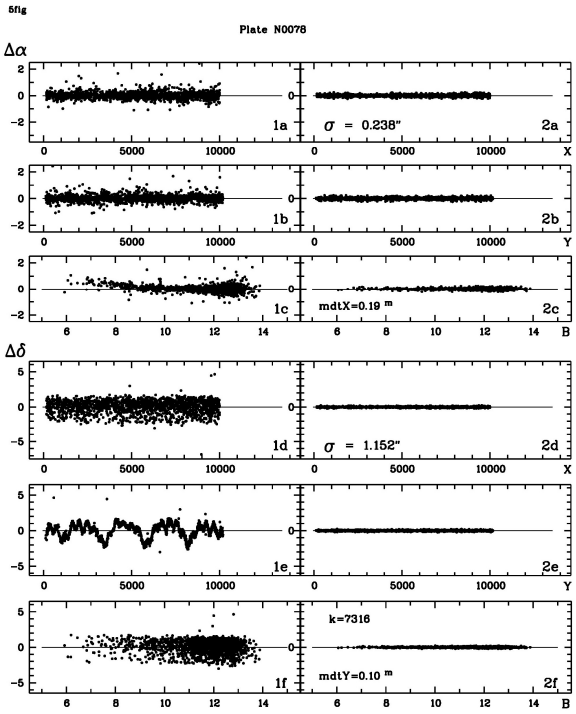

Figure 4: The residual differences in coordinates after the program corrections for plate N0078.

Preliminary analysis of the material obtained allows us to make some conclusions:

– Standard image processing of brightest stars requires improvement.

– Photometric data require additional account information (filters, emulsion, exposure time, etc.).

– Preparation of O-C coordinates on different epochs of observations demonstrate the manifestation of his own movements, which are known for certain stars reach 21 mas/year for RA and 47 mas/year Dec.

References

Andruk V.M. et al.: 2010, *Kinem. Phys. Cel. Bodies*, **26, N3**, 75.

Andruk V.M. et al.: 2005, *Kinem. Phys. Cel. Bodies*, **21, N5**, 396.

Andruk V.M. et.al.: 2014, *Odessa Astron. Publ.*, 27/1, 53.

Bouy H. at al.: 2015, *A&A*, **577, id. A148**, 17.

Hambaryan V. et al.: 2012, *PASRB*, **11**, 259.

Kazantseva L.V. et al.: 2015, *Kinem. Phys. Cel. Bodies*, **31, N1**, 58.

Protsyuk Yu.I. et al.: 2014, *Odessa Astron. Publ.*, 27/1, 59.

Protsyuk Yu.I. et al.: 2014, *Odessa Astron. Publ.*, 27/1, 61.

Somers G. et al.: 2015, *MNRAS*, **449, N 4**, 4131.

Tsvetkov M. et al.: 2005, *Kinem. Phys. Cel. Bodies*, *Supl., 5,* 567.

Vavilova I.B. et al.: 2012, *Kinem. Phys. Cel. Bodies*, **28, N2**, 85.

Yamamoto K. et al.: 2013, *PASJ*, **65, N 4**, 19

Zapatero Osorio M. R. et al.: 2014, *A&A,* **568, id A77**, 16.

CROSS-MATCHING OF VERY LARGE CATALOGS

M. V. Martynov, D. V. Bodryagin

Research Institution "Mykolaiv Astronomical Observatory"
Observatorna St., 54030, Mykolaiv, Ukraine

ABSTRACT. Modern astronomical catalogs and sky surveys, that contain billions of objects, belong to the "big data" data class. Existing available services have limited functionality and do not include all required and available catalogs. The software package ACrId (Astronomical Cross Identification) for cross-matching large astronomical catalogs, which uses an sphere pixelation algorithm HEALPix, ReiserFS file system and JSON-type text files for storage, has been developed at the Research Institution "Mykolaiv Astronomical Observatory".

Keywords: database, catalogs, virtual observatory.

1. Introduction

Cross-identification is a powerful tool which is used for solving many astrometric and astrophysical problems. Numerous programs and Web services (like CDS X-Match Service http://cdsxmatch.u-strasbg.fr/xmatch) has been developed for this in frames of Virtual Observatory (VO). Unfortunately, their functionality and options are restricted by next reasons:

– the limited list of catalogs which are available for cross-identification;

– rigorously specified object identification algorithms;

– some restrictions and difficulties in cross matching and uploading/downloading of large (hundreds of thousands or more objects) user data sets.

2. Cross-matching of the astronomical data with the software package ACrId (Astronomical Cross Identification)

This software product is a package of console scripts written in the Python programming language. There were implemented the following steps:

1) Data preparation (preprocessing and pixelation of selected catalogs);

2) Cross-identification of the objects;

3) Output and saving of the cross-matching results in the user formats.

Most of astronomical catalogs and surveys are available in two types: text (XML-format VOTable) or binary and have different patterns of records. The first stage is carried out to convert the selected digital catalogs into a common format of the JSON-type text file. This conversion allows you to describe all the different catalogs with help of uniform rules and makes easier adding other catalogs and lists of absolutely various structure, origin and type. Standard form of catalog description includes three files

1) General description;

2) List of files of the catalog (original, before pixelation);

3) Description format.

The next stage of the preparation data of "big data" type to cross-matching consists in partitioning the selected file into separate fragments. The pixelation of the sphere is frequent and efficient solution of many problems because in astronomy we have deal with data distributed on the celestial sphere. Pixelation means subdivision spherical surface on numbered fragments of equal area. Usage of pixelation allows not only to solve the problem of celestial map representation and analysis, but is also essential by constructing databases that require quick search of celestial objects. Pixelation also does possible to use several PC simultaneously for cross-matching of large surveys. There are some systems of pixelation. We used hierarchical grid with equal squares HEALPix (Hierarchical Equal Area isoLatitude Pixelization) (Górski et al., 2005). Pixelation sphere has a number of advantages over the previously used method of the sphere division using the equatorial coordinates. However, there is a technical problem when we divide sphere into pixels to place them on the HDD (if the pixel size is about half an arc minute, then their number will exceed 805 million). Not every system can create so many files. For example, the NTFS file system (OS MS Windows) allows you to create more than 4 billion files, but the creation of empty 805 million files of zero size takes about 320 GB of disk space. You can't also change the maximum number of files available without formatting the partition in the ext3 and ext4 file systems (OS Linux) and there is need more than 200GB (depending on the size of the cluster partition) for the creation of 805 million empty files. It turned out that the best choice for solving the problem is ReiserFS file system, which was designed specifically to work with a lot of small files. There are no restrictions on the maximum available number of system files and 805 million zero size files occupy only 82 GB. After the "zero" pixelation sphere, that is, after the creation of zero

size files, it is necessary to fill in their by respective objects from the catalogs. As noted earlier list of catalogs can be arbitrary because the unified files JSON-type text format were created for all catalogs before pixelation process. The actual process filling the pixels can last from several hours to several weeks depending on the computing capacity and size of the input catalog. It should be noted that this version of the data preparation for cross-identification requires high-capacity HDD for long-term storage of the results of catalogs pixelation. The advantage of this option is lack of necessity to build additional indexes to locate the data quickly, since the role of the search tree plays the file system itself in which files and folders are named and arranged so that they are playing the role of "frozen" fast path to data.

In general, the task of cross-identification astronomical objects in different catalogs is search the same source in some lists of coordinates. The main problems in this case are different epochs of observations and different limiting magnitudes of the catalogs. The first one requires taking account proper motions and their error. This leads to the fact that the use of only coordinate criterion for identification does not always yield successful results. The object may be absent in this neighborhood, or there may be several candidate objects from another catalog. Preliminary pixelation allows us to carry out a so-called "cascade" cross-identification with using more than two catalogs. This enables the construction of additional filters, which ultimately reduces the error of false identifications.

The ACrId software package has a wide range of applications in our observatory. HealPix pixelation of some basic astrometric catalogs, including the catalog of XPM (Fedorov et al., 2009), which is not in the database CDS, have performed. The results are used to calculate and the study of the proper motions of stars.

Usage the software allowed us to obtain the first version of the compiled catalog of stars with high proper motion (HPM) on the whole celestial sphere (about 968,251 objects). The distribution of the stars in the equatorial coordinates is shown in Figure 1.

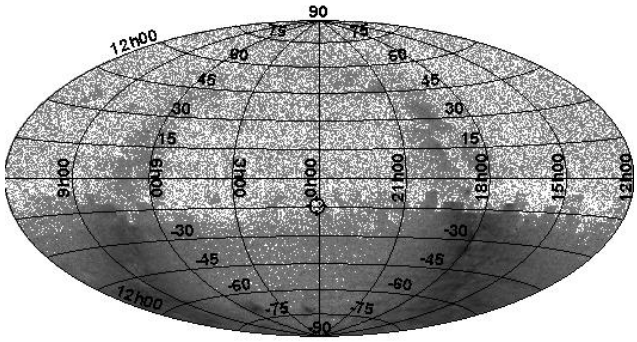

Figure 1: Distribution HPM stars on celestial sphere in equatorial coordinates.

As can be seen from the fig. 1, there are a huge number of HPM stars with proper motion more than 150mas/year on the Southern hemisphere. To validate this result, it is planned to get a second version of the catalog using the represented software with an expanded list of modern celestial catalogs and surveys.

3. Conclusion

The software package of extra-large astronomical catalogs pixelation and cross-identification "ACrId" is used to division the celestial sphere on small plots of equal area (pixels) for the following usage pixel numbering as search index. Program "ACrId" allows you to cross-matching an arbitrary number of catalogs with any format and carry out multi-stage objects cross-identification for the search common objects and determinations their parameters.

References

Górski K. M.: 2005, *AphJ*, **622**, **2**, 759.
Fedorov P.: 2009, *MNRAS*, **393**,133.
http://cdsxmatch.u-strasbg.fr/xmatch

DETERMINATION OF PROPER MOTIONS OF CIRCUMPOLAR STARS BY USING IMAGES FROM UKRVO PLATE ARCHIVES

Yu. Protsyuk[1], V. Andruk[2], A. Mazhaev[1], O. Kovylianska[1] , S. Protsyuk[1], V. Golovnya[2]

[1] Research Insitute: Nikolaev Astronomical Observatory (RI NAO), Ukraine, yuri@nao.nikolaev.ua , mazhaev@nao.nikolaev.ua

[2] Main Astronomical Observatory (MAO) of National Academy of Sciences (NAS), Ukraine, andruk@mao.kiev.ua , golov@mao.kiev.ua

ABSTRACT. UkrVO plate archives contain information obtained at different time periods and in different observatories for the same regions of the sky [3, 5, 6, 7, 8]. It allows us to carry out joint processing of plates and to receive new results for interesting objects. To obtain proper motions of stars in circumpolar areas, we selected 34 photographic plates from the RI NAO archive and 161 plates from the archive of the MAO NAS. A mean epoch difference between the plates from these archives is 55 years. Scanning of the plates and data processing were independently carried out by both observatories. A catalog of equatorial positions for 195 thousand stars up to 15^m was compiled in the RI NAO (black dots in Fig. 1). A catalog of equatorial positions for 1050 thousand stars up to 16.5^m was compiled in MAO (gray dots in Fig. 1). A comparison of positions for common stars contained in these catalogs was conducted. A catalog of proper motions for 30 thousand common stars up to 15^m was compiled using these two input catalogs. The obtained result suggests the advisability of processing of all observations to receive proper motions of stars up to $14\text{-}15^m$ in the declination zone of 65° to 90°.

Keywords: Astrometry – Proper motions – Astronomical data bases – Catalogs – Virtual observatory tools.

1. Introduction

We selected photographic plates containing circumpolar stars in declination zone of 65° to 90°. All plates in the RI NAO archive were obtained with the Zonal Astrograph (ZA, D/F = 12/204, 101"/mm, FoV 5°x5°). Selected plates from the MAO archive were obtained with the Double Wide-angle Astrograph (DWA, D/F = 40/200, 103"/mm, FoV 8°x8°). The plates were obtained with up to four fold overlap in MAO and usually without overlapping in the RI NAO. Therefore, the same star was observed two to four times in the MAO and one or two times in the RI NAO.

2. Virtual observatory tools

We compiled both catalogs in accordance with the VOTable standard, which was produced and endorsed by the Executive Committee of the International Virtual Observatory Alliance. Usage of the VOTable standard allows us to apply wide range of VO tools to visualize and examine tabular data. For example, Aladin sky atlas allowed us to visualize obtained equatorial positions, which are shown in Figure 1. Tool for OPerations on Catalogues And Tables (TopCat) allowed us to carry out cross correlation of stars contained in different astrometric catalogs and to examine linear correlation of proper motions for found common stars.

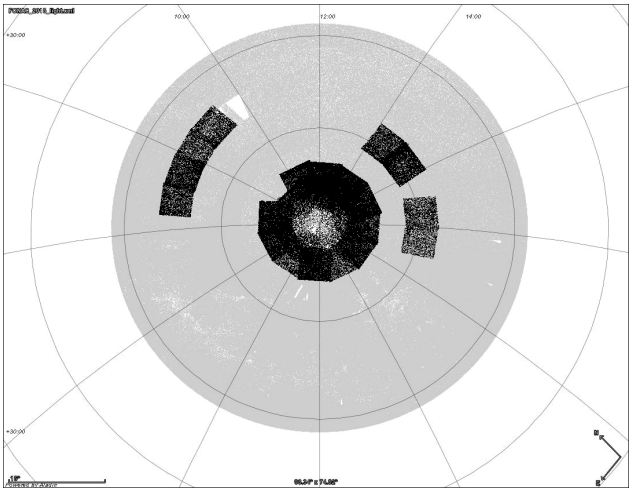

Figure 1: Equatorial positions of stars from two catalogs.

3. Data processing

The mean first epoch of 34 selected plates is 1930.3. Total number of plates for the first epoch of observations of circumpolar stars in the RI NAO archive is 196. The mean second epoch of 161 selected plates is 1985.7. The MAO archive contains about 2000 plates in the declination zone of 65° to 90°. These plates were obtained during the observation campaign of FON project. The Russian or Ukrainian acronym FON stands for Photographic Survey of the Northern Sky.

Each selected plate from the MAO archive was scanned only once with a resolution of 1200 dpi. Each selected plate from the RI NAO archive was scanned five or six times with a resolution of 1200, 1500 or 1600 dpi. As the result of plate scanning at the MAO, we obtained two to four equatorial positions for every star. The number of positions depends on number of available plates, which cover a given region of interest (ROI) in the sky. As the result of plate scanning at the NAO, we obtained six to twelve equatorial positions for each

star. The number of positions depends on number of scans for one or two available plates in a given ROI. Both observatories conducted the raw image processing by using the same procedures and MIDAS/ROMAFOT package to obtain (X, Y) coordinates [4]. Both observatories carried out astrometric reduction in the Tycho-2 system by using different software, namely 00plate in MAO and plate_gr in NAO [1] to compare obtained results of data processing.

4. Comparison of catalogs

The catalog of positions for 195 thousand stars up to 15^m was compiled in the RI NAO. The catalog of positions for 1050 thousand stars up to 16.5^m was compiled at the MAO. Numbers of stars versus magnitude are shown in the left part of Figure 2 as empty and filled circles for the RI NAO and the MAO catalogs respectively. Common ROI in the sky for both catalogs are shown in Figure 1. Numbers of stars in the common ROI are shown in the right part of Figure 2 as filled and empty circles for the RI NAO and the MAO catalogs respectively.

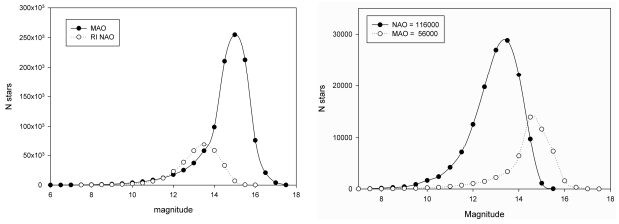

Figure 2: Number of stars for two input catalogs (left) and number of stars in common ROI (right) vs magnitude.

Standard deviations (SD) of positions of input catalogs are $\sigma_\alpha = \pm 0.24$" and $\sigma_\delta = \pm 0.23$" for the MAO catalogue, and $\sigma_\alpha = \pm 0.10$" and $\sigma_\delta = \pm 0.17$" for the RI NAO. Inner accuracies of equatorial positions versus declination are shown in Figure 3 for both input catalogs. The plate_gr software used in NAO provides us better results than 00plate software used in MAO, especially near 90° (Figure 3).

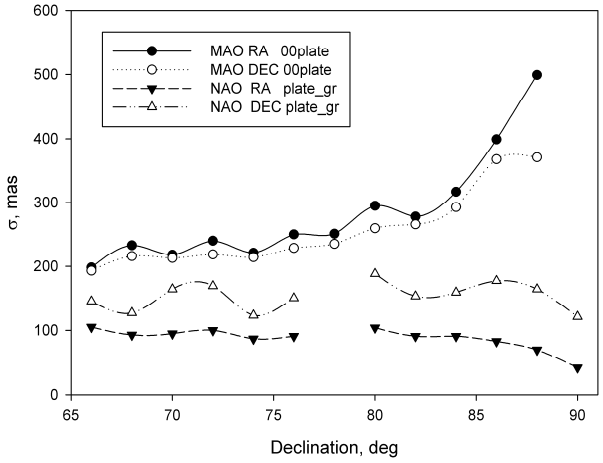

Figure 3: The SD of equatorial positions vs declination.

Using these two input catalogs as the first and the second epoch of observation, we obtained a resulting ZA_DWA catalog of positions and proper motions for about 30 thousand common stars. Number of stars versus magnitude for the ZA_DWA catalog is shown in the left part of Figure 4. We calculated inner accuracies of equatorial positions for the ZA_DWA catalog. The SD of positions in right ascension (RA) and declination (DE) are ±73 mas for both equatorial coordinates. The SD of equatorial positions versus magnitude are shown in the right part of Figure 4.

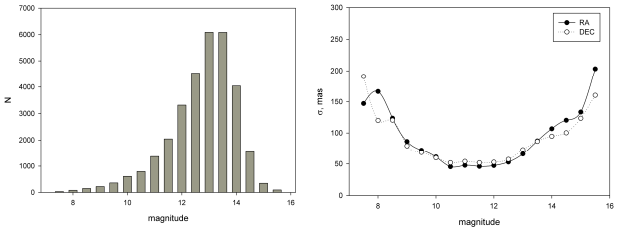

Figure 4: Number of stars (left) and SD of positions (right) in the ZA_DWA catalog vs magnitude.

We compared proper motions for the common stars in the ZA_DWA and Tycho2 catalogs. TopCat allowed us to find common stars for these catalogs and to calculate parameters of linear correlation (LC) for proper motions of stars in RA – $\mu_\alpha \cdot \cos\delta$ and DE – μ_δ. The coefficients of LC in $\mu_\alpha \cdot \cos\delta$ (Figure 5) and μ_δ are equal to 0.92 and 0.94 respectively for about 16 thousand common stars.

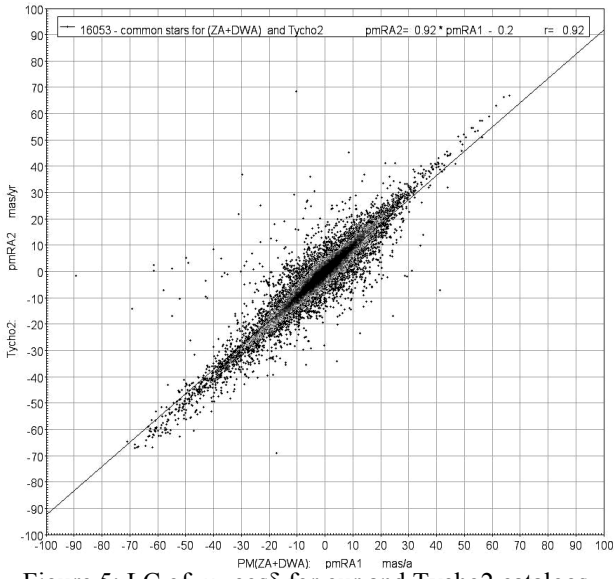

Figure 5: LC of $\mu_\alpha \cdot \cos\delta$ for our and Tycho2 catalogs.

The obtained result suggests the advisability of processing of all observations to receive proper motions of stars up to 14-15^m in the declination zone of 65° to 90°.

Acknowledgements. This research has made use of "Aladin sky atlas" developed at CDS, Strasbourg Observatory, France 2000A&AS..143...33B and 2014ASPC..485..277B TopCat as an interactive graphical viewer and editor for tabular data were helpful in this research work (2005ASPC..347…29T).

References

2. Andruk V. et al.: 2016, *KPCB*, **32**, 1 (in press).
3. Andruk V. et al.: 2014, *Odessa Astron. Publ.*, **27/1**, 53.
1. Protsyuk Yu. et al.: 2014, *Odessa Astron. Publ.*, **27/1**, 59.
4. Protsyuk Yu. et al.: 2014, *KPCB*, **30**, N6, 296.
6. Protsyuk Yu. et al.: 2014, ISBN: 978-80-7080-918-1, 131.
5. Vavilova I. et al.: 2014, ISBN: 978-80-7080-918-1, 8.
7. Vavilova, I.B. et al.: 2012, *KPCB*, **28**, N2, 85.
8. Vavilova, I.B. et al.: 2012, *BA*, **21**, N3, 356.

DATA PROCESSING OF PLATES CONTAINING IMAGES OF URANUS AND NEPTUNE FROM UKRVO DIGITAL ARCHIVE: STRUCTURE, QUALITY ANALYSIS

Protsyuk Yu.[1], Yizhakevych O.[2], Kovylianska O.[1] , Protsyuk S.[1], Andruk V.[2], Kashuba S.[3], Kazantseva L.[4]

[1] Research Insitute: Nikolaev Astronomical Observatory, Ukraine, *yuri@nao.nikolaev.ua*
[2] Main Astronomical Observatory, National Academy of Sciences, Ukraine, *andruk@mao.kiev.ua*
[3] Astronomical Observatory, Odessa National University, Ukraine, *sv.kashuba@gmail.com*
[4] Astronomical Observatory, Kyiv National University named after T. Shevchenko, Ukraine, *kazl@ukr.net*

ABSTRACT. To use accumulated resources of UkrVO digital archive, analysis of the available photographic plates containing images of Uranus and Neptune was conducted. Data processing of selected plates was also caried out to provide an estimate of positional precision and accuracy. Archives of the Research Institute: Nikolaev Astronomical Observatory (NAO), Main Astronomical Observatory of National Academy of Science (MAO), Astronomical Observatory of Odessa National University (AO ONU), Astronomical Observatory of Kyiv National University (AO KNU) were used. Numbers of plates containing images of Uranus and Neptune are, respectively, the following: 220 and 218 plates in NAO, 64 and 35 plates in MAO, 54 and 44 plates in AO ONU, 3 and 1 in AO KNU. Plates of NAO and MAO have 2 or 3 exposures per plate, and other plates have only one exposure per plate. The epoch of observation for most plates is 1960 to 1998, and for only one plate is 1908.

All plates were scanned with the resolution not less than 1200 dpi. Each plate of NAO was scanned 5 to 6 times. Plates containing images of Uranus and Neptune were, respectively, scanned 618 and 952 times in NAO. All plates of other observatories were scanned only once. Raw image processing for scans containing images of Uranus and Neptune was conducted for all scans obtained in observatories. (X, Y) coordinates, (I) intensities and FWHM values were obtained for images of all objects.

Star identification for scans containing images of Uranus and Neptune was, respectively, conducted for 600 and 936 scans in NAO and for 71 scans in MAO. Coordinates of all objects were obtained. Positional accuracy of reference stars was estimated for 244 plates of NAO and 66 plates of MAO, and has value of 0.08″-0.26″.

Keywords: astronomical data bases – astrometry – methods: data analysis – catalogs

1. Introduction

In 2014 we used Joint Digital Archive (JDA) database of UkrVO (Vavilova et al., 2012a, 2012b) to find and recalculate all Ukrainian observations of Pluto (Kazantseva et al., 2015). In 2015 we continue this work and analysis of the available photographic plates in JDA, containing images of Uranus and Neptune, was conducted.

Archives of the NAO (Zonal Astrograph (ZA, D/F=12/204, 101"/mm), MAO (Double Wide-angle Astrograph (DWA, D/F = 40/200, 103"/mm), Double Long Focus Astrograph (DLFA, D/F=40/550, 37"/mm)), AO ONU (Seven Wide Angle Astrograph (SWA, D/F=12/60, 313"/ mm)) and AO KNU were used. Then, we start scanning of this plates and make processing of a received images. Using different kind of software we obtained coordinate of the planets and comparing results with well known ephemerides.

2. Structure of archive and plate scanning

We found more than 600 plates with Uranus and Neptune in UkrVO. Structure of plate archives is shown in Table 1.

Table 1. Structure of plate archives

	Telescope, epoch	Uranus, plates	Neptune, plates
NAO	ZA 1961-1998	220	218
MAO	DLFA, DWA, Z600 1963-1991	64	35
AO ONU	SWA 1960-1989	42+12	32+12
AO KNU	AZT8, DAMR 1988, 1908	3	1

All plates in NAO and MAO have 2 or 3 exposures per plate. Another one have only one exposure. 12 plates of AO ONU have Uranus and Neptun in same plate.

After searching in JDA all plates were scanned with the resolution not less than 1200 dpi (part of plates in NAO were scanned with the resolution 1600 dpi). Current status of the scanning shows in Table 2.

Table 2. The current status of the plate scanning

	Uranus, plates	scaned, plates/scans	Neptune, plates	scaned, plates/scans
NAO	220	104/618	218	160/952
MAO	64	39/39	35	35/45
AO ONU	42+12	48/54	32+12	38/38
AO KNU	3	3/3	1	1/1

Each plate of NAO was scanned 5 to 6 times without turning. Plates containing images of Uranus and Neptune were, respectively, scanned 618 and 952 times in NAO. All plates of other observatories were scanned only once (ecsept one plate of MAO and AO ONU with 6 scans for testing purpose).

3. Data reduction and quality analysis

For raw image processing we used MIDAS/ROMAFOT software (Andruk et al., 2010; Protsyuk et al., 2014a, 2014b). Raw image processing for scans containing images of Uranus and Neptune was, respectively, conducted for 618 and 952 scans in NAO and for all scans obtained in other observatories. (X, Y) coordinates, (I) intensities and FWHM values were obtained for images of all objects. The current status of raw image processing shows in third column of Table 3 (considering that 1 plate in NAO usually have 6 scans).

Table 3. The current status of the raw image processing and identification

	scaned, plates	processed in MIDAS, plates	identified, plates	no identified, plates
RI NAO	264	264	244	8
MAO	74	74	66	8
AO ONU	86	85	2	-
AO KNU	4	4	1	-

For star identification we used two different software package for LINUX and WINDOWS system (Protsyuk et al., 2014; Andruk et al., 2016). Star identification for scans containing images of Uranus and Neptune was, respectively, conducted for 600 and 936 scans in NAO and for 71 scans in MAO. Some of plates no identified due to quality of images and errors in observation. After identification coordinates of all objects on plates were obtained in Tycho-2 system (Protsyuk et al., 2014; Andruk et al., 2016). Positional accuracy of reference stars shows in Table 4. In first column scale of one pixel in seconds of arc specified. In columns from 4 to 6 standart deviation (SD) of planet's position (in arcsec and pixel) and magnitude shows. Table 4 shows, that SD of planet's position is in ranges 0.10-0.12 pixel in main part of archive, that corresponds depending on the scale from 0."08 to 0."26. Plates of AO ONU have large scale and big distortion near the border, so, errors in seconds of arc also big.

Table 4. The current status of the reduction

	Proc., plates	Ident., plates	SD of planet RA position, arcsec|pix	SD of planet DEC pos., arcsec|pix	SD of mag
NAO 2.1|1.6	264	244	0.19|0.11	0.19|0.11	0.01-0.07
MAO DLFA 0.8	74	66	0.09|0.11	0.08|0.10	0.01-0.03
MAO DWA 2.2			0.22|0.10	0.26|0.12	0.04-0.05
AO ONU 16.9	85	2	2.2|0.13	2.7|0.16	0.01-0.03
AO KNU	4	1	-	-	

Since the NAO has a 6 scans for each plate we obtained inner accuracy of planets coordinate. Distribution of quantity of SD of positions in seconds of arc shows on Fig. 1 for Uranus and on Fig. 2 for Neptune.

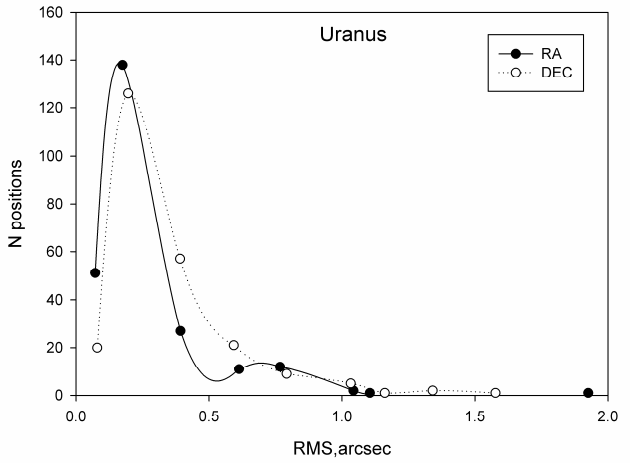

Figure 1: Distribution of quantity of SD of Uranus position in seconds of arc

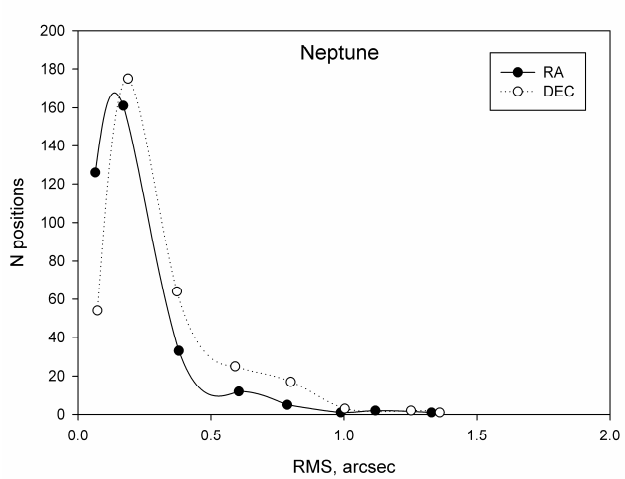

Figure 2: Distribution of quantity of SD of Neptune position in seconds of arc

Some plates of NAO have 5 exposures, so, we obtained track of planet position during time of observation (Fig. 3, Fig. 4).

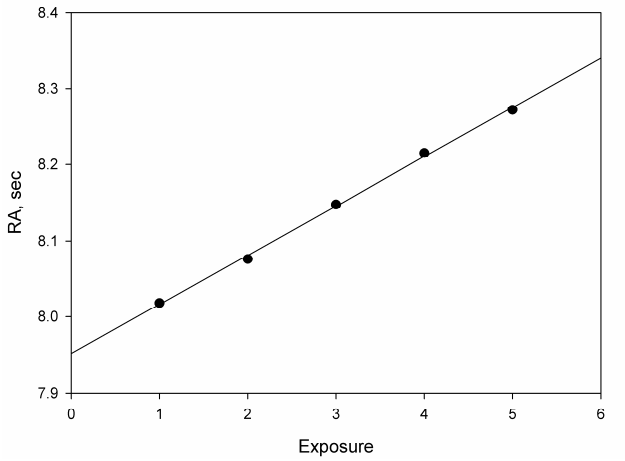

Figure 3: Track of the Uranus in RA direction on one of a plates

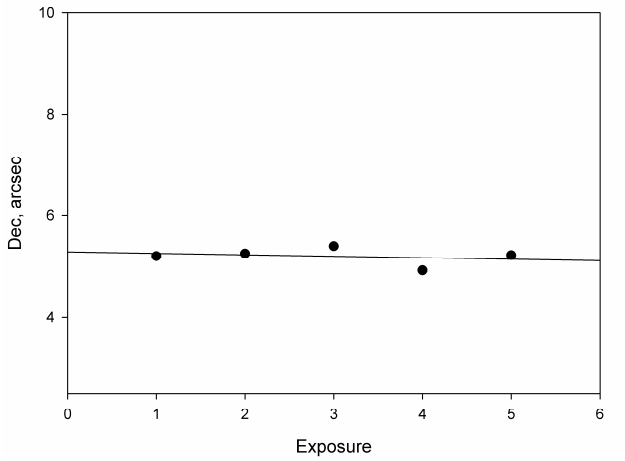

Figure 4: Track of the Uranus in DEC direction on one of a plates

For all moments of planet's observation we downloaded planet's position from The Institut de Mecanique Celeste et de Calcul des Ephemerides (IMCCE) ephemeris web-site and were compared our results with well known ephemerides.

4. Conclusion

We were found in UkrVO archive 627 plates with 1701 exposures of the Uranus and Neptune. Were scanned and processed in MIDAS software 428 plates on date. And were identified 313 plates with 932 positions of Uranus and Neptune. Obtained positions were compared with known orbital theories and were received (O-C) for them.

For next period we will modify program for processing AO ONU observations, finishing scan, reduction and identification of all UkrVO plates with Uranus and Neptune. Also we shall include satellites of the planets in workset and using of those coordinates for improvement of the orbital theory of the planets and their satellites.

Acknowledgements. The authors are thankful to anybody who has read this contribution to the end.

References

Andruk V.M. et al.: 2010, *Kinem. Phys. Cel. Bodies*, **26, N3**, 146.

Andruk V. et al.: 2016, *Kinem. Phys. Cel. Bodies*, **32, N1** (in press).

Kazantseva L.V. et al.: 2015, *Kinem. Phys. Cel. Bodies*, **31, N1**, 58.

Protsyuk Yu.I. et al.: 2014a, *Kinem. Phys. Cel. Bodies*, **30, N6,** 54.

Protsyuk Yu. et al.: 2014b, *Odessa Astron. Publ.*, **27/1**, 59.

Vavilova I.B. et al.: 2012a, *Kinem. Phys. Cel. Bodies*, **28, N2,** 85.

Vavilova I.B. et al.: 2012b, *Baltic Ast.*, **21, N3**, 356.

CREATION OF LARGE CATALOGUES BY USING OF VIRTUAL OBSERVATORIES

Yu.I.Protsyuk, O.M.Kovalchuk

Research Insitute "Nikolaev Astronomical Observatory",
Mykolaiv, Ukraine, *yuri@nao.nikolaev.ua*

ABSTRACT. We developed an application program to search images in the registers and databases of Virtual Observatories and to download them to local computer. The program has the ability to process XML file in VO Table format to generate links to images, as well as to work directly with the astronomical servers. To improve the efficiency for downloading of large number of images, we used multi-threaded mode. The program runs under the Windows operating system. Using the program in 2014 year, we found and downloaded more than 145 thousand of images of open clusters, having total volume of about 300 GB. Total download time was about 7 days. To process the downloaded images, we created and configured a complex of 10 virtual machines on two PCs for parallel image processing by using Astrometrica program. Total processing time was about 14 days. An application program was also created to analyse the obtained results, which were used to create four catalogues of stellar coordinates at the average epoch of 1953 to 1998. The total number of stars in the catalogues is more than 35 million. The standard error is 0.04" to 0.07", and the average number of observations is 4 to 6. The catalogs are used to improve proper motions of stars in and around of open clusters.

Keywords: Astrometry – Astronomical data bases – Catalogs – Virtual observatory tools.

1. Introduction

In recent years through the development of panoramic receivers and information technology astronomers must respond to an avalanche increasing amount of data that contain information on many celestial objects at different wavelengths. Existing and future huge databases can not afford to use in one isolated institution, but provides such opportunities for international cooperation and organization wide access to collected data. International Virtual Observatories Alliance (IVOA) created to pool resources astronomical data at the national and international levels and provide convenient unified search engine to access the data. Since 2011 Ukrainian Virtual Observatory (UkrVO) included to IVOA (Vavilova et al., 2010, 2011, 2012).

New scientific results can be obtained using data accumulated on different instruments for a long time. One example of this is the study of open clusters (OC) of our Galaxy, formations of stars that have a common origin. It helps solve a wide class of problems concerning formation of stars, structure and evolution of the Galaxy and others. Currently, the number of OC estimated near one hundred thousand and only a small percentage of them have been studied in detail. In particular, we don't know the exact distances and middle proper motions of about half of all known OC.

To solve this problem at the Research Institute: Nikolaev Astronomical Observatory (RI NAO) we studied of stars in regions around the OC several last years using the achievements of a decade of work on the creation and implementation of modern information technologies in astronomy, including the UkrVO creation (Protsyuk et al., 2007; Mazhaev et al., 2014; Vavilova I. et al.: 2010, 2011, 2012, 2014). With the assistance of our own observations and data from IVOA registries received at different times and at different telescopes, an accurate catalogs of positions and proper motions of stars around OC in creating (Protsyuk et al., 2014).

2. Develop an application program to search images in VO databases

Search and downloading of astronomical images obtained at different times and on different instruments through specialized astronomical websites or through existing specialized software requires a big amount of manual work and time if there is a need for a large number of observations. For this purpose we developed methodics and software to search for images in the IVOA registers and astronomical databases (DB) and automatically download them to computer. Software provides features for finding information about astronomical images and automatically download them to your computer when matching predetermined criteria. Search criteria, given in a prepared list, include the angular coordinates and search radius. The program has the ability to process XML files in VOTable format to create links to the images and work directly with astro-servers. Software running in the Windows operating system and consists of several functional modules – namely: content downloads module, module of content analysis of Web page and formation of links to files and image downloads module. The program works in multithreaded mode and provides full control of downloading and processing of possible network errors. Download speed is limited only by the speed of the Internet connection. TThe modular construction principle of the program provides high stability that is essential for automatic downloading large file sets.

3. Processing and analysis of the obtained images

We used developed program for 500 selected fields aropund OC and were found and downloaded more than 145 thousand images in 2014. Images were obtained at various of telescopes from 1952 to 1999 with total capacity near 300GB. Total duration of the work of program was about 7 days of continuous operation. By automating the process productivity increased about 200 times.

For processing the images arrays we created complex of 10 virtual machines on 2 PCs, which is configured for parallel automatic processing of large volumes of observations using Astrometrica *(http://www.astrometrica.at)* with additional program for automation. Images were downloaded from Aladin Images Server *(http://aladin.u-strasbg.fr)* for infrared photometric reviews 2MASS (Skrutskie M.F. et al., 2006.) and DENIS (DENIS Consortium, 2005) and from the server *http://archive.stsci.edu* for The Digitized Sky Surveys (DSS) array. Also we include near the 20 thousand own observations at the telescope Mobitel KT-50. The UCAC4 catalog (Zacharias et al., 2013) were used for all reduction as reference one. The total number of processed images – more than 160 thousand. Were received coordinates for more than 235 million objects with good precision. For processing of the entire array of images with 10 virtual machines took about 14 full days job.

Also software for the analysis of the results were created. The accuracy analysis of (O-C) (UCAC4 reference catalog) depending on the Mag, Dec, Ra and Color band. Calculation of the standard deviation and the mean (O-C) made in 3-iteration. This number of iterations is selected because the number of exceptions by the criterion 3σ in third iteration decreases sharply. Part of the results of calculations for one source (2MASS) set out in the form of a graphs of Figures 1-4.

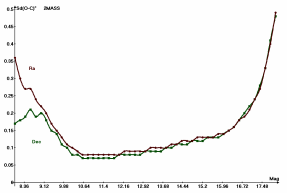

Figure 1: Dependence of the standard deviation (SD) of O-C to magnitude

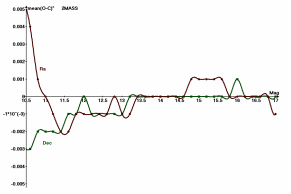

Figure 2: Dependence of the mean O-C to magnitude

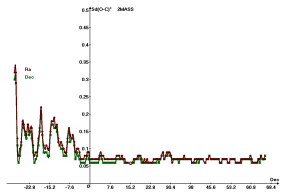

Figure 3: Dependence of the SD of O-C to declination

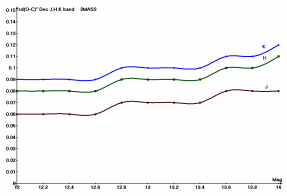

Figure 4: Dependence of the SD of O-C in declination to magnitude in bands J, H, K

We made analysis of accuracy of the results from all 4 sources by magnitude, coordinates and color band.

4. Creation and analysis of the catalogs

Image processing conducted using the program Astrometrica and additional program, created in the RI NAO, for batch mode processing. Were processed over 160 thousand images with UCAC4 reference catalog. All data is divided into five parts and we obtained five catalogs at different epochs.

First consider the catalog, obtained from 2MASS set. We received more than 135 million objects on it in sites containing OC. With this data we obtained astrometric catalog of over 19.7 million stars $(9\text{-}18.5)^m$ (Fig.5) which observed three and more times with the average number of observations (ANO) of a star about 6.3 times and the average accuracy of catalog position (AACP) in right ascension (RA) 40 mas and declination (DEC) 39 mas (Fig. 6). The average epoch of catalog is 1998.7.

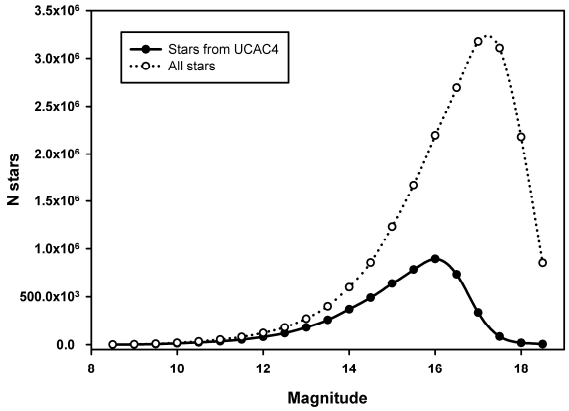

Figure 5: Distribution of stars of 2MASS set catalog to magnitude

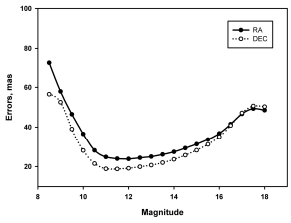

Figure 6: Dependence of precision of 2MASS set catalog to magnitude.

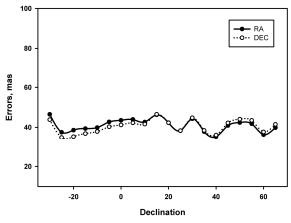

Figure 7: Dependence accuracy of 2MASS set catalog to DEC

As shown in Figure 7 the accuracy distribution to declination without major deviations. In comparison, the reference catalog on the same data, which includes over 5.1 million stars from UCAC4 that were observed 3 or more times with ANO of a one star about 4.9 times have AACP 32 mas by RA and 28 mas by DEC.

Next consider the catalog, obtained from the DENIS set. We received more than 24.5 million objects in regions, containing OC. With this data we obtained astro-

metric catalog of more than 3 million stars (9-18.5)^m (Fig. 8) which observed three and more times with the ANO of a star about 5.2 times and AACP in RA 52 mas and DEC 68 mas (Fig. 9). The average epoch of catalog is 1998.8.

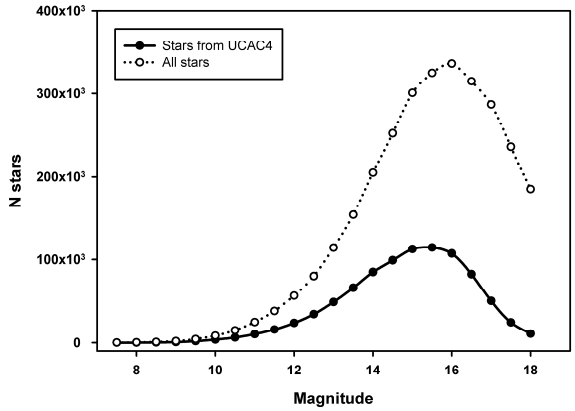

Figure 8: Distribution of stars of DENIS set catalog to magnitude

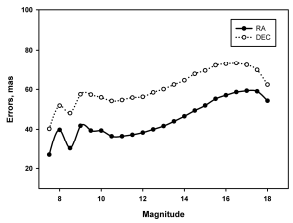

Figure 9: Dependence of precision of DENIS set catalog to magnitude.

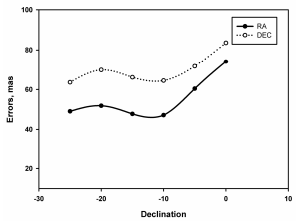

Figure 10: Dependence accuracy of DENIS set catalog to DEC

As shown in Figure 10 the accuracy distribution to declination have the noticeable dependence. In comparison, the reference catalog on the same data, which includes over 0.9 million stars from UCAC4 that were observed 3 or more times with ANO of a one star about 5.3 times have AACP 41 mas by RA and 52 mas by DEC.

Next consider the catalog, obtained from the DSS-A set. We received more than 19.5 million objects in regions, containing OC. With this data we obtained astrometric catalog of about 3 million stars (13-18.5)^m (Fig. 11) which observed three and more times with the ANO of a star about 4.1 times and AACP in RA 65 mas and DEC 70 mas (Fig. 12). The average epoch of catalog is 1953.2.

As shown in Figure 13 the accuracy distribution to declination have the noticeable dependence with accuracy deviation. In comparison, the reference catalog on the same data, which includes about 0.7 million stars from UCAC4 that were observed 3 or more times with ANO of a one star about 3.6 times have AACP 65 mas by RA and 70 mas by DEC.

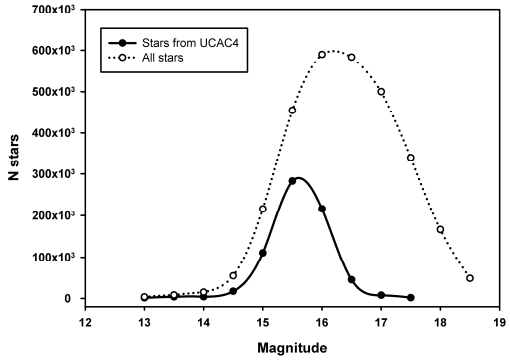

Figure 11: Distribution of stars of DSS-A set catalog to magnitude

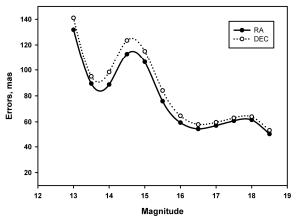

Figure 12: Dependence of precision of DSS-A set catalog to magnitude.

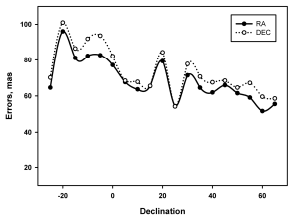

Figure 13: Dependence accuracy of DSS-A set catalog to DEC

Next consider the catalog, obtained from the DSS-B set. We received more than 52.5 million objects in regions, containing OC. With this data we obtained astrometric catalog of more than 8 million stars (13-18.5)^m (Fig. 14) which observed three and more times with the ANO of a star about 5.7 times and AACP in RA 47 mas and DEC 54 mas (Fig.15). The average epoch of catalog is 1988.3.

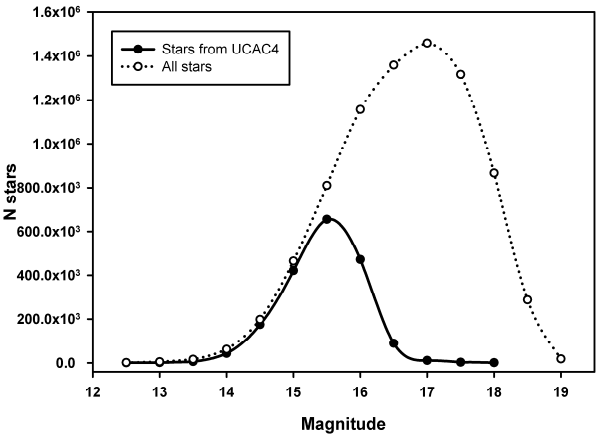

Figure 14: Distribution of stars of DSS-B set catalog to magnitude

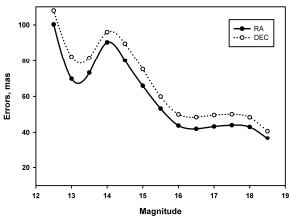

Figure 15: Dependence of precision of DSS-B set catalog to magnitude.

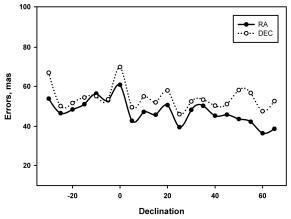

Figure 16: Dependence accuracy of DSS-B set catalog to DEC

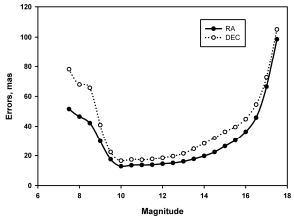

Figure 18: Dependence of precision of MOBITEL set catalog to magnitude.

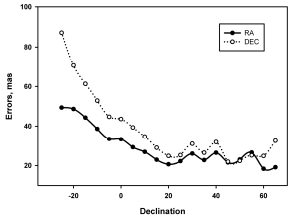

Figure 19: Dependence accuracy of MOBITEL set catalog to DEC

As shown in Figure 16 the accuracy distribution to declination have the some dependence and the picture is somewhat reminiscent of the behavior of the system in the Mobitel telescope (Fig. 19) but zero-point is not at zenith but around the equator. When you move to north accuracy difference between the two coordinates increases. In comparison, the reference catalog on the same data, which includes over 1.8 million stars from UCAC4 that were observed 3 or more times with ANO of a one star about 5.6 times have AACP 50 mas by RA and 56 mas by DEC. This is worse, than accuracy of general catalog and is associated with significantly worse accuracy of bright stars.

Finally consider the MOBITEL-2014 catalog, which include data from more than 20 thausands of CCD images, observed in RI NAO in 2011-2014. We received more than 90 million objects in regions, containing OC in the area of ± 20 ° from the Galactic plane. With this data we obtained astrometric catalog of over 3.7 million stars $(8\text{-}17)^m$ (Fig. 17) which observed three and more times with the ANO of a star about 21 times and AACP in RA 29 mas and DEC 38 mas (Fig. 18). The average epoch of catalog is 2013.6.

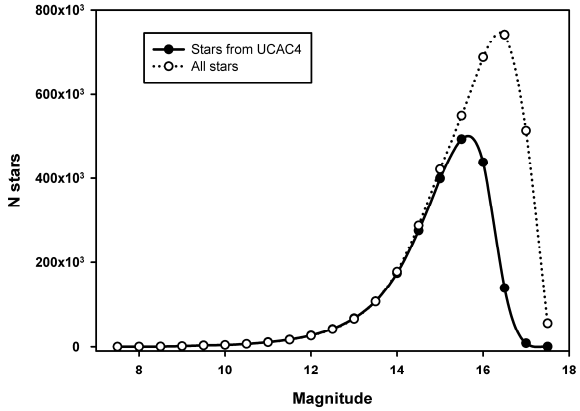

Figure 17: Distribution of stars of MOBITEL-2014 set catalog to magnitude

As clearly shown in Figure 19 the accuracy distribution to declination have the dependence from the zenith distance. Perhaps the reason is related to the lack of telescope alignment in south, which is usually performed only in the direction of the zenith ($\delta = 47°$) and pole ($\delta = 90°$) without alignment control to south of the zenith.

5. Conclusion

By using software, created in NAO in 2014, at 500 selected areas of sky within a 7 days of continuous operation more than 145 thousand astronomical images obtained at various telescopes from 1952 to 1999 was found and downloaded. For processing the arrays of images, including 20 thousand of own observations, the complex of 10 virtual machines was created on 2 PCs. Complex was set up to automatic processing of large volumes of observations in parallel and worked about 14 full days. As a result, we received more than 235 million coordinates of sky objects with good precision. All the processing is performed in a single system with the same software. And we obtained astrometric catalogs with more than 38 million stars.

Thus, the implementation of this investigation resulted in the increase performance of processes from 10 to 200 times. It shows how important for modern astronomy is to use modern information technology when working with large volumes of information.

Acknowledgements. The authors are thankful to Herbert Raab for the Astrometrica program, Yevgen Kozyryev for the Astrometrica automation program and anybody who has read this contribution to the end.

References

Mazhaev A. et al.: 2014, *Odessa Astron. Publ.*, **27/1,** 55.
Protsyuk Yu.I. et al.: 2007, *Proc. of IAU Symp.,* **N248**, 548.
Protsyuk Yu.I. et al.: 2014, *Kinem. Phys. Cel. Bodies*, **30, N6,** 54.
Skrutskie M.F. et al. : 2006, *AJ*, **131**, 1163.
Vavilova I. B. et al.: 2010, *Kosmichna Nauka i Tekhn.*, **16, N5**, 62 (in russian).
Vavilova I. B. et al.: 2011, *Kosmichna Nauka i Tekhn.*, **17, N4**, 74 (in russian).
Vavilova I.B. et al.: 2012, *Kinem. Phys. Cel. Bodies*, **28, N2,** 85.
Vavilova I. et al.: 2014, *Odessa Astron. Publ.*, **27/1,** 65.
VizieR Online Data Catalog: 2005, *The DENIS database*
Zacharias N. et al.: 2013, *AJ*, **145**, 44

THE COMPILED CATALOGUE OF PHOTOELECTRIC UBVR STELLAR MAGNITUDES IN THE TYCHO2 SYSTEM

E.Relke[1], Yu.I.Protsyuk[2], V.M.Andruk[3]

[1] Walter-Hohmann-Observatory, 159 Wallneyer St., 45133 Essen, Germany, *helena_relke@yahoo.com*

[2] Research Institute: Nikolaev Astronomical Observatory, 1 Observatornaya St., 54030, Mykolaiv, Ukraine,*yuri@nao.nikolaev.ua*

[3] Main Astronomical Observatory of National Academy of Sciences, 27 Akad. Zabolotnogo St., 03680, Kyiv, Ukraine, *andruk@mao.kiev.ua*

ABSTRACT. In order to calibrate the images of astronomical photographic plates from the archive of UkrVO was created the compiled catalogue of photoelectric UBVR stellar magnitudes. It is based on: the Kornilov catalogue of 13586 WBVR stellar magnitudes (Kornilov at al., 1991), the Mermilliod catalogue of 68540 UBV stellar magnitudes (Mermilliod, 1991) and the Andruk catalogue of 1141 UBVR stellar magnitudes (Andruk at al.,1995). All original coordinates have the different epoch and equinox. We performed the cross reference of stars from these three catalogues with the Tycho2, UCAC4 and XPM catalogues and created a new photometric catalogue on the epoch and equinox of J2000.0.

Keywords: Photometric – methods: data analysis – catalogues virtual observatory tools – astrometry - techniques

1. Introduction

For the goals and objectives of photometric calibration of the astronomical photographic plates exposed for the sky areas from -30° to 90º was created the first version of the compiled star catalogue of the positions, proper motions and photoelectric U(W)BVR stellar magnitudes in the Johnson system. The reason for the creation of this catalogue was the low precision of the equatorial coordinates and the absence of any information about the proper motions of stars, that have photoelectric U(W)BVR stellar magnitudes in all source catalogues. For our purposes were chosen three source catalogues:

1. Photometric catalogue of UBV stellar magnitudes (Kornilov et al., 1991)
2. Photometric catalogue of WBVR stellar magnitudes (Mermilliod et al., 1991)
3. Photometric catalogue of UBVR stellar magnitudes of the MEGA project (Andruk et al., 1995; Andruk 1996; Andruk 1996; Andruk 1996).

The corresponding number of stars with the photoelectric stellar magnitudes in three source catalogues is following: 13586 (down to $\delta \leq$ -26º), 47022 (down to $\delta \leq$ -30º) and 1141 (down to $\delta \leq$ -13º). Altogether the whole list has 61749 stars. The precision of the equatorial coordinates of the stars in these catalogues is not high enough, (especially for the second catalogue), that complicated the identification of the calculated coordinates of stars obtained as the result of the processing of digitized images of photographic plates. The difficulties by the identification are significant for the faint stars and growing up for the photographic plates recorded in the first half of the twentieth century.

2. The results of the identification with the Tycho2, UCAC4 and XPM catalogues

All stars of the created list were consistently identified with the stars of the Tycho2, UCAC4 (Zacharias et al., 2013) and XPM (Fedorov P. et al., 2009) catalogues. The corresponding amounts of stars of the individual source catalogues identified with the Tycho2 catalogue were following: the 38837, 13202 and 633 stars for the first, second and third catalogues respectively. Then the not identified stars from the whole list were compared with the UCAC4 catalogue. The results of this second identification were: the 7803, 289 and 460 stars for the first, second and third source catalogues respectively. The same procedure of the identification for the rest of not identified stars using the XPM catalogue gave out the following results: the 75, 3 and 7 stars. So the first version of our catalogue contain 61309 stars. Due to the errors of identification and because of the duality of a certain amount of stars, the number of the starts in the final catalogue will be decreased.

3. The using of the two exposures on the same photographic plate for the photometry

The combination of characteristic curves of the two exposures on the same photographic plate makes possible to build a new combined characteristic curve for the whole interval of stellar magnitudes on the photographic plate. The photoelectric stellar magnitudes (Bpe) from the source catalogues were used as the photoelectric standards. The steps and methods of the construction of such combined characteristic curves for photographic plates, are shown on the figures 1 and 2. The photometric field errors were also taken into account. The difference between stellar magnitudes of two exposures in the scale of the photoelectric standards (Bpe) is $\Delta B = 3.223$ mag. The errors of photome-

try are σ1 = ± 0.229 mag for the first exposure and σ2 = ± 0.374 mag for the second one. The characteristic curves for the binding of the instrumental photometric values of m1 and m2 with the scale of photoelectric standards Bpe are displayed on the d-panel. The photometric errors are σ1 = ± 0.146 mag and σ1 = ± 0.179 mag.

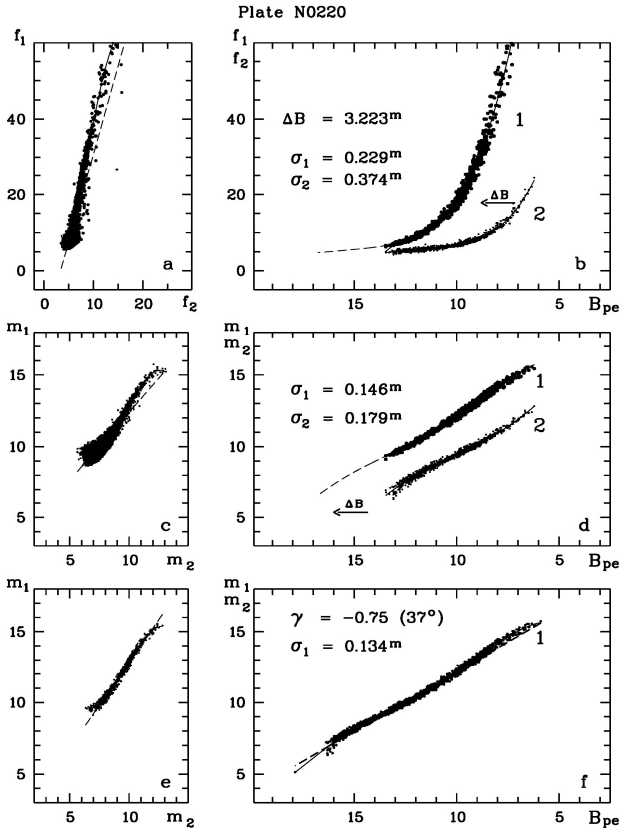

Figure 1: Photometry of stars using the information about the two exposures for the photographic plate N0220.

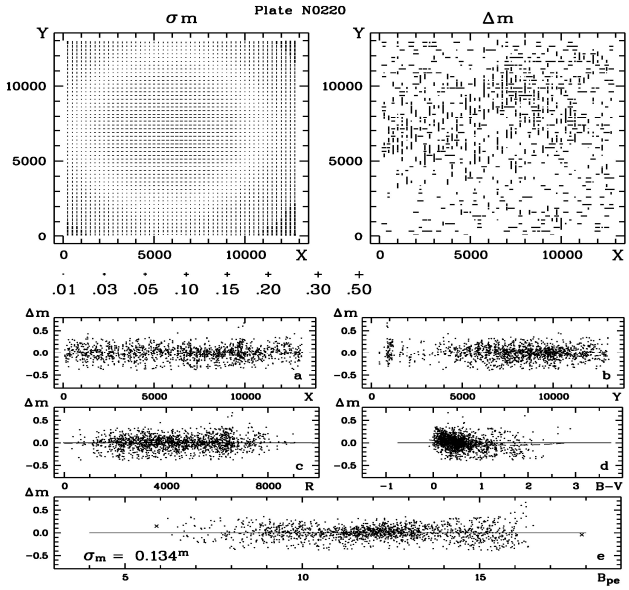

Figure 2: The photometric field errors (upper panels and panels a, b, c, d) for the photographic plate N0220.

4. About the compiled catalogue of photoelectric U(W)BVR magnitudes

As a result of this succeeding identification was created a compiled star catalogue of the equatorial coordinates and proper motions in the system of the Tycho2 catalogue and photoelectric U(W)BVR magnitudes adopted to the Johnson system. The electronic form of this catalogue is presented in the 14 columns. The first seven columns contain information from the original source catalogues: equatorial coordinates α, δ (1 and 2 columns); U(W), B, V and R magnitudes (3, 4, 5 and 6 columns); the 7 column contains the references on the original photometric catalogues (1 – Andruk et al., 1995, 2 – Kornilov et al., 1991 and 3 – Mermilliod et al., 1991). The next seven columns contain the results of the identification: the equatorial coordinates of the stars on the epoch and equinox 2000.0 (8 and 9 columns); the proper motions μαCosδ and μδ (arcsec/year, 10 and 11 columns); B and V magnitudes from the Tycho2, UCAC4 and XPM catalogues recorded in columns 12 and 13; the last column (14) contains the references on the catalogues where data taken from (1 – Tycho2, 2 – UCAC4 and 3 – XPM).

5. Conclusion

This work was performed within the framework of work on the creation of software for data reduction of Joint Digital Archive of Ukrainian Virtual Observatory (Vavilova et al., 2012; Vavilova et al., 2012). The photoelectric calibration of the photographic plates was already used by the authors in series of works (Andruk et al., 2010, Andruk et al., 2014, Andruk et al., 2016, Kazantseva et al., 2014, Protsyuk et al., 2014). The created catalogue will be posted on the websites of the RIO NAO (Ukraine), MAO NASU (Ukraine) observatories and as well as will be transferred to the Strasbourg astronomical Data Centre.

Acknowledgements. The authors are thankful to anybody who has read this contribution to the end.

References

Andruk V.M. et al.: 1995, *Astron. Nachr.*, **316, N4,** 225.
Andruk V.M. et al.: 1996, *Astron. Nachr.*, **317, N2,** 49.
Andruk V.M. et al.: 1996, *Astron. Nachr.*, **317, N2,** 127.
Andruk V.N.: 1996, *Kinem. Phys. Cel. Bodies*, **12, N4,** 60.
Andruk V.M. et al.: 2010, *Kinem. Phys. Cel. Bodies*, **26, N3**, 146.
Andruk V.M. et al.: 2014, *Odessa Astron. Publ.*, **27, N1,** 53.
Andruk V.M. et al.: 2016, *Kinem. Phys. Cel. Bodies*, **32, N1**, 56.
Fedorov P. et al.: 2009, *Mon. Not. R. Astron. Soc.*, **393**, 133.
Kazantseva L.V. et al.: 2015, *Kinem. Phys. Cel. Bodies*, **31, N1,** 58.
Kornilov V.G. et al.: 1991, *Trudy GAIS*, **63,** 1.
Mermilliod J.C.: 1991, *Homogeneous means in the UBV system*.
Protsyuk Yu.I. et al.: 2014, *Kinem. Phys. Cel. Bodies*, **30, N6,** 54.
Vavilova I.B. et al.: 2012, *Kinem. Phys. Cel. Bodies*, **28, N2,** 85.
Vavilova I.B. et al.: 2012, *Baltic Ast.*, **21, N3**, 356.
Zacharias N. et al.: 2013, *Astron. J.*, **145.** 44.

CATALOG OF ASTRONOMICAL POSITIONS OF SATURN'S MOONS OBTAINED BY PHOTOGRAPHIC OBSERVATIONS AT THE MAO NASU IN 1961-1991

O.M.Yizhakevych, V.M.Andruk, L.K.Pakuliak

Main Astronomical Observatory of National Academy of Sciences,
27 Akad. Zabolotnogo St., 03680, Kyiv, Ukraine, *izhak@mao.kiev.ua*

ABSTRACT. In the framework of UkrVO national project the new methods of plate digital image processing are developed. The photographic material of the UkrVO Joint Digital Archive (JDA, http://194.44.35.19/vo-mao/DB/archivespecial.php) is used for the solution of classic astrometric problem – positional and photometric determinations of objects registered on the plates including Saturn's moons. The results of tested methods show that the positional RMS errors are better than ±150 mas for both coordinates and photometric ones are better than $\pm 0.20^{m}$ with the Tycho-2 catalogue as reference.

Keywords: astrometry – methods: catalogs – planets and satellites: individual: Saturn

1. Introduction

A decade ago we created the database of metadata of photographic astronomical plates DBGPA on the base of the MAO NASU glass archive. Later it formed the basis for the creation of Ukrainian VO Joint Digital Archive (JDA) (Vavilova et al., 2012, Vavilova et al., 2012). The efficient structure of the JDA database facilitates a quick search and selection of the desired information for the solution of specific problems such as the determination of the coordinates of celestial bodies and creation of catalogues of stars and galaxies (Kazantseva et al., 2015).

Here we present the results of the reduction of photographic observations of Saturn and its moons, made in 1961 – 1991 at the MAO NASU using 4 telescopes. In DBGPA, we found the data of almost 300 photographic observations of these objects. For further processing, we select 253 plates matching the quality criteria. These plates were scanned using Epson Expression 10000XL (EE) commercial scanner. The complete reduction of the set of plates was made using the software package specially developed and customized for this case at the MAO NASU Department of Astrometry. The catalogue of more than 1100 astrometric positions of the eight Saturn's moons (S2-S9) was obtained in the system of the Tycho-2 star catalogue**.** The internal accuracy of RMS reduction on the data of three telescopes DLFA, DAZ, and Z600 is about ±0.03″ – ±0.11″, for the DWA plates the accuracy appears to be a little bit worse ±015″– ±0.21″. The temporal distribution of calculated positions of moons is presented in the histogram of Fig.1.

The most effective observations were those done in 1980 and 1982 with DWA and the observations conducted in 1990 with Z600 (Yizhakevych et al., 2014).

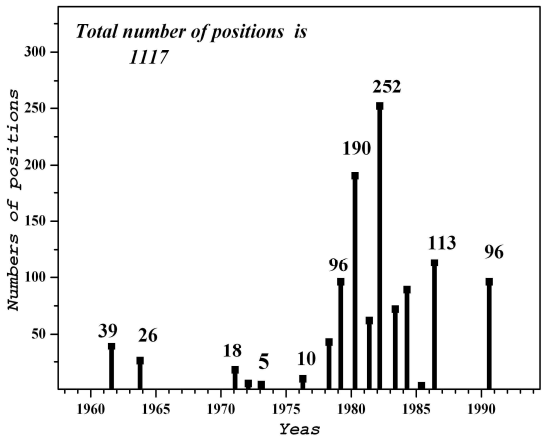

Figure 1: The distribution of the calculated positions of Saturn's moons observations using 4 telescopes of the MAO NASU.

2. Observational data

The first series of photographic observations (**193** plates, 71 observational nights*)* were obtained during 1961–1988 using two astrographs: Double Long Focus Astrograph DLFA (D/F=400/5500 mm) and Double Wide Angle Astrograph DWA (D/F= 400/2000). A few short series of observations were made in field conditions: in 1986 with the Double Zeiss Astrograph DAZ (D/F= 400/3000) in Kitab observatory of the Tashkent University (Uzbekistan) **(8** plates, 7 observational nights*)* and in 1989 (7 observational nights), 1990 (9 nights), 1991 (7 nights) with the Zeiss Reflector Z600 (F = 7500 mm; mt. Maidanak, Usbekistan **(54** plates*)*. Table 1 presents the more information about the telescopes and the observational material.

The most efficient observers for 30 years who collected data for more than 10 plates each were Ledovskaya (Kulyk) I.V., Lysiakova R.F., Major S.P., Onegina A.B., Sereda E.M., Shatokhina S.V., Yizhakevych O.M.

The technique of observations of moving objects with a different brightness (from 8^{m} to 14^{m}) is the exposition of multiple images of varying duration on the same plate. Obviously, the effectiveness of such observations depends

on the mutual random placement of the Saturn's moons at the moment.

Table 2 shows the availability of Saturn's moons observations using MAO NASU telescopes. The highlighted data apply to the maximum distances between the moon and the planet (in mm) on the plate depending on the telescope scale. In the other words, they concern the cases when the moon being in the opposition can be found on the plate.

Table 1. Additional information about telescopes.

Telescope, Tube	Scale ″/mm	Field degree	Emulsion	Years
DLFA, I	37.5	2.5x2.5	ORWO -ZU21, -ZU2	1961-1984
DLFA, II	37.5	1.8x2.5	ORWO -NP27	1982
DWA, I,II	103.1	8.0x8.0	ORWO -ZU21	1976-1988
DAZ, I,II	68.8	0.5x0.5	ORWO -ZU21	1986
Z-600	27.5	5.5x5.5	ORWO -ZU21, -ZU2, -NP27	1989-1991

Table 2. The availability of the observations of Saturn's satellites (S2–S9) with telescopes of the MAO NASU.

Satellite	MgV	Distance from the Planet (mm) on the plate depending on the telescope scale			
		DLFA 37"/mm	DWA 103"/mm	DAZ 68"/mm	Z600 27"/mm
1	*2*	*3*	*4*	*5*	*6*
S2	11.7	**1.1**	0.4	0.6	**1.5**
S3	10.3	**1.4**	0.5	0.7	**1.8**
S4	10.4	**1.7**	0.6	**0.9**	**2.3**
S5	9.7	**2.4**	**0.9**	**1.3**	**3.2**
S6	8.3	**5.5**	**2.2**	**3.1**	**7.5**
S7	14.2	6.7	2.7	3.7	**9.1**
S8	11	**16.1**	**5.9**	**8.9**	**21.8**
S9	16.4	111.	41.	62.	152.
T exposure: from some seconds of time to some minutes					

In fact, various reasons make the chance for the satellite detection lower, for example, because of photographic irradiation, mismatched exposure duration, unfavorable mutual placement of moons, and others.

The special attention was paid to the estimation of the moments of observation. As a rule, the observer recorded the moments of cassette shutter opening and closing at the hearing using stellar chronometer or stellar clock with the further connection to the precise time signals by the «6 points» technique. Before the start of the processing, the corrections of chronometers and stellar clocks were newly qualified and the UT moments of the middle of the exposition were also redefined for each image in contrast to DBGPA data, where the moments of observation have the different format of presentation. They are the start moments of the exposure and its duration.

Search files for the identification of the moons were prepared due to the IMCCE (Paris) ephemeris (http://www. imcce.fr/hosted_sites/aimirror/nssephe.php).

3. Reduction

The algorithm of calculation of the positions by photographic observations is as follows: the first step is the determination of the rectangular coordinates ***x, y*** of objects in the plate coordinate system; on the second step, the objects are identified in the reference star catalogue, and finally the positions in the equatorial coordinate system **α, δ** are derived.

The connection between two coordinate systems ***x, y*** and **α, δ** is determined by the infinite power series, whose members depend on many factors. Among them are the quality of the telescope optics, the field of view of the telescope, the tilt of the plate to the focal plane of the optical system, the reference system used, the number of reference stars on the plate and other factors. The calculations using the formulae of the linking are possible only after the application of restrictions on the number of members of the power series in the result of the evaluation of their relevance on the basis of the adopted model of aberrations. By varying this number, we can get results with the highest level of accuracy, leaving only the significant members of the series (Andruk et al., 2005; Andruk et al., 2014). The scanning of plates was made using Epson Expression 10000XL scanner at 16-bit gray levels and a resolution of 1200 dpi. (Golovnya et al., 2010). Previously, the detailed study of the device, namely the additional errors, connected with the scanner mechanics behavior, has showed its applicability to the solution of problems of ground-based astronomy (Protsyuk et al., 2014).

The software package, specially developed and customized for the case in the LINUX-MIDAS-ROMAFOT environment (Andruk et al., 2007; Andruk et al., 2010), allowed to make a reduction of **253** scans with Saturn's moons images. In fact, the amount of processed material appeared to be approximately three times larger because of multiple images on the each plate. It requires the additional efforts to improve the software algorithm for splitting the digitized image into separate files according to the number of exposures on the plate.

Initially, the software was developed for the processing of the astronegatives of the FON project (Yatsenko et al., 2011). Its plates have large fields of view and are obtained with two expositions: long (16–20 min.) and short (30–60 sec) ones. This allows selecting a few hundred reference stars from the Tycho-2 catalogue homogeneously distributed across the plate field. The more reference stars are on the plate, the more accurate solution for the relation of two coordinate systems could be obtained. In our case, the number of exposures exceeds two.

The processing of the DWA (8°x8°) and DAZ (5°x5°) plates was made using the polynomial of the sixth degree. In addition to them in the observations of Saturn's moons another two telescopes were involved having different

scales of images and star fields (Table 1). So, the reduction of DLFA plates (2°x2°) needs the polynomial of the third degree, and the linear model was applied to the reduction of Z600 (0.5°x 0.5°) plates**.**

The first step of the reduction includes the full analysis of the image for detecting the blemishes and damages of the emulsion on the plate as well as their removal. The elimination of scanner errors is done on the same step too.

The next step was the full reduction of the selected plates. On this step, the plates with failed observations were found and excluded from the processing. These include plates with aiming errors (plates of Z600, obtained in 1991), improper exposition duration when observing faint objects (plates with Phoebe – S9, 16.4^m; plates of Z600, obtained in 1989), errors in the recording of times and in the determination of chronometer corrections, etc.

Finally, we obtained the catalogue of 1100 astro-metric positions of eight Saturn's moons (S2–S9) using 193 photographic plates exposed on four telescopes during 87 productive observational nights.

The comparison of observed positions with the theory of moons' motion DE431 was made using the ephemeris of IMCCE, France, and the residuals $(O–C)_\alpha$ and $(O–C)_\delta$, as well as their standard deviations σ, were obtained according to (1):

$$\sigma = \sqrt{\Sigma((o-c)_i - \overline{(o-c)})^2 / (n-1)} \,. \qquad (1)$$

The results of the comparison are given in Table 3. The internal accuracy of the astrometric reduction into the Tycho-2 reference system lies within ±0.03″ – ±0.11″ for the three telescopes DLFA, DAZ, Z600. For the DWA, the internal accuracy is worse, and it is equal ±015″– ±0.21″.

Figures 2, 3, 4, 5 show the scattering of (O–C) deviations from their average value for S6 satellite as the most efficient object for all four telescopes. The comparison between these four histograms demonstrates that the scattering of O-C from their average value lies in the limits of 1″ and is random for DLFA, DAZ and Z600. In the case of DWA, this scattering is much larger and lies within ±2″. The dispersion analysis for the Fisher test shows that it may indicate the presence of an undetected source of residual systematic errors.

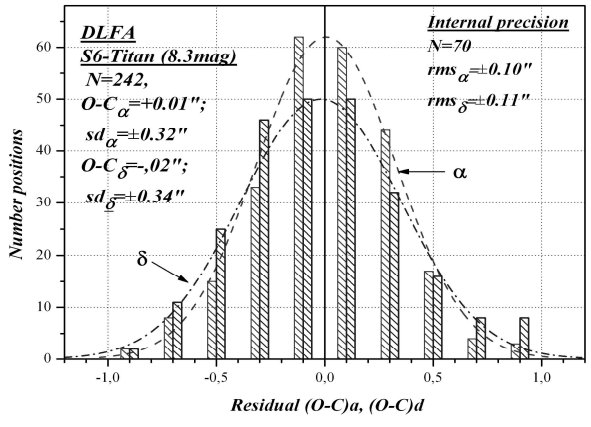

Figure 2: Residuals (O–C); DLFA

Table 3. Statistic parameters of the results of the astrometric solution for 7 satellites and 4 telescopes.

Obj	DLFA (1961–1984 yrs)				
	N	O-C$_\alpha$″	σ$_\alpha$″	O-C$_\delta$″	σ$_\delta$″
S2	9	+.402	0.32	+.184	0.17
S3	71	-.094	0.38	+.085	0.46
S4	118	-.015	0.33	+.067	0.39
S5	186	+.071	0.34	+.018	0.35
S6	248	+.005	0.32	-.018	0.37
S8	212	-.019	0.36	+.019	0.37
Σ	844	+.007	±.34	+.022	±.37
Obj	DWA (1978–1986 yrs)				
	N	O-C$_\alpha$″	σ$_\alpha$″	O-C$_\delta$″	σ$_\delta$″
S5	5	-.744	0.85	-.214	1.11
S6	55	+.209	0.60	+.109	0.64
S8	36	-.744	0.85	-.214	1.11
Σ	96	-.198	±.72	-.004	±.87
Obj	Z600 (1990)				
	N	O-C$_\alpha$″	σ$_\alpha$″	O-C$_\delta$″	σ$_\delta$″
S3	4	+.166	0.25	+.041	0.30
S4	11	-.160	0.30	+.089	0.24
S5	12	-.252	0.46	+.183	0.26
S6	35	-.032	0.43	-.219	0.30
S7	5	-.252	0.51	+.099	0.39
S8	29	+.313	0.41	+.016	0.34
S9	1	+.439		-.268	
Σ	97	+.027	±.41	-.035	±.31
Obj	DAZ (1986)				
	N	O-C$_\alpha$″	σ$_\alpha$″	O-C$_\delta$″	σ$_\delta$″
S4	4	-.451	0.27	+.096	0.15
S5	18	-.093	0.47	+.070	0.29
S6	29	-.052	0.34	+.040	0.27
S8	29	-.012	0.31	-.012	0.31
Σ	80	-.055	±.33	+.025	±.26

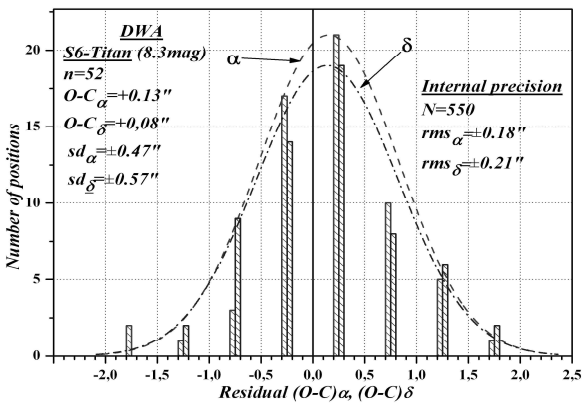

Figure 3: Residuals (O–C); DWA.

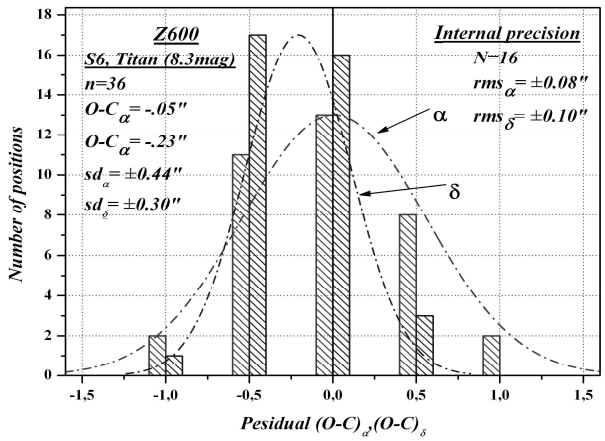

Figure 4: Residuals (O–C); Z600.

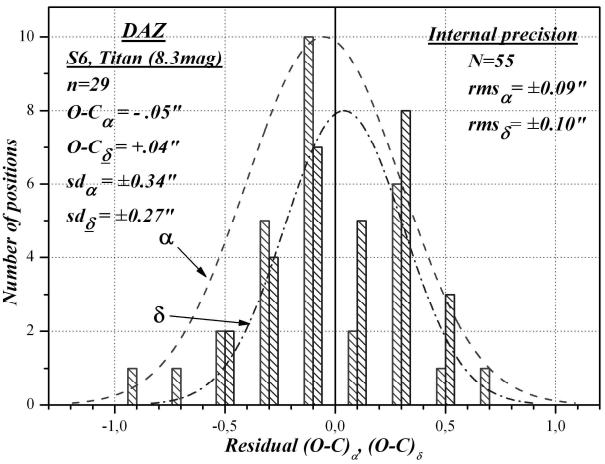

Figure 5. Residuals (O–C); DAZ.

4. Conclusion

The catalogue of 1100 astrometric positions of eight Saturn's moons S2-S9 was obtained based on the reduction of four independent series of observations from different telescopes. For the moment, we have processed 193 plates from the set of 253 plates found in the database of UkrVO JDA.

The internal accuracy of the reduction for three telescopes with the scales from 28 to 68 arcsec/mm lies within ±0.03″ – ±0.11″. The fourth instrument with the scale 103 arcsec/mm gives the accuracy in the interval ±015″–±0.21″ and the larger dispersion of O–C.

For three telescopes DLFA, DAZ, Z600 standard deviations **σ** are in the range from ±0.25″ to ±0.37″ for both coordinates**,** while those for DWA exceed the above values of 1.5–2 times.

The dispersion analysis for the Fisher test shows that the larger dispersion of O-C for DWA may indicate the presence of an undetected source of residual systematic errors. In order to identify the cause of these errors, we assume to perform the additional analysis of the reduction of DWA observations.

The problem of the reduction of Z600 plates exists. Most of them were eliminated because of insufficient results of the preliminary digital analysis of images for defects and damages of emulsions. The considerable number of moons' images close to the planet was not found on the scans of those plates using the digital procedure in contrast to the previous reductions based on the classic technique of measurements (Izhakevich, 1991; Yizhakevych, 1991; Yizhakevych, 1994, Kaltygina, 1992; Pakuliak, 2012; Yizhakevych, 2012). These points to the possible limitations of the processing algorithm, which could misidentify the few pixel images of faint moons as the "dirt" on the emulsion. This requires the further improvement of the software for the processing of digital images of plates with the Solar System bodies.

Acknowledgements. This work was partially supported by the Ukrainian Astronomical Association.

References

Andruk V.M. et al.: 2005, *Kinem. Phys. Cel. Bodies*, **21, N5**, 396.

Andruk V.M. et al.: 2007, *J. Phys. Studies*, **11, N3**, 329.

Andruk V.M. et al.: 2010, *Kinem. Phys. Cel. Bodies*, **26, N3**, 75.

Andruk V.M. et al.: 2014, *Kinem. Phys. Cel. Bodies*, **27, N1**, 53.

Golovnya V.V. et al.: 2010, *J. Phys. Studies*, **14, N2**, 2902.

Izhakevich E.M.: 1991**,** *Scientific paper deposited in All-russian institute of scientific and technical information***, No. 4553-B91**, 1991PDRII4553_I.

Kaltygina S.V. et al.: 1992, *Scientific paper deposited in All-russian institute of scientific and technical information***, No. 1044-Uk92**, 5.

Kazantseva L.V. et al.: 2015, *Kinem. Phys. Cel. Bodies*, **31, N1**, 58.

Pakuliak L. et al.: 2012, in *Proc. of the Conf. NAROO–GAIA "A new reduction of old observations...", June 20–22, 2012, France, Paris*, p. 161.

Protsyuk Yu.I. et al: 2014, *Odessa Astron. Publ.*, **27/1,** 59.

Vavilova I.B. et al.: 2012a, *Kinem. Phys. Cel. Bodies*, **28 N2**, 85.

Vavilova I.B. et al.: 2012b, *Baltic Asronomy*, **21, N3,** 356.

Yatsenko, A.I. et al.: 2011, *Kinem. Phys. Cel. Bodies*, **27, N5**, 249.

Yizhakevych O.M. et al.: 1991*, Kinem. Phys. Cel. Bodies*, **7, №2**, 98.

Yizhakevych O.M. et al.: 1994, *Kinem. Phys. Cel. Bodies*, **10, №1,** 88.

Yizhakevych Ye. et al.: 2012, in *Proc. of the Conf. NAROO–GAIA "A new reduction of old observations…", June 20-22, 2012, France, Paris*, p. 153.

Yizhakevych O. et.al.: 2014, *Odessa Astron. Publ.*, **27/1,** 67.